This is to certify that the
thesis entitled

CHARACTERISTICS AND MODELING OF MINIATURE
MICROWAVE PLASMA DISCHARGES CREATED WITH
MICROSTRIPLINE TECHNOLOGY

presented by

JEFFRI JULLIARSA NARENDRA

has been accepted towards fulfillment
of the requirements for the

M.S. degree in ELECTRICAL ENGINEERING

Timothy Grotjohn
Major Professor's Signature

8/6/04
Date

CHARACTERISTICS AND MODELING OF MINIATURE MICROWAVE PLASMA DISCHARGES CREATED WITH MICROSTRIPLINE TECHNOLOGY

By

Jeffri Julliarsa Narendra

A THESIS

Submitted to
Michigan State University
in partial fulfillment of the requirements
for the degree of

MASTER OF SCIENCE

Department of Electrical and Computer Engineering

2004

ABSTRACT

CHARACTERISTICS AND MODELING OF MINIATURE MICROWAVE PLASMA DISCHARGES WITH MICROSTRIPLINE TECHNOLOGY

By

Jeffri Julliarsa Narendra

Recently, interests in the development of a system on a chip, MEMS and their related micro system applications have suggested the possibility of numerous applications for mini and micro plasma sources. The primary objective of this thesis is to develop such a miniature plasma source and understand the discharge behavior created by it. The plasma source designed in this research is based on the microstrip transmission line structure. The stripline has a characteristic impedance of 50 ohms and is connected to a 2.45 GHz microwave power operating at 1 - 100 Watts. The plasma was created inside a tube, with an inner diameter of 2 mm or less, that was orientated perpendicular to the stripline conductor. This design allows the creation of an electrodeless plasma discharge.

Several diagnostic techniques were utilized to characterize the miniature discharges. Gas temperature and electron density analysis was performed using optical emission spectroscopy (OES). The electron temperature and electron density measurements were performed using the double Langmuir probe (DLP). The results from the OES and DLP experiments are compared to the global analytical model. The power densities for argon discharges created by this source vary from 10's to over 800 W/cm^3 and the plasma densities as indicated by the modeling work are in the range of 10^{12}-10^{15} cm^{-3}.

ACKNOWLEDGMENTS

I would like to take this opportunity to thank my major professor, Dr. Timothy A. Grotjohn, for his constant encouragement and excellent guidance that led me through the work presented here. Along with my advisor, I would like to thank Dr. Jes Asmussen and Dr. Donnie K. Reinhard for being part of the examining committee. Their valuable suggestions and advice are greatly appreciated.

I would also like to thank Kadek W. Hemawan, Andy Wijaya, and Stanley Zuo, who have helped me in the course of this study. A word of thanks is also due to Dr. John T. Hinnant for proof reading the manuscript.

Finally I would like to thank my family for their love and their constant support for my graduate studies.

TABLE OF CONTENTS

LIST OF TABLES

LIST OF FIGURES

Chapter 1

Introduction

1.1 Motivation

This research project involves investigating and establishing the scientific basis and engineering principles for the design and operation of small microwave plasma sources with discharge dimensions ranging from 1.0 mm – 2.0 mm. Past investigations on microwave discharges by researchers have primarily focused on discharges that were a few centimeters to almost a meter in size. However, careful investigations of microwave discharges with dimensions on the order of few millimeters have not been done, especially in the GHz frequency range. The emphasis in this project is on developing plasma sources that will operate without the electrode erosion and contamination problems of small plasma electrode-based systems that are used in arc systems and plasma displays. Small microwave discharges operate with a low input power. This allows the sources to operate with coherent and controllable power supplies currently available for mobile communication system with power levels of one to a few watts.

The thesis intends to experimentally evaluate and subsequently model the behavior of microwave discharges as the discharge size is decreased. The microwave plasma system being used is a microstripline based plasma source. Some of the experimental conditions/structures investigated include varied discharge radii, a variety of discharge gas types (inert gas-argon, and molecular gases-nitrogen and hydrogen), both low and high pressure regimes, a range of

flow rates giving short to long gas residence times in the discharge chamber, and range of plasma discharge geometric aspect ratios.

1.2 Objectives

The primary objective of this work is to design a new miniature plasma source based on microstripline technology and to develop an understanding of the fundamental characteristics of the discharge created by this source.

To achieve this objective, two microstrip transmission line coupling structures were designed and tested. The performance of those structures was compared in terms of the coupling efficiency needed to generate the discharge. The fundamental characteristics studied were the electron temperature, gas temperature, and electron density. The studies were performed on A_r, H_2, N_2, and mixtures of A_r - H_2 and A_r - N_2 discharges at various pressures ranging from 0.5 Torr to 760 Torr.

1.3 Thesis outline

This thesis will focus on observing the characteristics of a discharge that is generated using two microstripline coupling structures. Chapter 2 discusses the literature on miniature microwave plasma sources and diagnostic techniques used in the research. The discussion includes a description of the microstripline transmission line. Chapter 3 explains the experimental systems. These include the testbed system and diagnostic equipment used in the experiments. Chapter 4 details the performance of the microstripline plasma source. The observations for various modifications on the system along with the interpretations are

discussed. In chapter 5, the rotational temperature measurements of hydrogen and nitrogen plasmas using optical emission spectroscopy (OES) are presented. The study of the Stark broadening effect in a hydrogen plasma, which can determine the electron density, is discussed as well. The relevant details needed to understand the optical emission spectroscopy methods are provided. In chapter 6, the electron temperature and density measurements, using double Langmuir probe (DLP), in low pressure argon discharge are presented. Chapter 7 discusses the numerical modeling of argon discharges' characteristics. The results are compared with the OES and DLP results. Finally, chapter 8 concludes the research and provides recommendations for future research.

Chapter 2

Literature on Miniature Plasma Sources and Diagnostic Techniques

2.1 Miniature microwave plasma sources

The definition of plasma according to Chen [1] is a quasineutral gas of charged and neutral particles which exhibits collective behavior. There is always some small degree of ionization in any gas; however, any ionized gas cannot be called a plasma. The plasma is quasineutral; that is, neutral enough so that the density of electrons and ions are equivalent ($n_e \cong n_i$), but not so neutral that all the interesting electromagnetic forces vanish.

A fundamental characteristic of the behavior of a plasma is its ability to shield out electric potentials that are applied to it. This shielding is called the Debye shielding. The quantity λ_D, called the Debye length, is a measure of the shielding distance or thickness of the sheath.

$$\lambda_D \equiv \sqrt{\frac{\varepsilon_o K_B T_e}{n_e e^2}} \qquad (2.1)$$

where ε_o is the permittivity of free space, K_B is the Boltzmann's constant, T_e is the electron temperature, n_e is the charged density far away from the shield, and e is the electron charge. Often, the Debye length can be approximated as:

$$\lambda_D \approx 743\sqrt{\frac{T_e}{n_e}} \text{ (cm)} \qquad (2.2)$$

where T_e is in eV and n_e is in cm^{-3}.

The criterion for an ionized gas to be a plasma is that it be dense enough that λ_D is much smaller than the dimension of the system (L). In addition, the number of particle (N_D) should be large enough inside the shielding so that the concept is statistically valid. Lastly, the frequency of typical plasma oscillations (ω_{pe}) times the mean time between collisions with neutral atoms (τ) should be greater than 1 for the gas to behave like a plasma rather than a neutral gas. Those three criterions can be represented as:

$$1.\ \lambda_D << L$$

$$2.\ N_D = n_e \frac{4}{3}\pi \lambda_D^3 >> 1 \qquad (2.3)$$

$$3.\ \omega_{pe}\tau > 1$$

The first criterion of a plasma indicates that the small-scale plasma source will create a high density discharge. Different small-scale plasma sources have been developed by several research groups. Yin et al. [2] has investigated a miniaturization of inductively coupled plasma (ICP) sources. The discharge in this ICP source is confined within the 4 mm i.d. of a discharge tube. The electron temperature of the argon plasma created using this ICP source is found to vary between 3 eV and 9 eV and the charge density is in the range of 10^9-10^{10} cm^{-3}.

A plasma gun, developed by Hartog et al. [3], is capable of producing a clean, high density (10^{13} – 10^{14} cm^{-3}), low temperature ($T_i \approx T_e \approx 5-15\, eV$) plasma for pulse length of at least 40 ms. The gun operates using molybdenum electrodes and it produces a plasma about 5 cm length and 3 cm diameter. A stack of washers is used to define the arc channel between the anode and cathode. The major impurities reported in this gun plasma are boron, carbon, and nitrogen from the boron nitride washers and molybdenum from the metal electrodes.

Stoffels et al. [4] designed a plasma needle for fine surface treatment of bio materials. This radio-frequency (RF) excited plasma source operates under atmospheric pressure. Plasma appears as a small glow at the tip of a metal pin with a dimension of 5 cm long and 1 mm diameter. The characteristic dimension of a helium plasma generated using this source does not exceed 0.1 – 0.2 mm and the electron density is on the order of $10^{13} - 10^{14}$ cm^{-3}.

At Michigan State University, small microwave discharges' characteristics have been studied since the early 1980's by Asmussen et al. [5 – 7]. Rogers [5] investigated the discharge properties of argon plasma columns with diameters of 1 – 3 mm and length up to 16 cm. The discharge was excited using a 2.45 GHz magnetron inside a microwave cavity. Quartz tubes of varying diameter were used to confine the gas. The tubes ran coaxially inside the cavity. Typical electron densities for argon discharges at 1 atm were 3×10^{13} cm^{-3} to 3×10^{14} cm^{-3}.

Brake [6] studied the Stark broadening effect of a mixture of hydrogen – argon discharge generated using a surface wave launcher. The plasma was contained in a 4 mm i.d. quartz tube, situated vertically, with pressure ranging from 50 – 1000 Torr. The electron density measurements of this work agreed with Rogers' data.

The electron density of microwave-generated surface wave discharges in argon have been measured using Stark broadening and calculated from the

measured wavelengths of the standing surface wave by Brake et al. [7]. Results obtained from these two techniques compare well. The electron density varies from 10^{13} cm^{-3} to 10^{14} cm^{-3} for pressures ranging from 50 to 800 Torr.

2.1.1 Microstripline structure

Microstripline is one of the most popular transmission line structures. The structure of a microstrip transmission line is shown in figure 2.1. The structure consists of a ground plane, a dielectric layer, and a stripline trace.

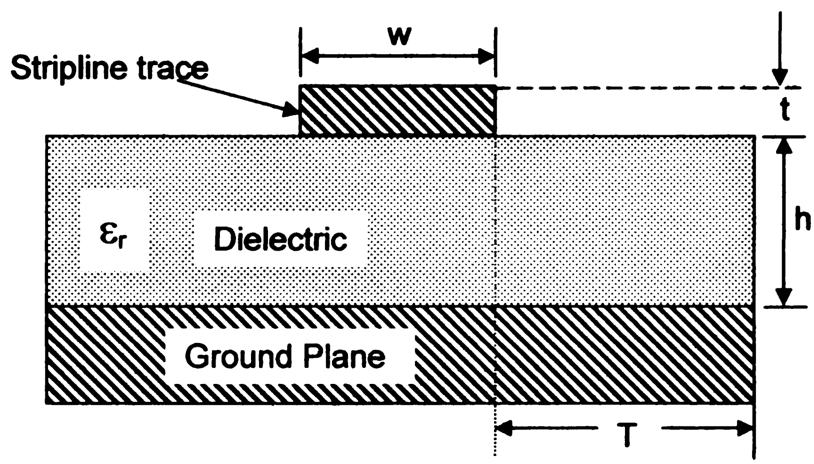

Figure 2.1 Microstripline with trace structure

There are various calculation techniques used to determine the characteristic impedance for this structure. Wadell [8] summarized Bogatin's experimental comparison of these calculations and recommended using the Wheeler equation with Schneider's ε_{eff}.

$$Z_0 = \frac{\eta_o}{2\sqrt{2}\,\pi\sqrt{\varepsilon_{eff}+1}} \ln\left\{1 + \frac{4h}{w}\left[\frac{14 + \frac{8}{\varepsilon_{eff}}}{11}\frac{4h}{3} + \sqrt{\left(\frac{14+\frac{8}{\varepsilon_{eff}}}{11}\right)^2\left(\frac{4h}{w}\right)^2 + \frac{1+\frac{1}{\varepsilon_{eff}}}{2}\pi^2}\right]\right\} \tag{2.1}$$

where η_o is the characteristic impedance of free space (in Ω), ε_{eff} is the effective relative dielectric constant, *h* is the dielectric height, *w* is the conductor strip width.

For $w/h \le 1$:

$$\varepsilon_{eff} = \frac{\varepsilon_r + 1}{2} + \frac{\varepsilon_r - 1}{2}\left[\left(1 + \frac{12h}{w}\right)^{-0.5} + 0.04\left(1 - \frac{w}{h}\right)^2\right] \tag{2.2}$$

and for $w/h \ge 1$:

$$\varepsilon_{eff} = \frac{\varepsilon_r + 1}{2} + \frac{\varepsilon_r - 1}{2}\left(1 + \frac{12h}{w}\right)^{-0.5} \tag{2.3}$$

where ε_r is the relative dielectric constant. The equations for ε_{eff} are accurate to within 1% for:

$\varepsilon_r \le 16$ (< 2% error ε_r >16)

$0.05 \le w/h \le 20.0$ (< 2% error w/h <0.05)

The thickness of the trace *t* can be corrected for by relating it to an equivalent change in the width (Δw) using the following equation:

$$\frac{\Delta w}{t} = \frac{1}{\pi} \ln \left[\frac{4e}{\sqrt{\left(\frac{t}{h}\right)^2 + \left(\frac{\frac{1}{\pi}}{\frac{w}{t} + 1.1}\right)^2}} \right] \quad (2.4)$$

The error in Z_0 is less than 2% for any ε_r and w.

The minimum width of the ground plane and the dielectric layer (T) should be more than the width of the trace (w) to minimize the effect on Z_0 and ε_{eff}. The effect is a function of frequency. At DC, the ground current will be spread equally through the ground cross-section; however, as frequency increases, it will concentrate into a strip directly below the microstripline. The ideal ratio is $T/w \geq 2$.

2.1.2 Microstripline plasma source

Bilgic et al. [9-10] have designed a miniature plasma source using microstrip technology. The microstrip plasma source (MSP) basically consists of a planar microstripline on fused silica used as the dielectric substrate and a massive copper ground plate which also serves as a heat sink. The microstrip transmission lines are designed for about 50 Ohms wave impedance without the plasma. The plasma-gas channel(s) are inside the dielectric substrate below the microstripline with a cross section of 1 mm^2. The plasma is encapsulated within the dielectric, and is not affected and contaminated by the surrounding atmosphere. A stable argon plasma can be achieved for a gas flow range of 50 – 1600 ml min^{-1} at a microwave forward power of 10 – 40 W. When the plasma gas is very low, no homogeneous plasma is formed in the MSP device but some small stable discharges between the two edges of the gas channel close to the electrodes can be observed. When increasing the Ar gas flow, these discharges start to overlap in the direction of the gas flow and to form one plasma, which homogeneously fills the whole discharge channel cross section.

2.2 Plasma diagnostic techniques

There are many different methods for measuring the plasma parameters. The diagnostic techniques which are presented here deal with the measurement of the microwave energy density, gas temperature, electron temperature, and charge density. Those discharge characteristics are considered to be the important features that can describe the nature of a discharge. The most commonly used diagnostic techniques are Optical Emission Spectroscopy and Langmuir probe diagnostics.

2.2.1 Optical emission spectroscopy

Optical Emission Spectroscopy (OES) analyzes the spectrum of light (photons) emitted by the species in the plasma. One of the simpler applications of OES is species identification, because different atoms or molecules emit different wavelengths in the spectrum. The OES can also provide semi-quantitative information on the concentration of the species. In this research, however, species and its concentration are provided as the input parameters.

The OES is also able to measure the translational temperature from a Doppler-broadened discharge. Broadening arises from the Doppler shift caused by thermal particle motion giving rise to the line profile. However, the perturbation of rotational energy levels by molecular collisions (pressure broadening) becomes the limiting factor for the line resolution.

For a molecule which has quantum states of rotation, rotational temperature can be measured for the emission spectrum. A number of experiments investigating the rotational temperature of hydrogen [11, 12] and nitrogen [4, 13, 14] discharges have been found in the literature. This technique is used in this research to obtain the gas temperature of the discharge. The detailed description of this diagnostic is presented in section 5.2

The electron density in a discharge can be measured by observing the Stark effect using an OES system [3, 15]. The Stark effect phenomenon occurs when an emitting species is in an electric field. An experiment to obtain the electron density from the Stark effect is explained in section 5.3.

2.2.2 Langmuir probe diagnostics

A Langmuir probe is a metal probe inserted into a discharge. The probe is usually small; therefore, the perturbation to the discharge is minimal. The concept of probe diagnostics is that a bias voltage is applied to the probe to collect the electron or ion current. Common configurations for the probe diagnostic includes: a single Langmuir probe, a double Langmuir probe, and an emissive probe. The electron temperature, electron density, discharge floating potential, discharge potential, and electron energy distribution function of a discharge can be identified using the single Langmuir probe configuration. However, this configuration needs a ground electrode in the discharge.

If there is no well-defined ground electrode in the discharge, as in the microstripline plasma source developed in this research, the double probes or emissive probe configurations are used to do the diagnostics. The double Langmuir probes can identify the electron temperature and electron density. Thus, the double probe configuration is used in this research. A detailed discussion of the double Langmuir probe diagnostics for the discharge generated using microstripline coupling structure can be found in chapter 6.

Chapter 3

Equipment and Experimental Methods

3.1 Introduction to equipment

This chapter describes the features of the miniature plasma source apparatus. In the first section, the testbed system is explained, including the microwave system and gas/vacuum system. The microstripline coupling structures' design are explained in detail in section 3.3.

The equipment setup for measurements and characterizations of the discharges are also described in this chapter. There are two techniques used in these experiments, Optical Emission Spectroscopy (OES) and Double Langmuir Probes (DLP) Diagnostics.

3.2 Plasma reactor system

3.2.1 Introduction

The system used for the experiment can be divided into three main parts; they are the microwave system, the gas/vacuum system, and the microstripline coupling structure.

3.2.2 Microwave system

Microwave energy is supplied by a 2.45 GHz Opthos Instrument, Inc. microwave power supply which has an operating power range from 1 Watt to 120 Watts. The actual output power from the power supply was calibrated using a

simple test circuit, as shown in figure 3.1. The reading from the Opthos power supply was compared to the reading from the power meter. The power meter was connected to the -10 dB directional coupler. A directional coupler has an input port, an output port, and a sampling port. 10 dB of the signal from the input port goes to the sampling port, whereas the rest of the signal goes to the output port. The reverse transmission from the output port to the input port of the directional coupler is lossless. The signal from the directional coupler was further attenuated by a proper attenuator to maintain the signal at the power meter range. A calibrated directional coupler and attenuator were used in this setup. The forward line of the directional coupler was connected to a dummy load. Microwave power coming from the attenuator was detected by a HP 432 power meter. The conversion of the power meter reading by the microwave power supply and the actual output power is given in table 3.1.

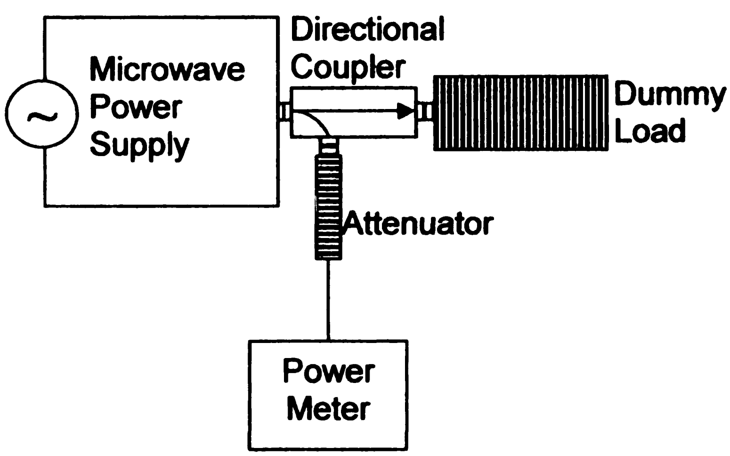

Figure 3.1 Schematic of the test circuit to calibrate the microwave power supply

Table 3.1: Conversion of Opthos microwave power supply output power reading to the actual output power

Opthos (W)	Actual (W)	Opthos (W)	Actual (W)
2	1.5	30	19
4	2.6	40	25.6
5	3.2	50	33
6	3.5	53	35.3
8	5.2	60	40.5
10	6.4	70	49
12	7.4	80	57.1
14	8.8	90	65.6
16	10	100	74.1
18	11.2	104	77.6
20	12.8	110	82.7
23	14.6	120	91.2
24	15.2		

The microwave circuit is designed to have a characteristic impedance of 50 ohms. The circuit includes a CT-3695-N UTE Microwave three port circulator, a 50 ohms Thermaline Coaxial resistor model 8085 as the dummy load, two Narda model 3003-10 coaxial directional couplers, three feet and six feet coaxial cables with N-type connectors, a HP 432A power meter, a General Radio Type-874 20 cm adjustable stub, and attenuators.

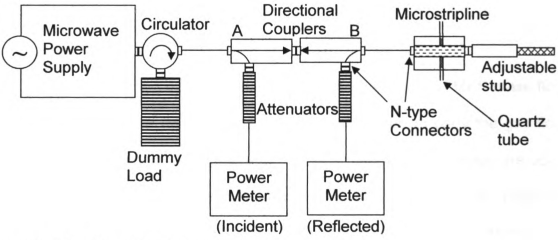

Figure 3.2 Schematic of the Microwave system

The configuration of the microwave circuit is shown in figure 3.2. The circulator transfers the microwave energy from the microwave power source into the system. A dummy load connected to the circulator is used to protect the power supply by absorbing the reflected microwave signal from the system.

Two directional couplers were used in this system to measure the incident power and the reflected power. The input port of the directional coupler (A) was connected to the circulator via a 3-feet coaxial cable. The directional coupler (B) was connected in reverse to the directional coupler (A) in order to measure the reflected power from the microstripiline. The power meters were connected to the sampling ports of each directional coupler. The signals coming from the sampling ports were reduced by 40 dB attenuators to meet the operating range of the meter. The total attenuation of the reflected power is measured to be -47.5 dB.

The other end of the microstripline is connected to an adjustable stub which is used to tune the microwave energy so that the maximum amplitude of the standing wave in the microstripline is in the vicinity of the quartz tube. The details of microstripline structure will be discussed in section 3.3.

3.2.3 Gas/vacuum system

Gas flow into the discharge tube is controlled through an MKS mass flow controller. Plastic hose with a diameter of ¼ inch is used to carry the gas flow between gas/vacuum system apparatus. Various discharge tube sizes are used in this experiment. Discharge pressure is monitored by a HEISE pressure monitor. The pressure monitor is connected to the plastic hose line between the quartz tube and the vacuum chamber using a T-branch Swagelok connector. The vacuum chamber/pump apparatus used for lowering the discharge pressure has been described elsewhere [12].

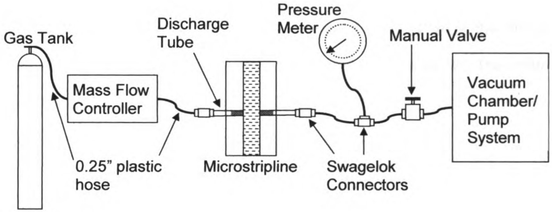

Figure 3.3 Schematic of the gas/vacuum system

There are two ways to control the gas/discharge pressure: first by using the MKS Pressure controller which is embedded into the vacuum chamber/pump and, second, by adjusting the manual valve opening. The MKS pressure controller is used for low pressure (1 – 100 Torr) experiments due to the ease of controllability. For pressure higher than 100 Torr, the manual valve opening is adjusted to obtain a desired pressure in the discharge tube.

3.3 Microstripline design

Plasmas were generated by applying a high electric field via the microstripline into the feed gases which flow inside the discharge tube. The discharge tube is orientated perpendicular to the stripline conductor. Two discharge tube placement designs were investigated. In the first design, the tube was placed between the microstripline and the ground plane (Figure 3.4) and in the second design, the tube was placed across a gap in the microstripline (Figure

3.6). The inner conductors of two N-type connectors were soldered to the copper line and outer conductors were screwed onto the aluminum ground plane. A Teflon plane was placed on top of the ground plane as the dielectric medium. The structure's dimensions have been calculated so they meet the 50 ohms impedance matching requirement as discussed in chapter 2. The material characteristics and dimension are listed in table 3.2.

Table 3.2 Dimension of the microstripline coupling structure

Materials	Length (mm)	Width (mm)	Thickness (mm)	ε_r
Copper	102	12	1	
Teflon	102	50	3.3	2.1
Aluminum	102	50	10	

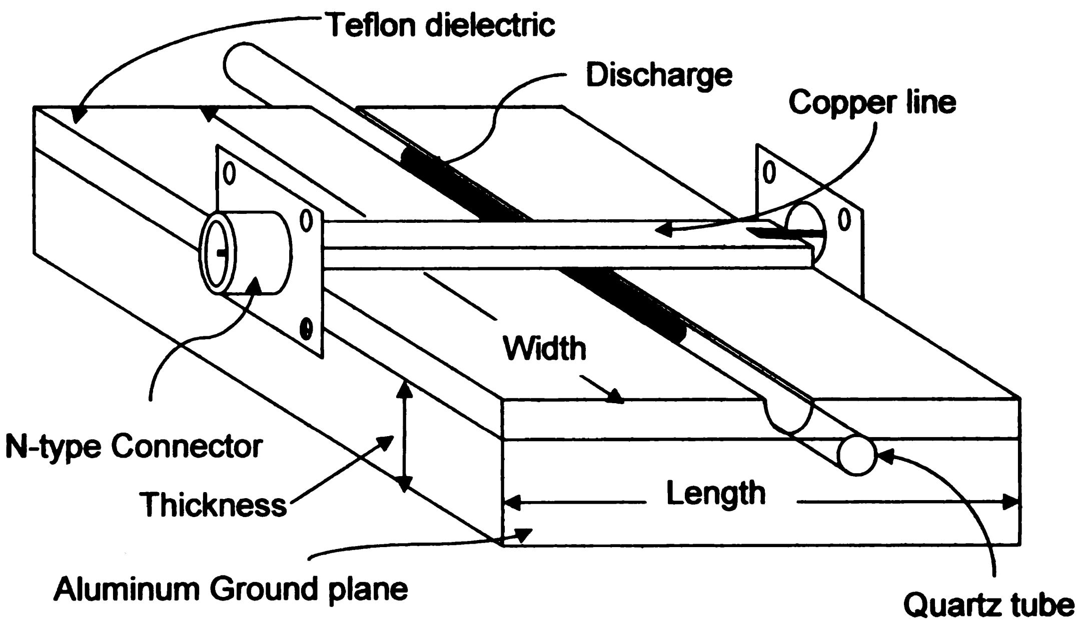

Figure 3.4 Microstripline coupling structure with discharge tube placed underneath the copper line

3.3.1 Microstripline coupling structure #1

Microstripline coupling structure #1 as shown on figure 3.4 and 3.5 was the first system that was used in the experiment. In this applicator, discharge tube was placed in between the copper and the aluminum ground plane. The tube was orientated perpendicular to the microstripline.

Transmission efficiency was measured by calculating the energy loss along the transmission line. A low power 2.45 GHz frequency generator was used to supply 1 Watt of microwave energy into the transmission lines without the discharge (empty load). The microwave circuit configuration in figure 3.2 was modified to measure the transmission efficiency. The microstripline structure together with the adjustable stub was replaced with a power meter. The efficiency of the transmission line using this configuration was 74%. However, when the microstripline structure was added to the circuit, the transmission efficiency was dropped to 45%. This indicated that the microstripline coupling structure is a lossy media or a microwave reflecting structure. Nevertheless, since a plasma is a power absorbing medium, it changes the matching conditions. The transmission efficiency was assumed to be higher than the empty load measurement. The approximation of power transmitted into the discharge is 59% of the input power.

Microwave power absorbed by the discharge can be calculated using the following formula:

$$Pabs = (Pinc \times 59\%) - (Pref \times 56{,}300) \quad \text{(Watts)} \qquad (3.1)$$

Where P_{inc} is the actual power coming from the Opthos microwave power supply, 59% comes from the approximation of the transmission efficiency, P_{ref} is the reflected power reading from the power meter and 56,300 comes from the -47.5 dB attenuators.

Microstripline structure #1 was used in a number of experiments to determine the discharge characteristics. A variety of discharge tube sizes can be used as long as the dimension of the outer diameter of the tube does not exceed the thickness of the Teflon dielectric layer, which is 3.3 mm. Thus a quartz tube with an inner diameter (i.d.) of 2 mm and an outer diameter of 3 mm can be used in the experiments. Optical emission spectroscopy and double Langmuir probes diagnostic were performed using microstripline structure #1 with a 2 mm i.d. discharge tube. In addition to the 2 mm i.d. tube, a 1 mm i.d. discharge tube was also utilized in discharge volume and power density measurements.

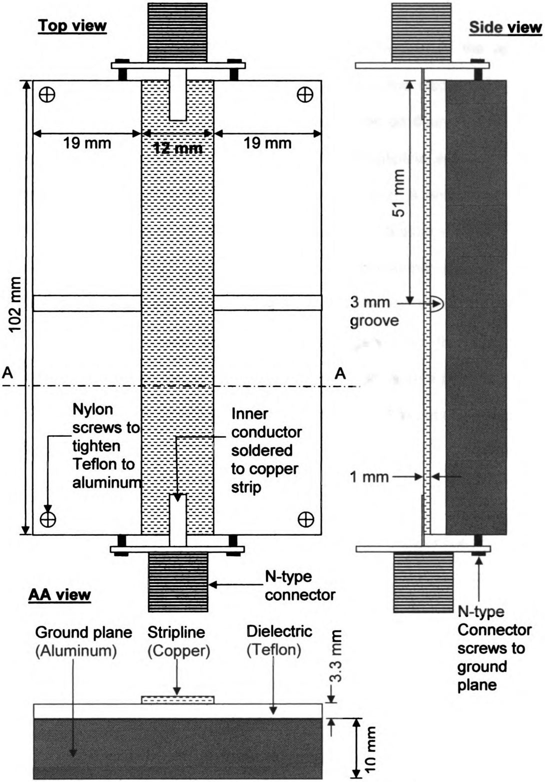

Figure 3.5 Two dimensional view of the Microstripline coupling structure

3.3.2 Microstripline coupling structure #2

Microstripline coupling structure #2 is a modification of the applicator mentioned in the previous section. In this applicator, the discharge tube was placed across a gap on the copper stripline as shown on figure 3.6. The other parts of the structure remain the same as the microstipline structure #1. The advantage of the structure #2 is that the dielectric layer is uniform across the plane. Thus, the characteristic impedance of the microstripline is not far off from the calculated value. However, the gap on the copper stripline promotes a big radiation leak and a lot of the microwave power reflected back into the circuit before the plasma is ignited. Once the plasma is generated, the radiation leak and the reflected power are greatly reduced. This is because a plasma acts as a conductor therefore the gap on the conducting microstripline acts as a microwave energy absorbing load.

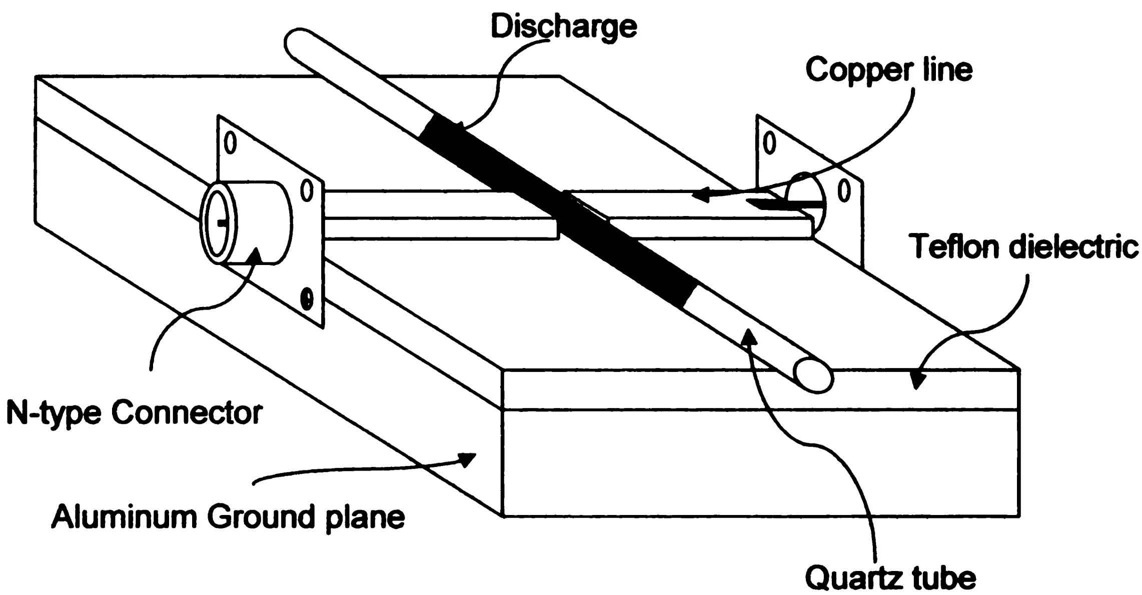

Figure 3.6 Microstripline coupling structure with discharge tube placed across a gap in the copper line

3.4 Optical Emission Spectroscopy setup

Some of the discharge characteristics were obtained using the Optical Emission Spectroscopy technique. In this subsection, the setup and equipment descriptions for OES measurements are explained.

3.4.1 Spectrometer system

The spectrometer used for all of the OES measurements was a McPherson Model 216.5, 0.5 meter, f/8.7, plane grating monochromator. The grating has 2400 grooves/mm designed to operate in the wavelength range of 1050 Å – 5000 Å. The entrance slit and the output slit were set at 20 μm wide.

The principle of operation of the monochromator is diffraction. The grating inside the monochromator diffracts the incoming light and the angle of diffraction varies with the wavelength. Hence, at any given time, only diffracted light at particular wavelength comes out to the exit slit. Choosing a specific wavelength can be done by rotating the diffraction grating about the axis at a specific angle.

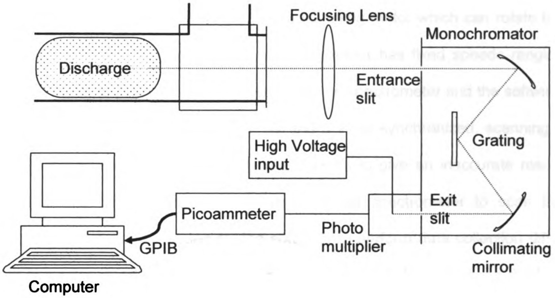

Figure 3.7 Schematic of the Optical Emission Spectroscopy measurement

3.4.2 Optic collection

The optic signal was collected at the end of the cylindrical discharge, thus data taken were the average over the whole length of the discharge. In order to see the discharge at the end of the tube, one of the ports in a T-shape Swagelok tube connector was modified to become a viewing window by attaching a 1 mm thick glass using epoxy. The other two ports in the connector served as a regular connection for gas flow. Distance between the discharge and the viewing window was kept as close as possible to minimize the signal loss. A biconvex lens with the focal length of 5 cm was used to focus the optic signal into the entrance slit of the monochromator. A black cloth was used to cover the path between the viewing window and the monochromator in order to block the ambient light, thus enhancing the signal-to-noise ratio.

3.4.3 Data collection

The McPherson spectrometer has a scanning motor which can rotate the grating to scan the wavelength. The scanning motor has fixed speeds ranging from 0.5 Å/min to 2000 Å/min. However, since the spectrometer and the software for data collection are run independently and are not synchronized, scanning a wide spectrum using a low scanning speed tends to give an inaccurate result. This happens because the time it takes for the spectrometer to scan the spectrum and the time needed for the software to perform data collection differ by a few milliseconds. Thus, a fix scanning speed of 5 Å/min to scan 50 Å of spectrum was chosen to get a maximum result in the spectrum quality factor without noticeable offset.

The McPherson spectrometer houses an EGI-GENCOM RPI QL/20 photomultiplier tube (PMT). The PMT converts light signals into electrical signals. A bias voltage of -900 V is applied to the PMT from the ORIEL 70705 High Voltage Supply. The output current from the PMT is detected by a Keithley 6485 picoammeter. The picoammeter is connected to a computer by an IEEE-488 (GPIB) interface. The GPIB bus is connected to a National Instrument GPIB card installed in the computer. A Quick BASIC program is used to record the signals at the desired interval. The software code is included in appendix B. The recorded data is then analyzed in Microsoft Excel.

3.5 Double Langmuir Probe setup

3.5.1 Probe

A double Langmuir probe was used to measure the electron characteristics such as the electron density and electron temperature. It is convenient to use the DLP setup over a single Langmuir probe because there is no well-define ground in the plasma created in the glass tube.

Two identical probes are inserted in the discharge with a separation distance of 0.18 mm. The distance between two probes needs to be longer than the discharge sheath (s), which is approximately four times the Debye length (λ_D), as described by [16]:

$$s \approx 4 \times \lambda_D \approx 4 \times 743\sqrt{\frac{T_e}{n_e}} \text{ (cm)} \tag{3.2}$$

where T_e is the electron temperature in eV, and n_e is the electron density in cm^{-3}. Using approximation values of T_e around 2 eV and n_e is in the order of 10^{12} cm^{-3}, the sheath is on the order of a few microns.

The probes were made of tungsten wires with a diameter of 0.1 mm. The length of the wires exposed to the discharge was 1 mm. Silica tubing with outer diameter of 0.33 mm and inner diameter of 0.15 mm was used as an insulator to cover the tungsten wires, with the exception of the tip area.

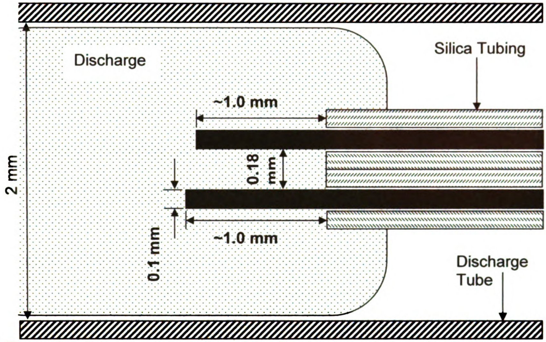

Figure 3.8 Cross sectional view of the Double Langmuir probe tips

3.5.2 Data Collection

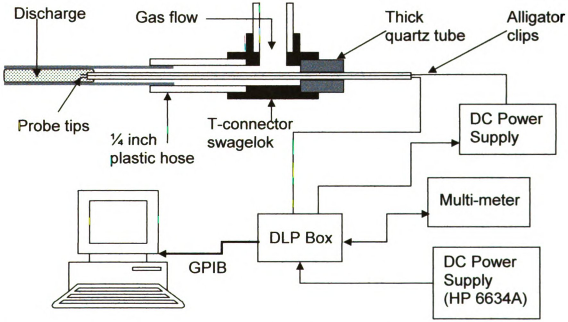

Figure 3.9 Schematic of the Double Langmuir Probe measurement

Shown in figure 3.9 is the system setup for DLP data collection. A DC Power Supply (HP 6634A) delivers potential to the probe via DLP box. The potential is set by a software consisted of a Quick BASIC program to increase from 1 Volt to 100 Volts. Since the I-V characteristic desired is in the range of -50 – 50 Volts, a bias voltage of -50 Volts is supplied by another DC power supply to get the desired voltage range. The current from the probes is recorded by a multi-meter and collected by the computer. The software code is included in appendix C. The recorded data is then analyzed in Microsoft Excel.

Chapter 4

Microstripline Plasma Source Performance

4.1 Introduction

This chapter describes the discharge behavior and its basic characteristics. In section 4.2, the ignition procedure is explained for various gases, pressure, flow rates, and incident powers. Section 4.3 explains the tuning behavior used to attain maximum power coupling into the plasma. Next, the volume of the plasma and the power density measurements are presented. Finally, the behavior of plasma in modified discharge tubes and the behavior of the discharge at atmospheric pressure are presented.

4.2 Ignition Process

The procedure for igniting a discharge in this miniature microwave plasma source is straightforward. First, the mechanical pump was turned on to lower the pressure in the discharge tube. Second, feed gas was delivered into the discharge tube by adjusting its flow rate from the mass flow controller. The third step entailed applying the microwave energy. Prior to conducting the experiment, a low power test was performed on the microwave circuit. The test was performed to check the circuit for radiation leaks that may occur and to calibrate the length of the adjustable stub to achieve a minimum reflected power. Appropriate stub tuning minimizes the reflected power, thus enhancing the performance of the discharge. Plasma acts as a load to the microwave circuit.

The plasma existence changes the impedance of the microwave circuit. Hence, the adjustable stub needs to be re-tuned after the plasma is ignited.

The incident power needed to ignite an argon discharge is around 5 Watts. However, for hydrogen and nitrogen feed gases, around 20 – 30 Watts of microwave power is needed to ignite the plasmas. The suitable pressure to ignite those discharges is around 1 – 3 Torr. An aluminum mesh was used as a microwave screen to enclose the microstripline coupling structure to prevent microwave radiation. Once the microwave system and gas/vacuum system were set, a high voltage spark from a tesla coil was applied to the discharge tube to ignite the plasma.

For argon feed gas, the discharge can be ignited in the pressure range from 1 Torr up to 300 Torr. Higher incident power are needed to ignite the plasma as the pressure increases.

Table 4.1 Operating condition for igniting argon discharge in 2 mm diameter tube.

Incident Power (Watts)	Flow Rate (sccm)	Maximum Pressure (Torr)
6.4	25	50
10	25	80
10	35	100
12.8	25	200
19	25	300

4.3 Tuning behavior

Transmission line impedance matching for this system was done by using a 20 cm single stub tuner. The operating frequency of the microwave system was 2.45 GHz. The microwave energy creates a standing wave in the microstripline and the adjustable stub. The stub was used to tune the standing wave so that the maximum electric field was at the discharge tube as shown in figure 4.1.

The medium inside the stub is air. The wavelength of the microwave propagation in air can be found using the following:

$$\lambda_g = {c}/{f} \qquad 4.1$$

where *c* is the speed of light and *f* is the microwave frequency. As seen in figure 4.2, the distance between the maximum power transfers to the load is at ${\lambda_g}/{2}$ or 6.12 cm.

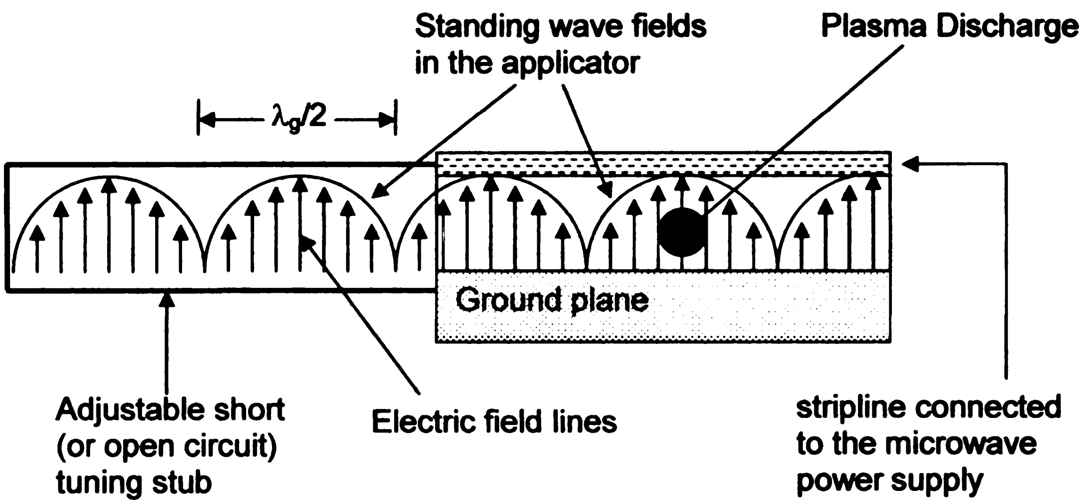

Figure 4.1 Tuning characteristic of the microstripline applicator

Plasma length in figure 4.2 is the length of the plasma expansion in the axial direction (along the tube). The value was obtained by measuring the distance between both ends of the plasma. As seen in figure 4.2, the maximum length is achieved when the absorbed power is at the maximum.

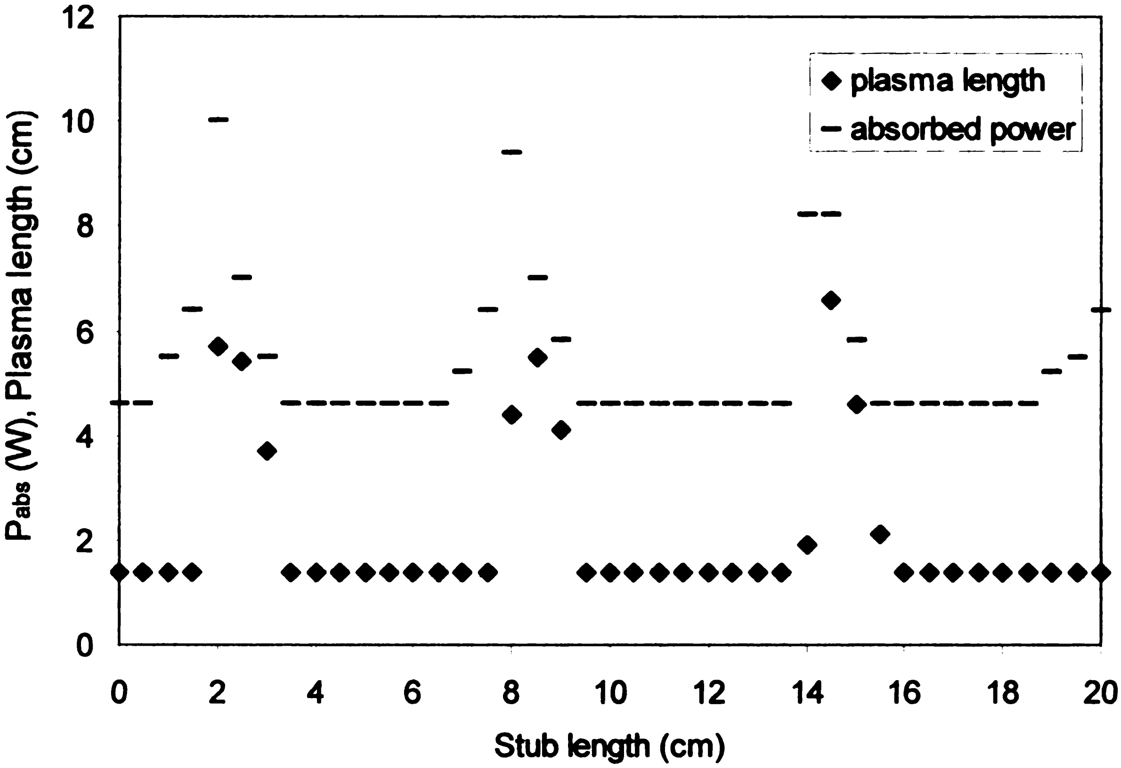

Figure 4.2 Variation of argon discharge length and absorbed microwave power at different stub positions. Discharge diameter: 1 mm, Input power: 13 W, flow rate: 50 sccm, pressure: 20 Torr, Microstripline system #2.

4.4 Volume of plasma

Plasma generated using the miniature microwave plasma source is confined in the radial direction by the tube. The quartz tube prevents the expansion of the plasma other than along the tube length. The plasma length can be adjusted by varying the input power or tuning the adjustable short. Maximum length of a discharge can be achieved when the adjustable short is tuned properly as explained in the previous subsection. Thus, the volume of the plasma is the cylindrical volume that depends on the cross sectional area of the discharge tube used in the system and maximum length of the discharge. The plasma sheath was on the order of a few microns as stated in section 3.5. Thus, the sheath was not incorporated in the calculation and the radius of the plasma was assumed equal to the radius of the tube.

An interesting phenomenon occurred for argon discharge when the power delivered into the discharge was increased. At very low powers the length of the discharge matches the width of the Microstripline. In this condition, the microstripline delivered the power into the discharge in a similar fashion as in the parallel plate system. However, as the absorbed power increases, the discharge expanded along the tube. In this case, in addition to the power transferred into the discharge by a parallel plate, the discharge was maintained by a plasma surface wave that traveled inside the quartz tube along the discharge.

The analysis of the plasma volume was done for the following gases: argon, hydrogen, nitrogen, and a mixture of argon-hydrogen. Parameters that were varied include the microstripline structures, the discharge tube size, the absorbed power, the pressure, and the gas flow rates. All of the experiments that use microstripline structure #2 and use discharge tubes that were 1 mm or less in inner diameter were performed for pure argon gas only.

Some of the experimental results are shown in figures 4.3 – 4.9. A complete data listing for different discharge sizes for power density measurements can be found in appendix D.

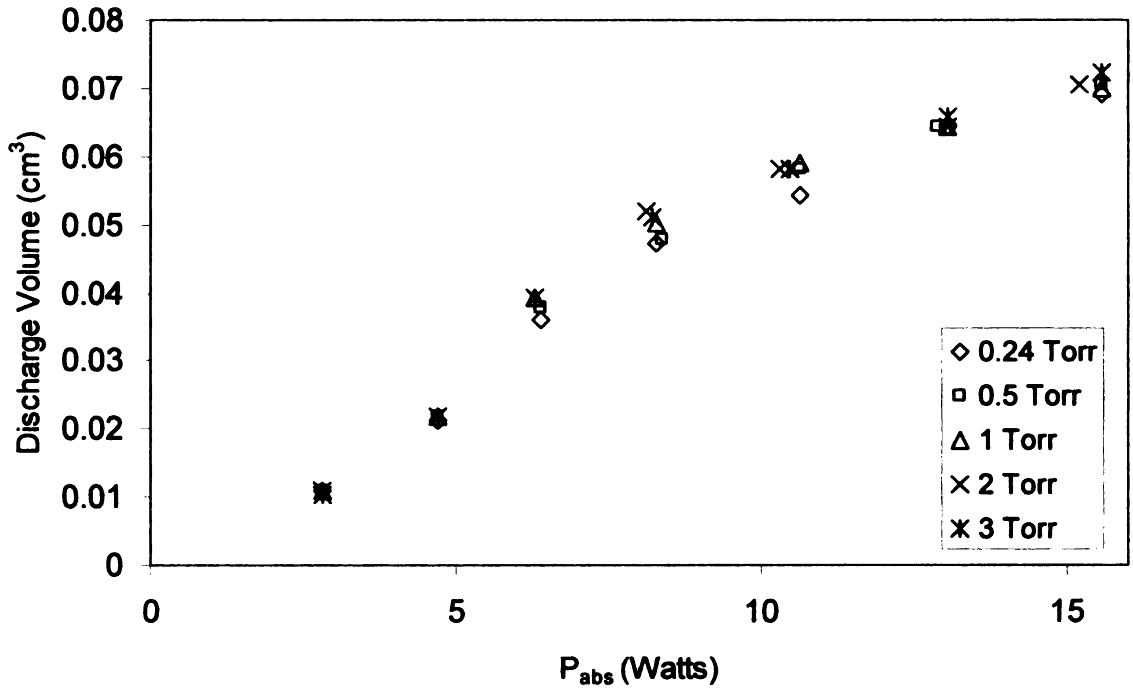

Figure 4.3 Variation of discharge volumes at different P_{abs}. Discharge tube diameter: 1 mm, Pressure: 0.24 – 3 Torr, feed gas: pure argon, flow rate: 20 sccm, microstripline system #2.

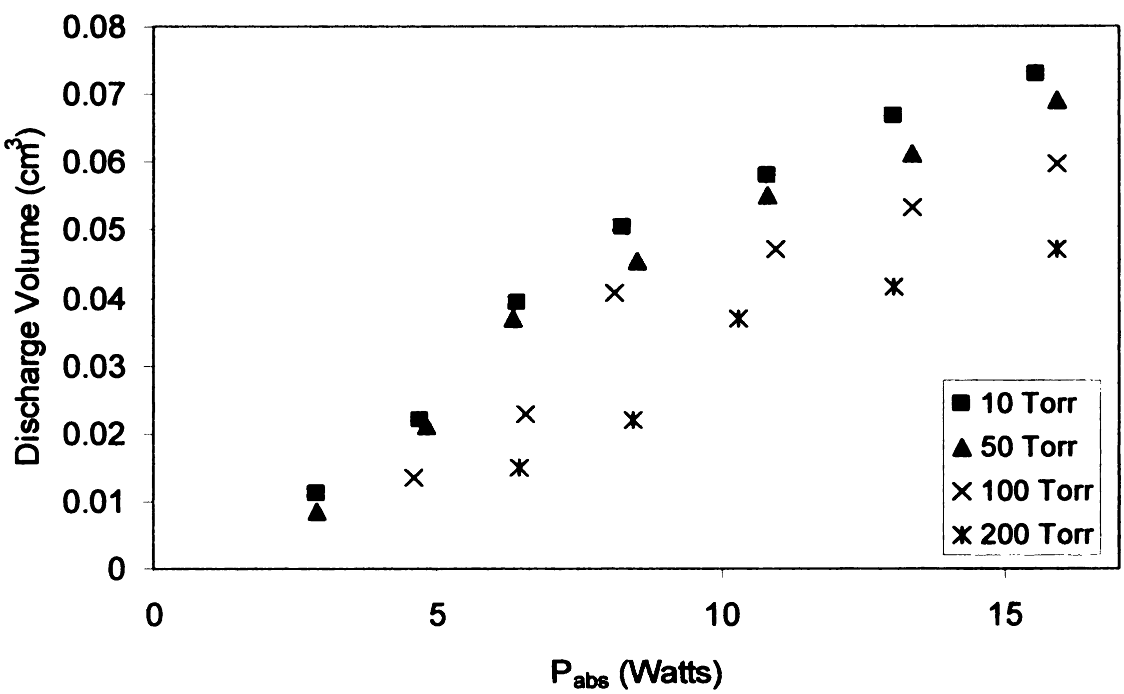

Figure 4.4 Variation of discharge volumes at different P_{abs}. Discharge tube diameter: 1 mm, pressure: 10 – 200 Torr, feed gas: pure argon, flow rate: 20 sccm, microstripline system #2.

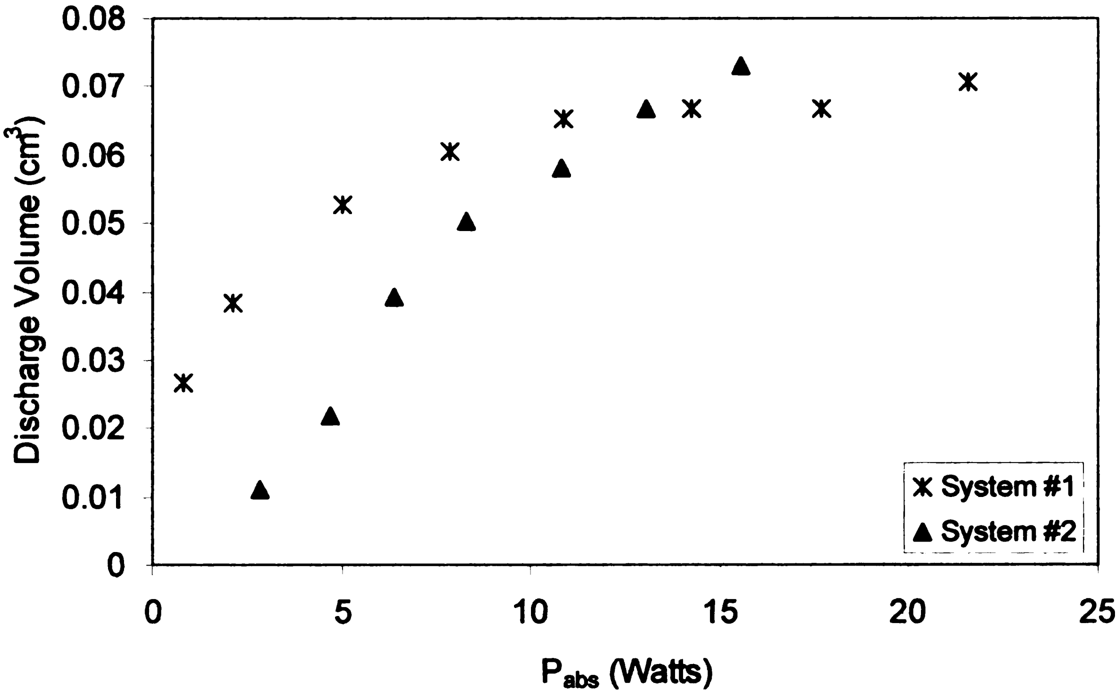

Figure 4.5 Comparison of discharge volume vs. P_{abs} of different microstripline applicators. Discharge tube diameter: 1 mm, pressure: 10 Torr, feed gas: pure argon, flow rate: 20 sccm.

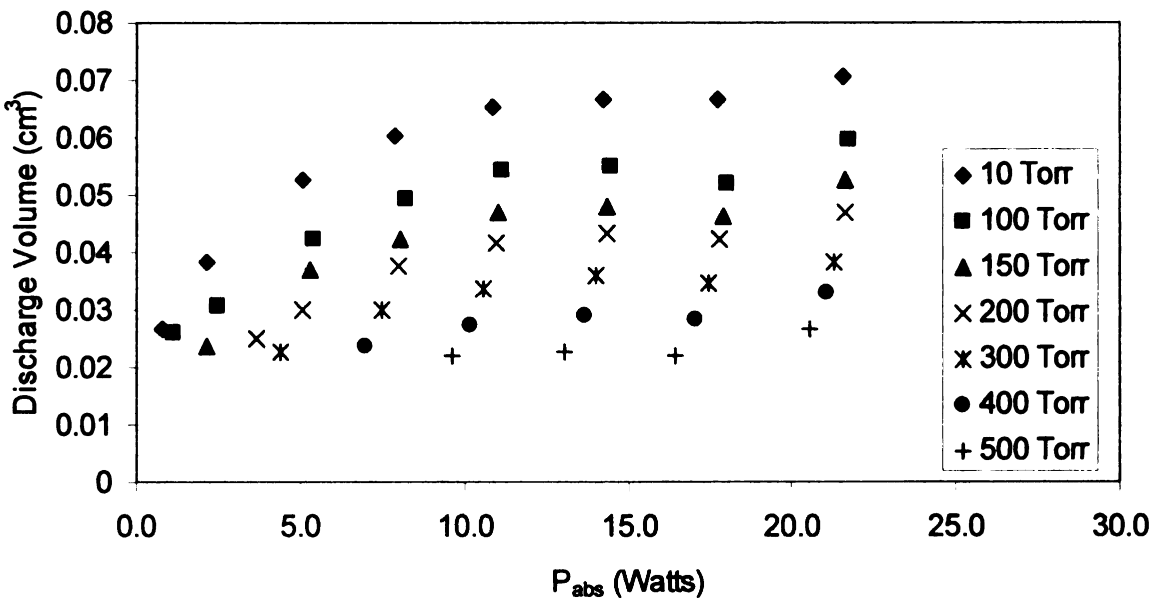

Figure 4.6 Discharge volumes variations at different P_{abs} for argon discharges created using microstripline system #1. Flow rate: 20 sccm, discharge tube size: 1 mm.

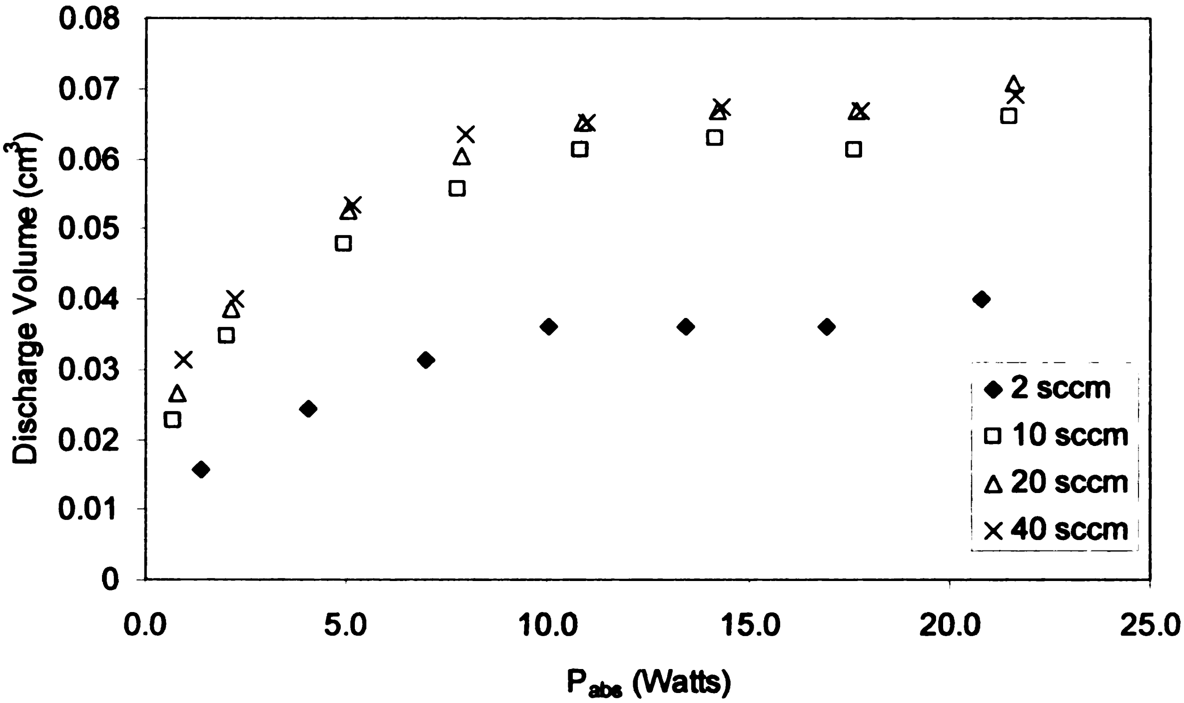

Figure 4.7 Discharge volume variations for different P_{abs} in argon discharges created using microstripline system #1. Pressure: 10 Torr, discharge tube size: 1 mm.

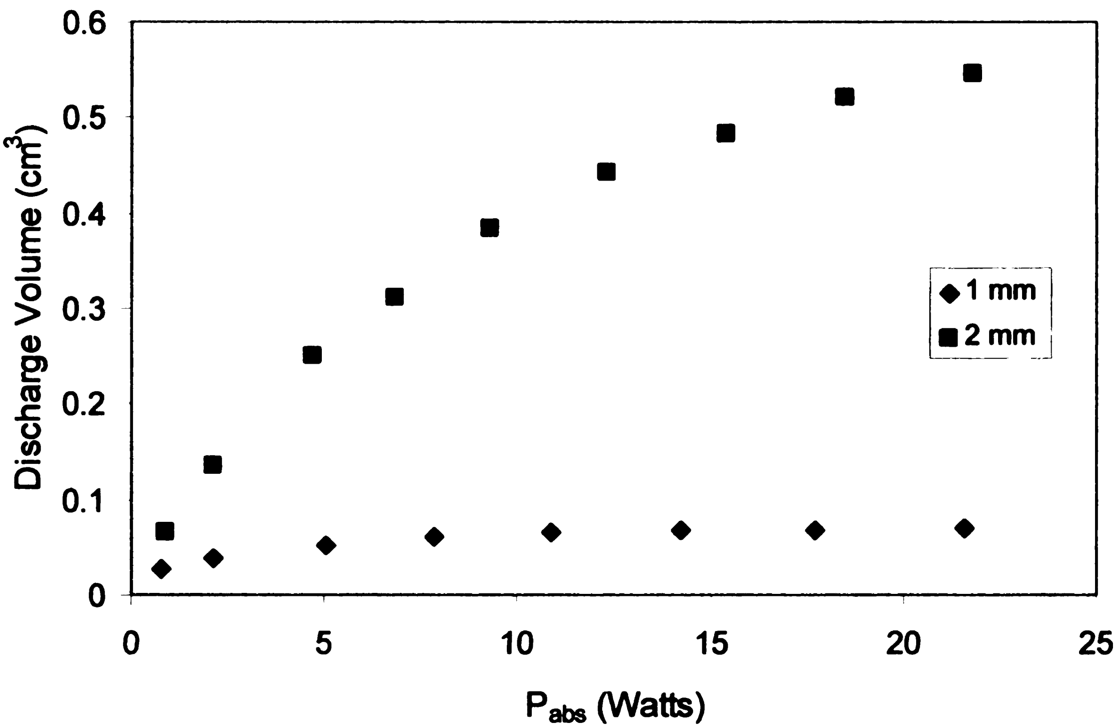

Figure 4.8 Discharge volume variations for different P_{abs} in argon discharges created using microstripline system #1. Pressure: 10 Torr, flow rate: 20 sccm.

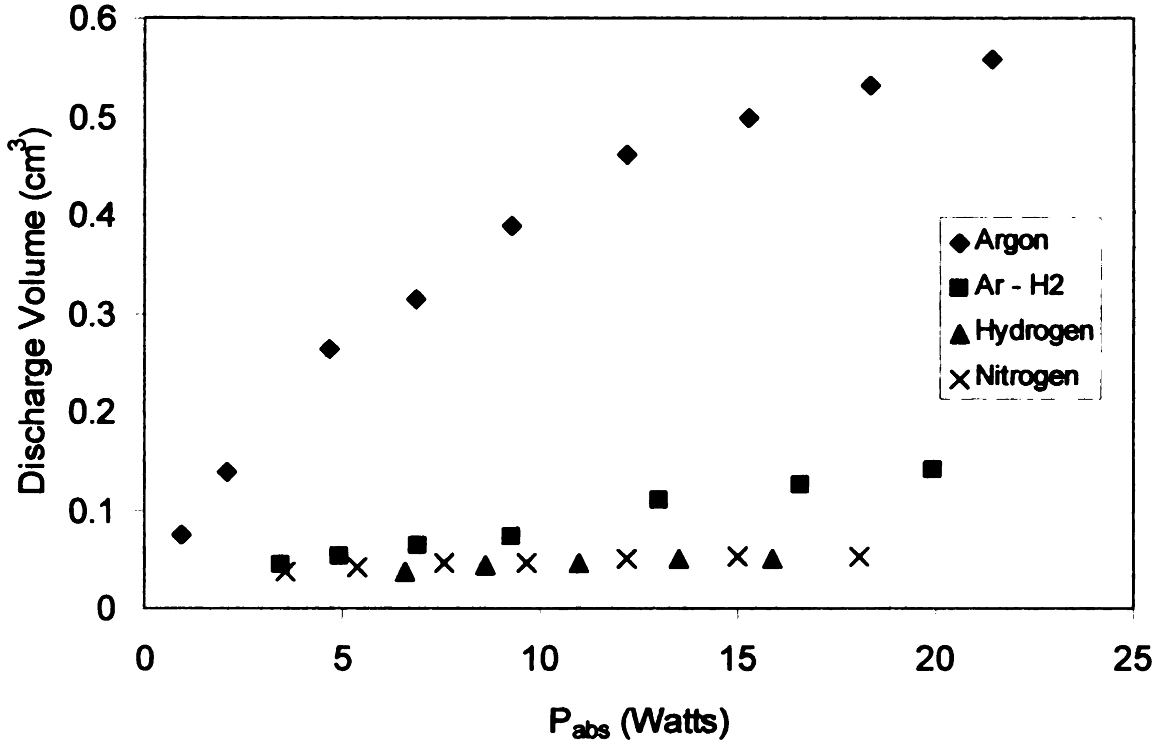

Figure 4.9 Discharge volume variations for different P_{abs} for Ar, Ar-H_2 (95%-5%), H_2, and N_2 created using microstripline system #1. Pressure: 5 Torr, discharge tube size: 2 mm.

From figure 4.3 and 4.4 it is seen that the volume of argon plasma increases as the absorbed power increases. In the low pressure range (0.24 – 3 Torr) the discharge volume shows little variation versus pressure. However, for higher pressure range (10 – 200 Torr), the volume of argon plasma decreases as the pressure increases. The maximum volume for argon discharge, created using microstripline system #2, inside a 1 mm tube, was 0.07 cm^3. A maximum discharge volume can be reached when the pressure is set to 10 Torr or lower and the absorbed power is around 16 Watts.

Figure 4.5 shows a comparison for different microstripline coupling structure designs. It can be seen that, with similar input parameters, system #1 gave a better performance for P_{abs} less than 10 Watts. However, the volume expansion tends to saturate for P_{abs} higher than 10 Watts. On the other hand, discharge volume and P_{abs} have a linear relationship for system #2. The observed argon plasma volume never exceeds 0.08 cm^3 for both systems using 1 mm discharge tube.

Argon discharges created using microstripline system #1 show little variation in their volume for pressures higher than 300 Torr, as can be seen in figure 4.6.

When the flow rate of the gas through the system was varied with the other parameters held constant, a slight decrease in discharge volume was observed with decreasing flow rate in the range 10 – 40 sccm as seen in figure 4.7. However, at 2 sccm, the discharge volume was noticeably smaller compared to the higher flow rate. With higher flow rate, supply of the argon species to the system was higher. Consequently, the volume of the discharge increased as the flow rate increased.

From figure 4.8, it can be observed that argon plasma created inside the 2 mm tube had a bigger volume than those created inside the 1 mm tube. Plasma length can be derived from the discharge volume since the cross sectional areas of both tubes differed by a factor of 4. By investigating the plasma length, it can be concluded that the surface wave maintained discharge is slightly larger for the 2 mm tube.

Figure 4.9 shows that the surface wave excitation was dominant in maintaining the argon discharge, whereas hydrogen and nitrogen discharges showed only a little variation in volume as the absorbed power increases.

4.5 Power density measurement

Power density in Watts per cubic centimeter (W/cm^3) was determined by taking the ratio of the absorbed microwave power and the plasma volume. The total absorbed power calculation has been described in section 3.4, whereas the volume of the plasma is given in section 4.4. All of the absorbed power was assumed to go into creating the plasma.

The analysis of the power density was done for the following gases: argon, hydrogen, nitrogen, and a mixture of argon-hydrogen. Parameters that were varied include the microstripline structures, the discharge tube size, the absorbed power, the pressure, and the gas flow rates. All of the experiments that use microstripline structure #2 and use discharge tubes that were 1 mm or less in diameter were performed for pure argon gas only.

Some of the experimental results are shown in figures 4.10 – 4.16. A complete data listing for different discharge sizes for power density measurements can be found in appendix D.

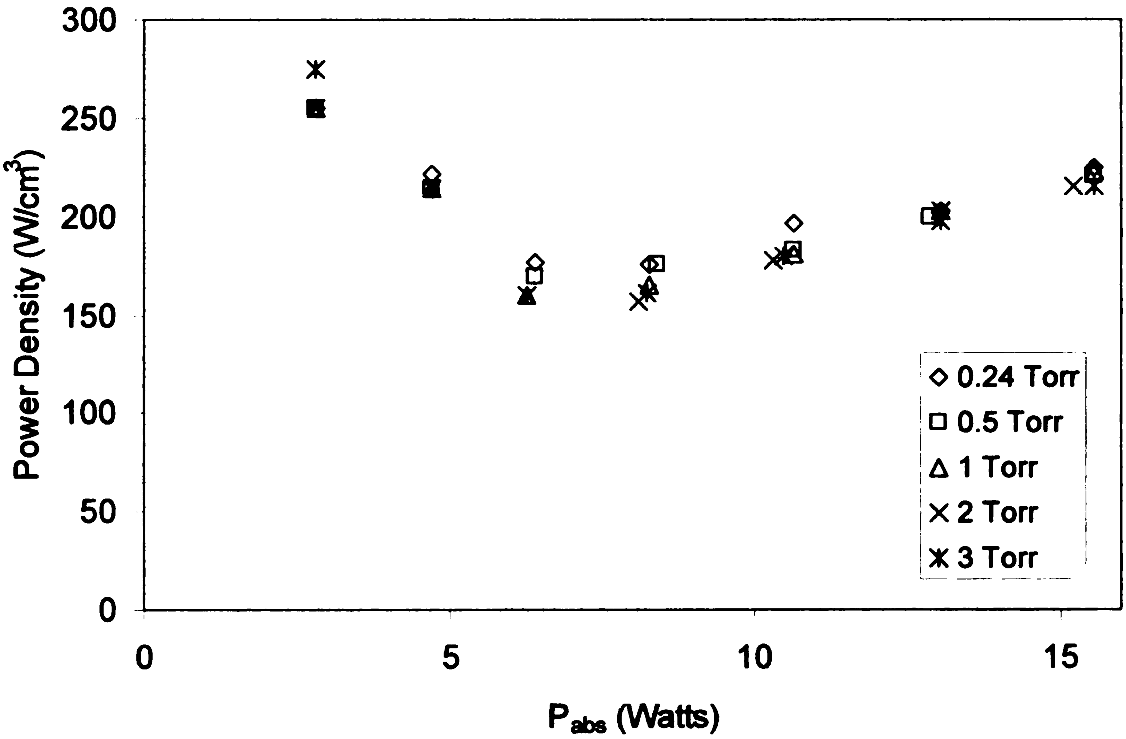

Figure 4.10 Variation of discharge power density at different P_{abs}. Discharge tube diameter: 1 mm, Pressure: 0.24 – 3 Torr, feed gas: pure argon, flow rate: 20 sccm, microstripline system #2.

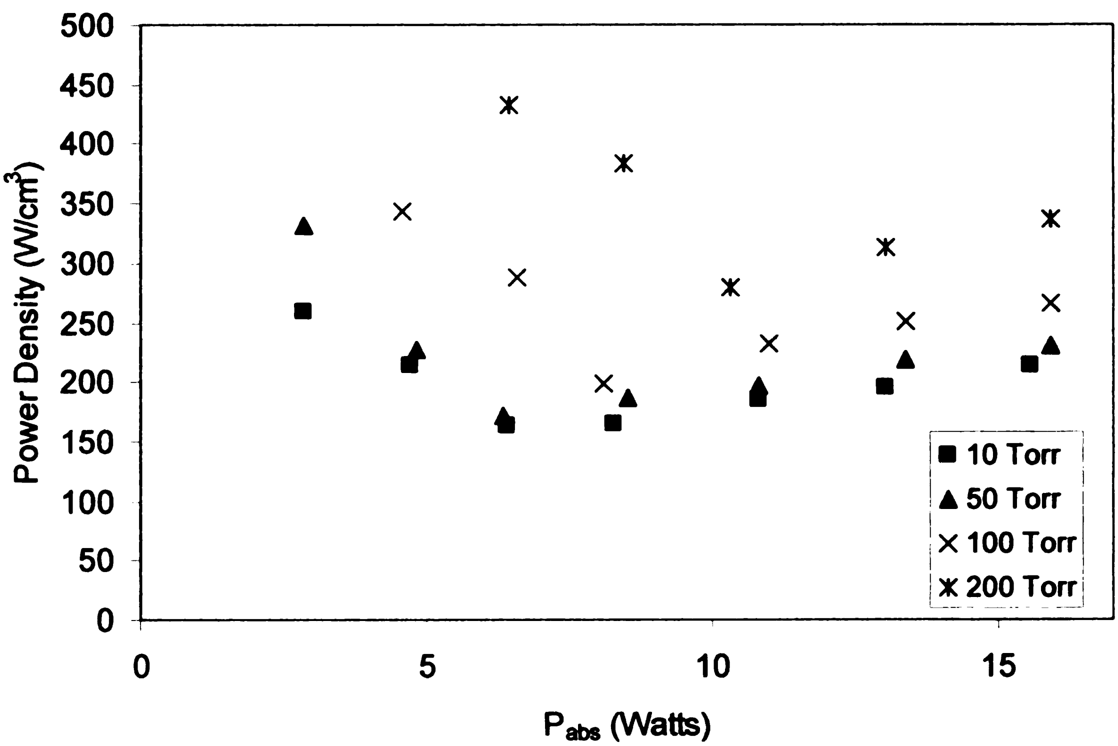

Figure 4.11 Variation of discharge power density at different P_{abs}. Discharge tube diameter: 1 mm, Pressure: 10 – 200 Torr, feed gas: pure argon, flow rate: 20 sccm, microstripline system #2.

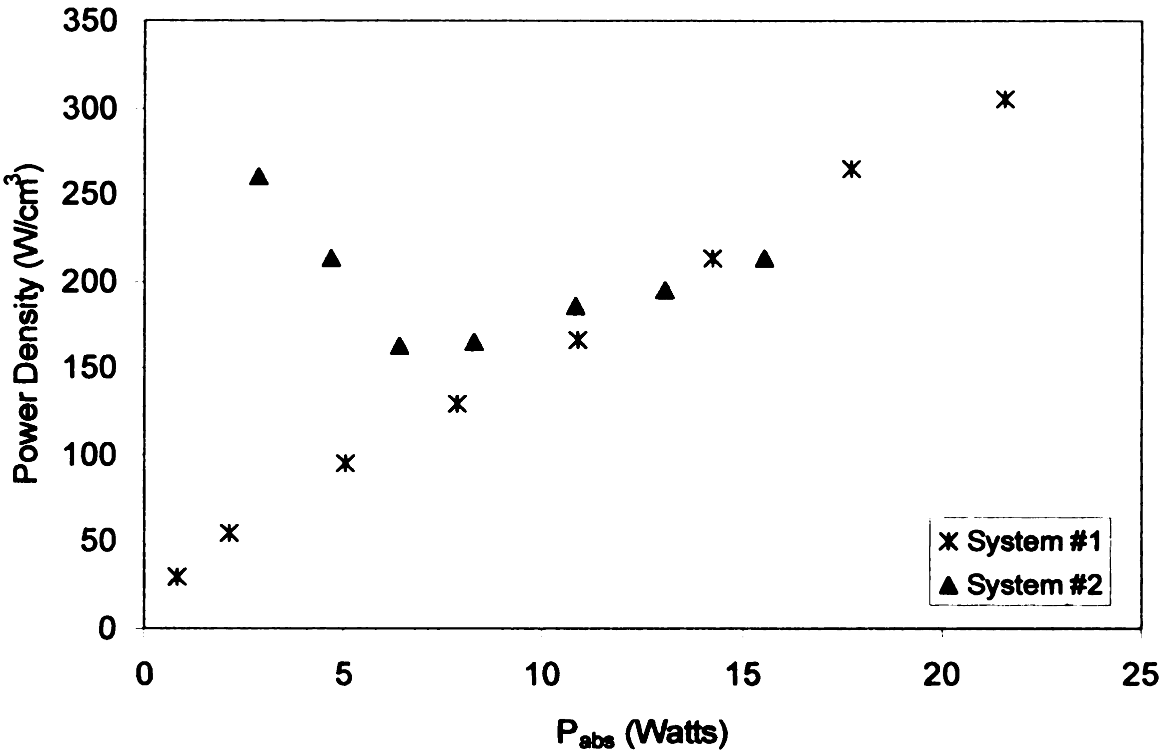

Figure 4.12 Comparison of discharge power density vs. P_{abs} of different microstripline applicators. Discharge tube diameter: 1 mm, pressure: 10 Torr, feed gas: pure argon, flow rate: 20 sccm.

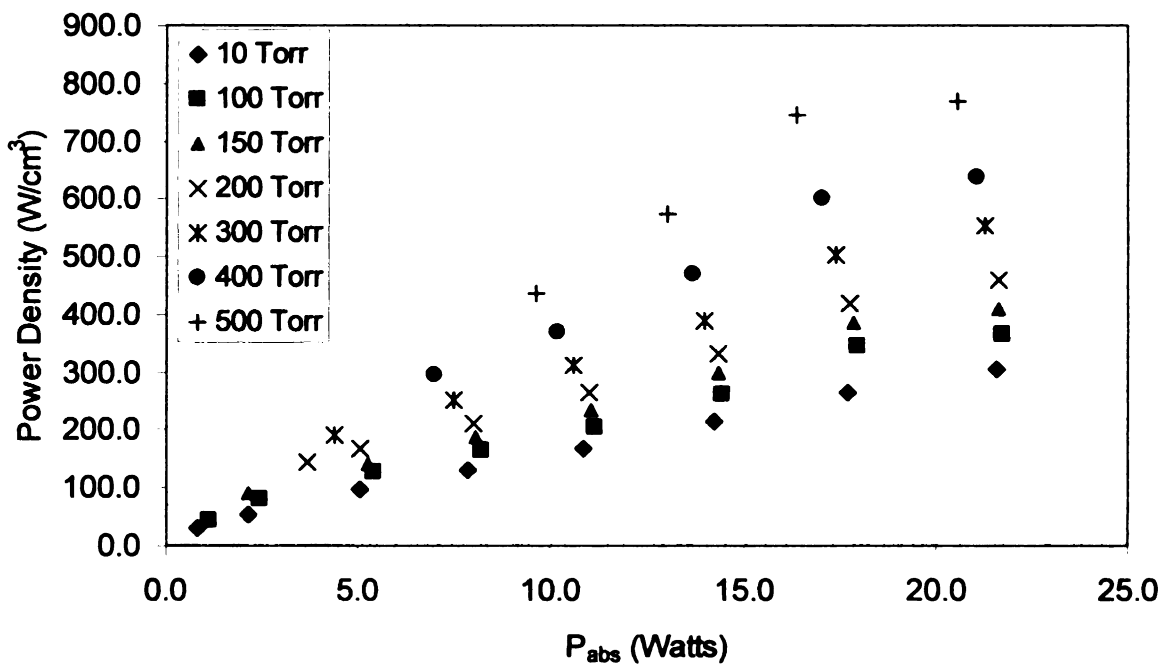

Figure 4.13 Discharge power density variations at different P_{abs} for argon discharges created using microstripline system #1. Flow rate: 20 sccm, discharge tube size: 1 mm.

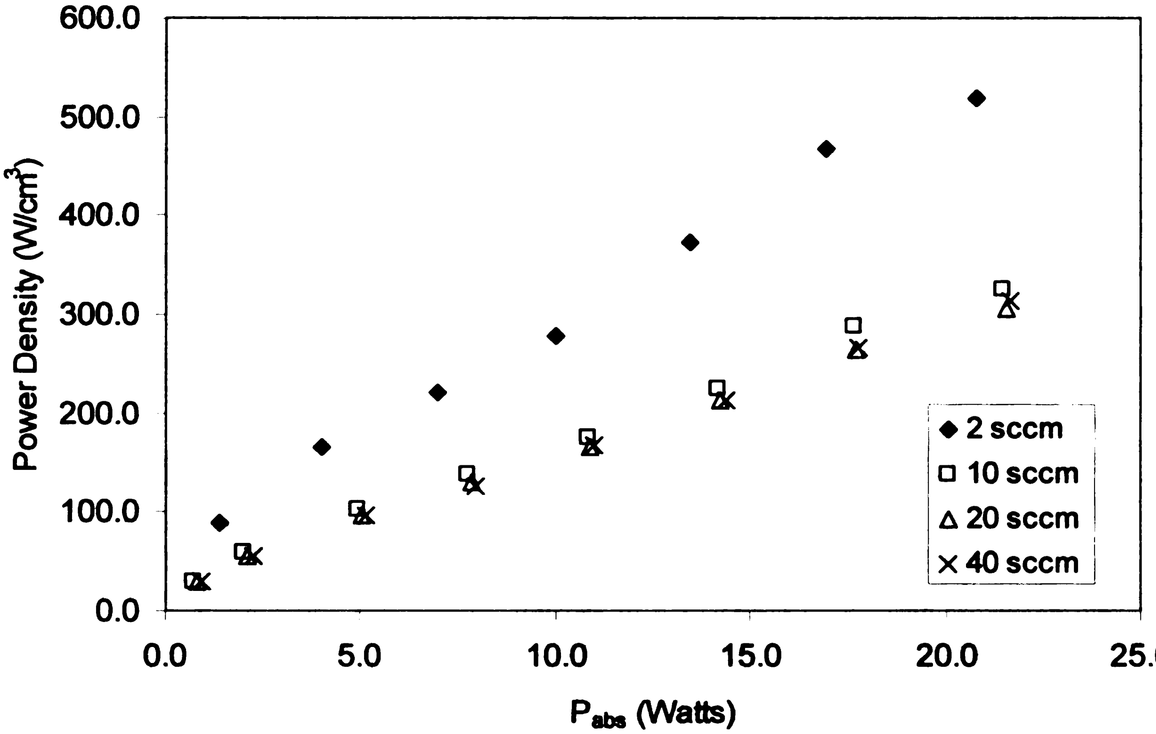

Figure 4.14 Discharge power density variations for different P_{abs} in argon discharges created using microstripline system #1. Pressure: 10 Torr, discharge tube size: 1mm.

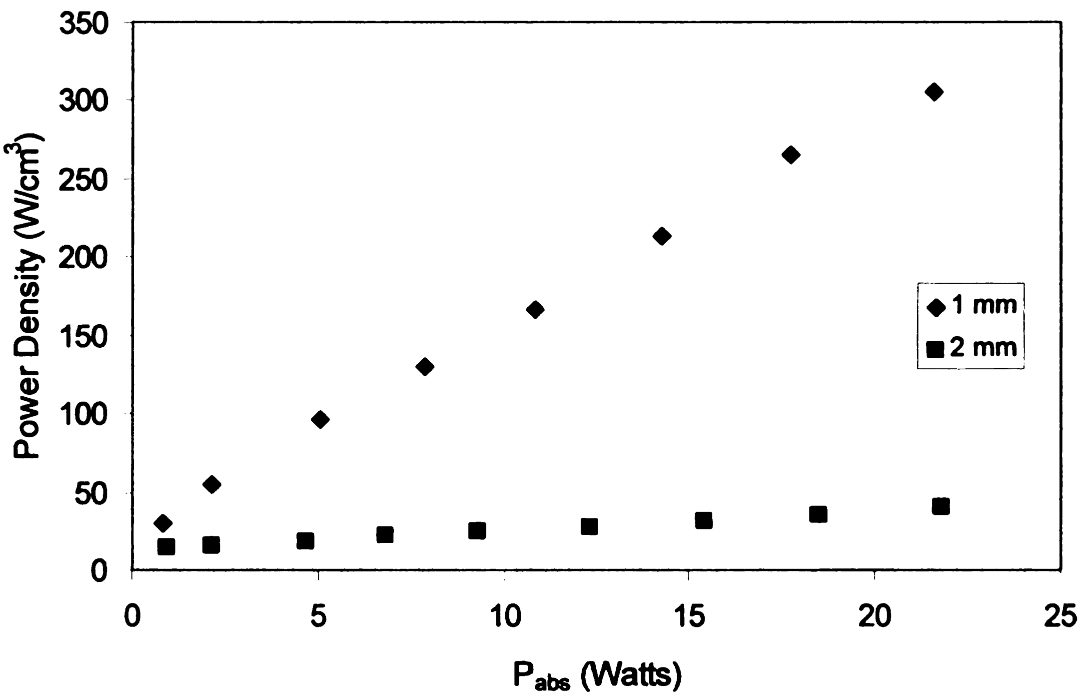

Figure 4.15 Discharge volume variations for different P_{abs} in argon discharges created using microstripline system #1. Pressure: 10 Torr, flow rate: 20 sccm.

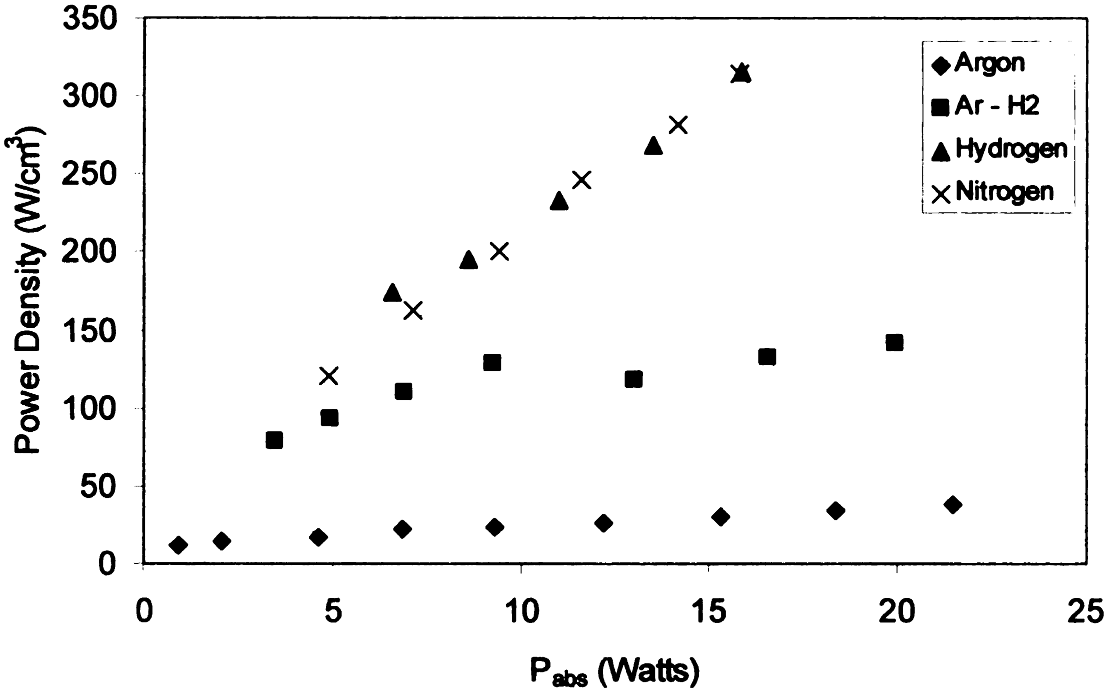

Figure 4.16 Discharge power density variations for different P_{abs} for Ar, Ar-H_2 (95%-5%), H_2, and N_2 created using microstripline system #1. Pressure: 5 Torr, discharge tube size: 2 mm.

From figure 4.10 and 4.11 it is seen that the power density of argon plasma, created using system #2, decreases as the absorbed power increases up to 6 Watts. Power density decreases because the discharge length expands rapidly. However, as the power becomes greater than 6 Watts, the power density increases with P_{abs}. Power density at higher pressure is higher than the lower pressure discharges but the profile is similar.

A linear profile of power density versus P_{abs} can be obtained from system #1, as shown in figure 4.12. Figure 4.13 also shows, for system #1, that the power density increases as both the absorbed power and pressure increase. Low P_{abs} data for high pressure discharges are not available due to the ignition constraint explained in section 4.2.

Figure 4.14 shows that when the flow rate of the gas through the system was varied with the other parameters held constant, a slight increase in discharge power density was observed with decreasing flow rate in the range 10 – 40 sccm. However, at 2 sccm, the discharge power density was noticeably bigger compared to the higher flow rates.

Figure 4.15 shows a comparison of power density for system #1 between 1 mm tube and 2 mm tube. Power density increases faster versus P_{abs} in 1 mm discharges.

Figure 4.16 shows that increase in the absorbed power for hydrogen, nitrogen, and a mixture of hydrogen – argon plasmas generates higher power density discharges. However, for argon plasma, the absorbed power is used to expand its volume rather than increase the power density.

4.6 Discharge branch and loop

The discharge tubes were modified in two ways in order to study the behavior of argon discharges as they expand. The first modification involved creating a branch on the 2 mm quartz tube as shown in figure 4.17. The main line of the discharge tube was connected to the argon gas flow meter and the vacuum chamber using a setup similar to that mentioned in chapter 3. The end of the branch line was terminated using epoxy. The branching point should be kept as close as possible to the copper stripline so that the discharge expansion can reach over it. With enough absorbed power, branching of the argon discharge can be made. The distance between the branching node and the end of the discharge in the branching line (B in figure 4.3) was shorter than the main line

discharge (A in figure 4.3). This may have happened because the pressure in the branching line is relatively higher than in the main line.

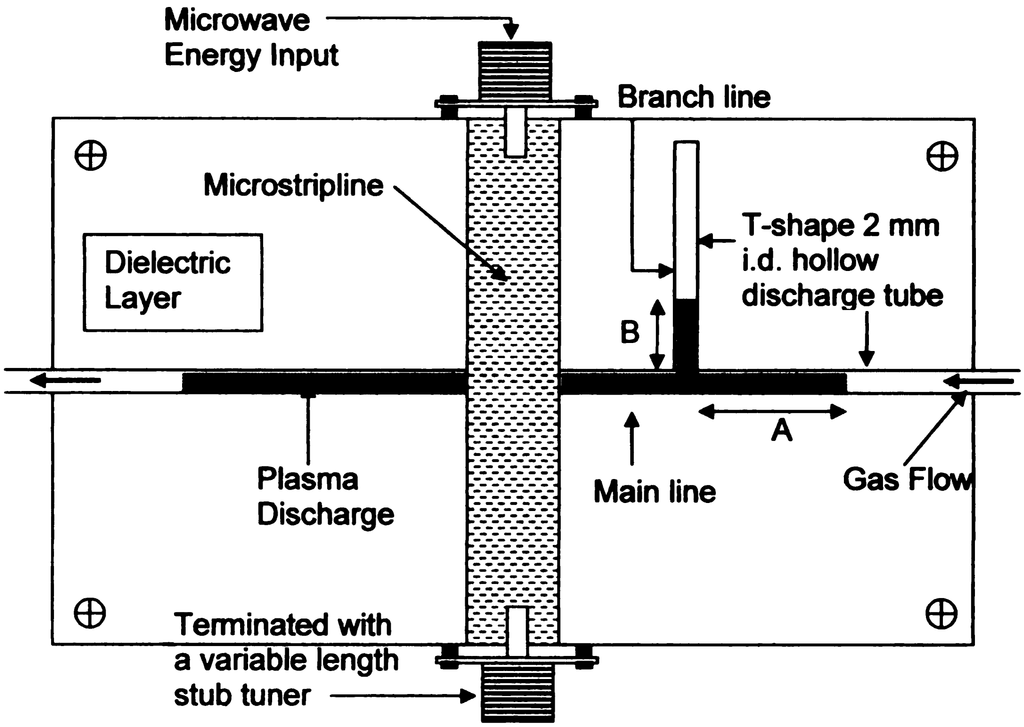

Figure 4.17 Top view of argon discharge branching inside the 2 mm i.d. quartz tube.

The other modification involved creating an oval loop circling the microstripline as shown in figure 4.18 and 4.19. At low microwave power, the argon plasma was generated underneath the microstripline and partially filled the oval shape of the discharge tube. Two independent discharges existed in each section of the tube that passed under the stripline. As the power increased, the discharge filled up the volume inside the oval. The oval tube could not be filled up completely as there was a gap at the top of the oval discharge that could not be eliminated with a high microwave power. This gap is believed to be caused by two surface waves meeting and reflecting at the gap. All of these experiments were performed at 1 Torr pressure because the volume of argon plasma is larger at low pressure.

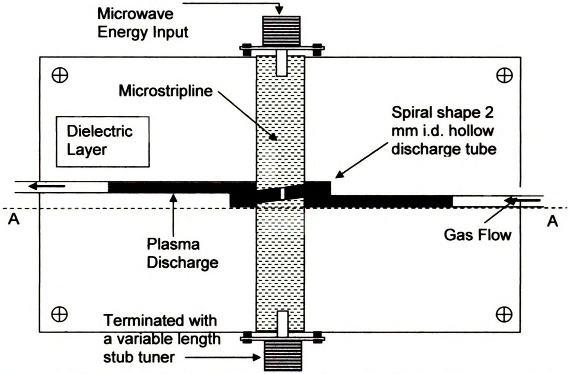

Figure 4.18 Top view of argon discharge inside a loop of 2 mm i.d. quartz tube.

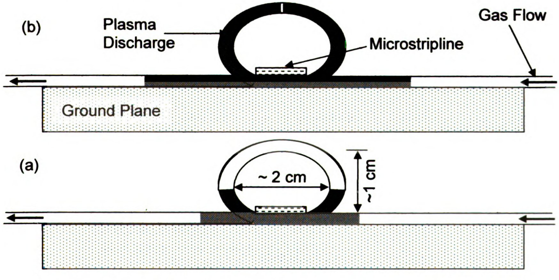

Figure 4.19 Side view of argon discharge inside a loop of 2 mm i.d quartz tube. At low P_{abs}, discharge does not completely fill up the loop (a); at high P_{abs}, argon discharge fills the loop completely (b) with the exception of a small gap on the top of the oval.

In conclusion, argon discharges created using a microstripline coupling structure will, with enough microwave power, have the behavior of expand their volume. The expansion follows the behavior of a fluid. An anomaly from a fluid behavior occurred when two discharges are placed closed to one another as shown in figure 4.19.

Another interesting phenomenon was observed for argon discharges in the microstripline system #2 at atmospheric pressure. With a proper adjustment of the variable stub tuning, filament-like discharges can be created using argon feed gas at atmospheric pressure. Different input powers, ranging from 5 – 20 Watts, generated different numbers of filaments, ranging from 1 – 14 filaments.

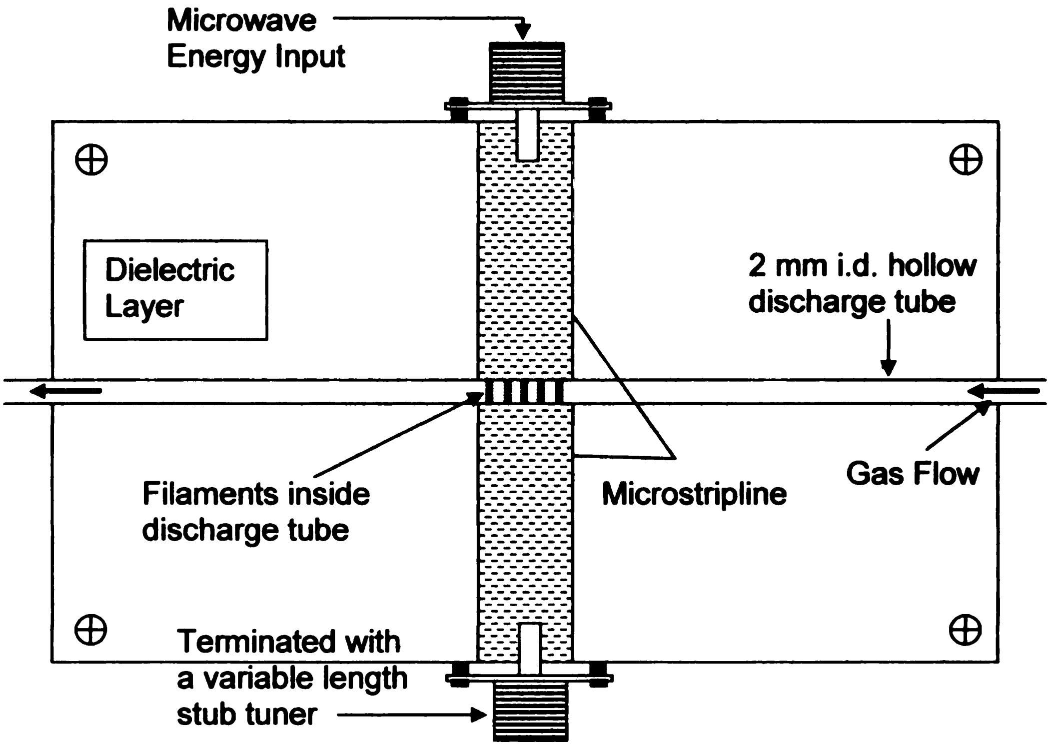

Figure 4.20 Filament-like discharges observed for argon feed gas at atmospheric pressure.

4.7 Conclusion

A series of experiments to determine the discharge volume and power density have been demonstrated. Both microstripline coupling structure designs were capable of generating Ar, H_2, N_2, and a mixture of Ar-N_2 plasmas. However, for molecular gases, there are some limiting factors in generating stable discharges. Pure molecular gas discharges were difficult to generate at pressures higher than 20 Torr. Moreover, the plasma length (volume) for these gases was very small compared to argon discharge.

The surface wave excited plasma behaviors were examined by modifying the discharge tube. Branching and looping of the discharge tube are possible.

Chapter 5

Investigation Using Optical Emission Spectroscopy

5.1 Introduction

This chapter describes the plasma discharge diagnostics using Optical Emission Spectroscopy (OES). The advantage of using OES diagnostic is that the measurement is done without perturbing the discharge. Gas temperature and electron density of the discharge can be obtained using this diagnostic method. Discharges used in this study are the homonuclear diatomic molecules hydrogen and nitrogen. The gas temperature measurements are explained in section 5.2 whereas the electron density measurements made by investigating the Stark broadening of hydrogen are explained in section 5.3.

5.2 Gas temperature

5.2.1 Gas temperature measurement theory

The total energy of a given state of a diatomic molecule is given by the formula (in wave number units)

$$T = T_{elc} + T_{tr} + G + F \tag{5.1}$$

where T_{elc} is the electronic energy, T_{tr} is the translational energy, G is vibrational energy, and F is rotational energy. In general, F is a small number since the energy separation between rotational levels in a given vibrational and electronic state are typically small compared with the thermal translational energy. Nearly all gas kinetic collisions produce a change in the rotational quantum number, whereas collisions producing a change in the vibrational or electronic quantum numbers usually occur much less frequently. Consequently, the relative rotational population distribution in a sufficiently long-lived vibrational state has a Boltzmann distribution and the rotational temperature reflects the gas kinetic temperature [15].

Further, breaking down these different forms of energy in equation 5.1, the rotational energy F in a given vibrational level is given by [14]

$$F = B_v J(J+1) - D_v J^2 (J+1)^2 + \cdots \tag{5.4}$$

where J is the rotational quantum number, B_v is the rigid rotator rotational spacing, and D_v is the first anharmonic correction to the rotational spacing. In addition, there are nonrigid rotator corrections to both B_v and D_v. These corrections are given by

$$B_v = B_e - \alpha_e \left(v + \tfrac{1}{2}\right) + \cdots \tag{5.5}$$

and

$$D_v = D_e + \beta_e \left(v + \tfrac{1}{2}\right) + \cdots \tag{5.6}$$

where v is the vibrational state, B_e and D_e are constants that corresponds to the equilibrium separation, α_e and β_e are the first anharmonic corrections. Values for those constants that correspond to the experiments are listed in table 5.1.

Table 5.1 Rotational constants for the electronic states of hydrogen and nitrogen

State	B_e	α_e	D_e (cm^{-1})	β_e
H_2 ($G^1\Sigma_g^+$)	28.4			
N_2 ($C^3\Pi_u$)	1.8259	0.0197	1.09E-5	

Based on the selection rule, the upper and lower state may have different electronic angular momentum Λ. Thus, two or three series of lines (branches) may appear which are the P, Q, and R branches. If $\Lambda=0$ in both upper and lower electronic states, the transition with $\Delta J=0$ is forbidden, hence only $\Delta J= \pm 1$ are allowed. The $\Delta J=+1$ transition gives rise to the R branch and $\Delta J= -1$ transition gives rise to the P branch. The electronic transitions involved in the experiments for both hydrogen and nitrogen rotational temperature measurements have $\Delta\Lambda=0$, thus the Q branch is not present. However, it is possible to pick an electronic transition which has a different angular momentum to observe all the branches; P, R, and Q. A simple representation of vibrational and rotational energy levels including the transitions which give rise to the P, Q, and R branches are shown in figure 5.1.

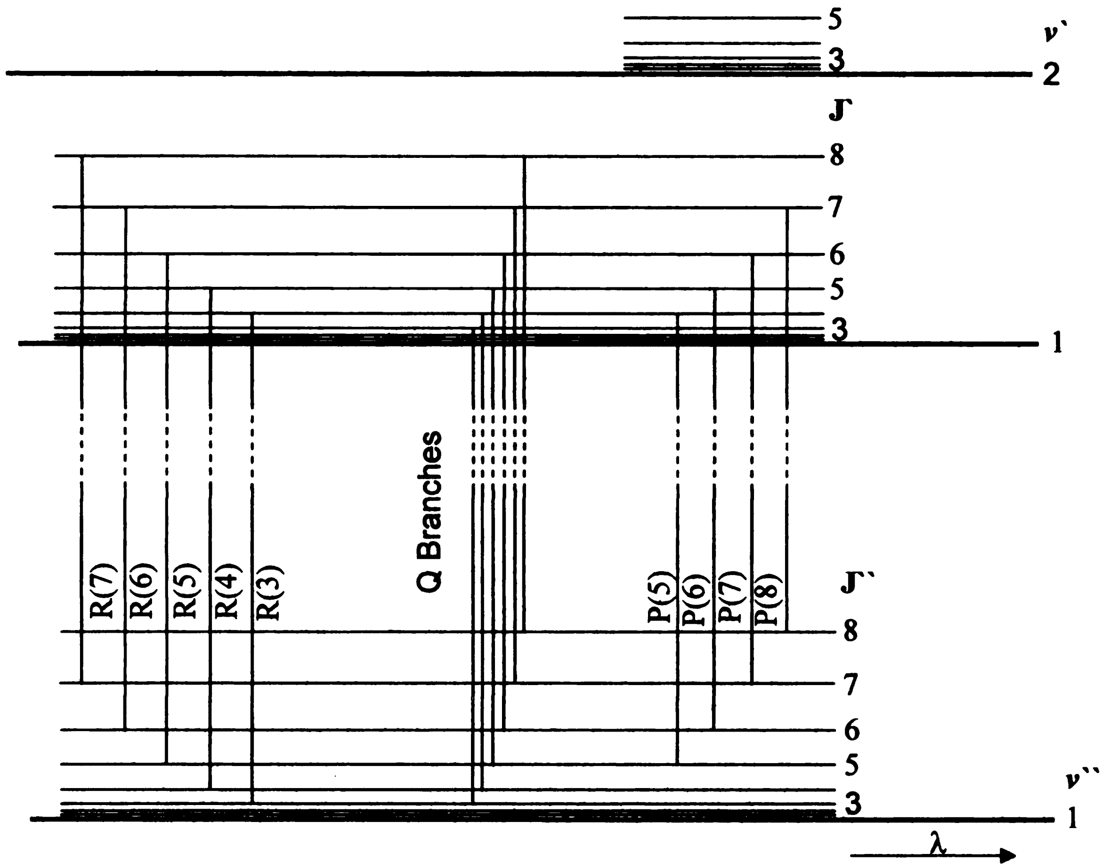

Figure 5.1 An example of vibrational and rotational energy levels with a number of transitions in the P, Q, and R Branches.

The relative rotational line intensities I of a Boltzmann distribution are described by [8]

$$I = Kv^4 S_{J'J''} \exp\left(-\frac{B_{v'} J'(J'+1)hc}{kT_r} \right) \tag{5.7}$$

where K is a constant for all lines originating from the same electronic and vibrational level, v is the frequency of the radiation, $S_{J'J''}$ is the appropriate Honl-London factor, $B_{v'}$ is the molecular rotational constant for the upper vibrational level, J is the rotational quantum number, h is the Planck's constant, c is the speed of light, k is the Boltzmann's constant and T_r is the rotational temperature.

Quantum numbers associated with the upper energy level are denoted with a prime, and those corresponding to the lower level with a double prime.

Honl-London factor describes the line strength of rotational spectra that depends on *J*. The Honl-London formulae for emission of the $\Delta\Lambda$=0, R-branch is described by [Herzberg]:

$$S = \frac{(J'+\Lambda')(J'-\Lambda')}{J'} \tag{5.8}$$

where J' is the rotational quantum number of the upper level state and Λ' is the electronic angular momentum of the upper level state. In most emission cases this factor can be simplified to S=J+1 from the approximation of equation 5.8.

5.2.2 Gas temperature of H_2

5.2.2.1 Experiment procedure

Several OES experiments, using the spectrometer apparatus setup described in chapter 3, were performed to obtain the rotational temperature of hydrogen discharges. The feed gases used in the experiments were pure H_2 and a mixture of H_2 and Ar. The parameters that were varied include the input power, pressure, and the ratio of the feed gasses flow rates.

The rotational temperature for hydrogen discharge was determined using the R branch of the $G^1\Sigma_g^+ \longrightarrow B^1\Sigma_u^+$ (0-0) band of H_2 molecule, where $G^1\Sigma_g^+$ is the upper electronic level and $B^1\Sigma_u^+$ is the lower electronic level of the 0 vibrational quantum number. Eleven emission lines (R_0 – R_{10}) in the spectrum range of 4530 Å – 4650 Å were identified as shown in figure 5.2.

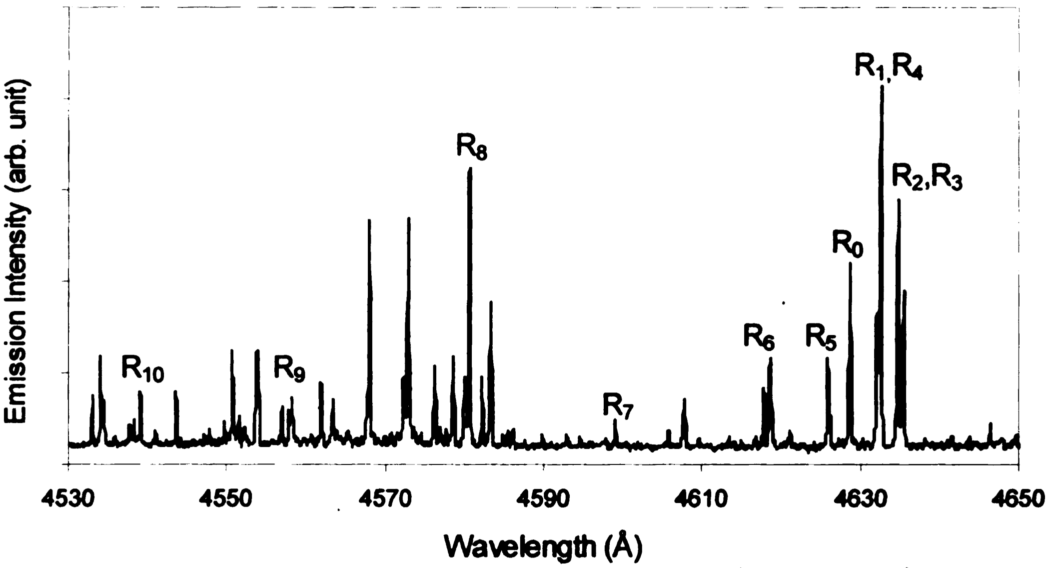

Figure 5.2 Emission spectra of the R Branch of the $G^1\Sigma_g^+ \longrightarrow B^1\Sigma_u^+$ (0-0) band of H_2 molecule.

It is found that the plot of *ln(I/S)* for this band is a linear function of the upper rotational energy under a variety of conditions, except for the R_6 and R_9 components [8]. Those lines usually are perturbed by nearby upper energy levels that have different lifetimes. In the Boltzmann plot, *I* is the intensity of the line and *S* is the corresponding Honl-London factor. The R_1, R_2, R_3, R_4 lines were not included in calculation since they were not resolved.

Table 5.2 Energy Level for the R branch of the $G^1\Sigma_g^+ \longrightarrow B^1\Sigma_u^+$ (0-0) band of H_2 molecule.

Rotational Line	Wavelength (Å)	Relative upper level energy (cm^{-1})	S
R0	4627.5	292.86	60.01
R5	4624.7	895.24	86.17
R6	4618.4	1150	315.83
R7	4598.1	1490.48	113.09
R8	4581.3	1835.71	356.69
R9	4557.4	2238.1	199.34
R10	4537.9	2666.67	642.39

Table 5.2 shows the upper energy level of the R-branch rotational lines and the corresponding value of S, the Honl-London factor. The intensity (*I*) was obtained from the peak intensity of the line subtracted by the average noise. The value of *ln(I/S)* was calculated and plotted against the upper level energy, as shown in figure 5.3. The line of best fit was obtained for the plot. The slope of this line corresponds to $-\frac{hc}{kT_r}$, where *c* is the speed of light. From the value of the slope, the rotational temperature of H_2 is obtained.

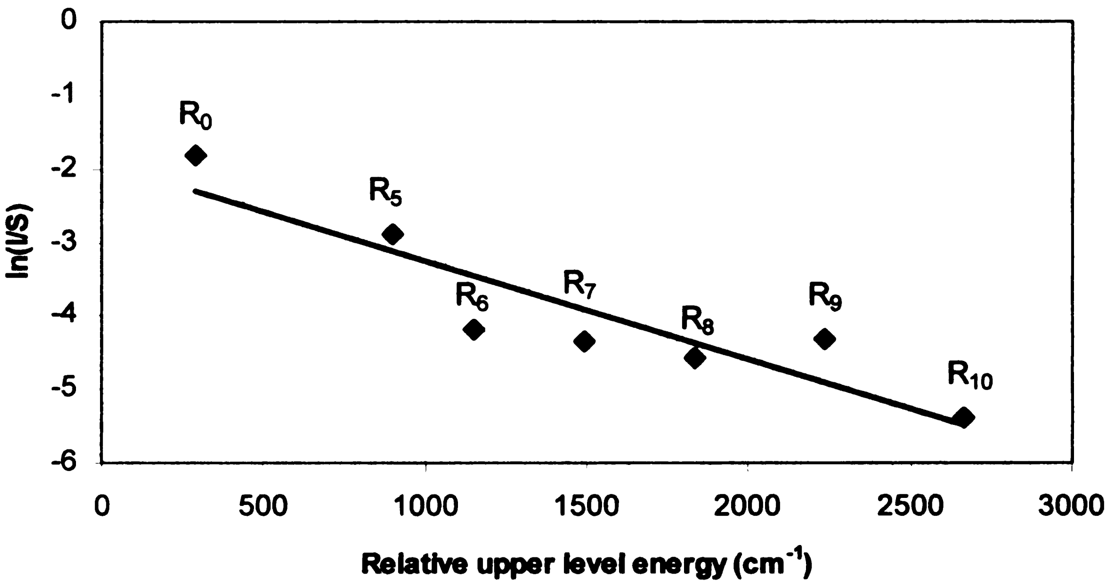

Figure 5.3 Boltzmann plot for the lines R_0 and $R_5 - R_{10}$ of H_2 plasma.

The data shown in figure 5.3 was for a H_2 plasma operated at 0.5 Torr pressure, 3 sccm flow rate, and 33 W microwave incident power.

5.2.2.2 Experimental results

The experiment results for the hydrogen rotational temperature are presented below. The accuracy of rotational temperature, determined using this method, is found to be within $\pm$ 100 K. This is estimated from the reproducibility of the data obtained.

When the flow rate of the gas was varied with the other parameters held constant, a slight increase in the rotational temperature of pure hydrogen discharge was observed with increasing flow rate.

The presence of argon cools down the discharge as can be seen in figure 5.5. The higher percentage of argon gas fed into the discharge, the lower rotational temperature of H_2 measured.

Figure 5.6 shows that the rotational temperature of hydrogen has little variation for different pressures from 0.5 to 5 Torr.

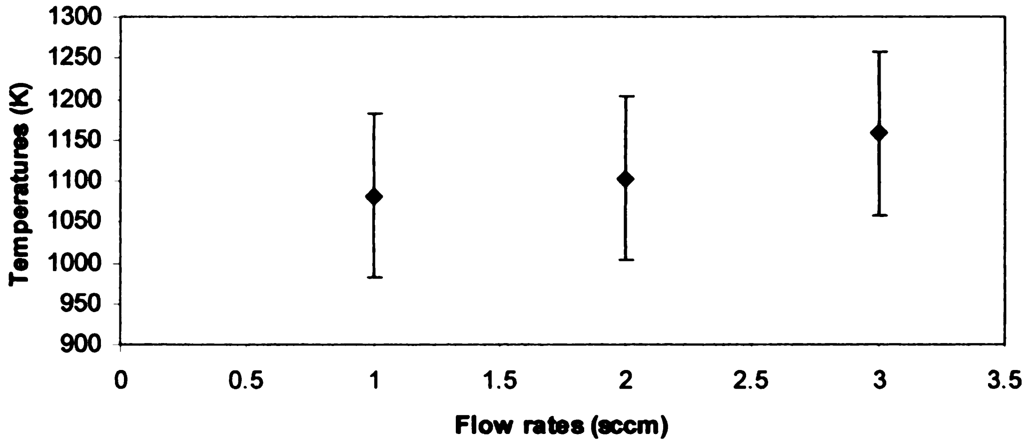

Figure 5.4 Variation of rotational temperature of H_2 with flow rates for pure H_2 plasma. Pressure: 0.5 Torr, P_{inc}: 33 W.

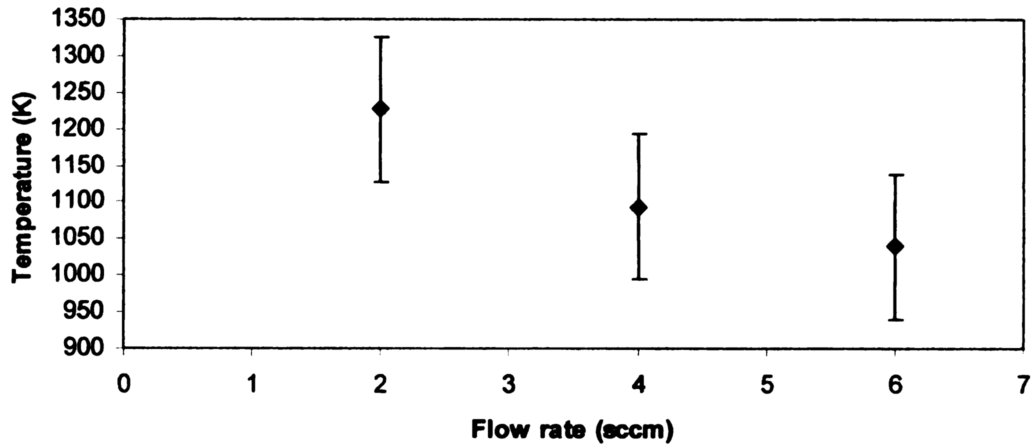

Figure 5.5 Variation of rotational temperature of H_2 with different Ar flow rates in H_2 – Ar plasma. Pressure 0.5 Torr, P_{inc}: 33 W, H_2 flow rate: 2 sccm.

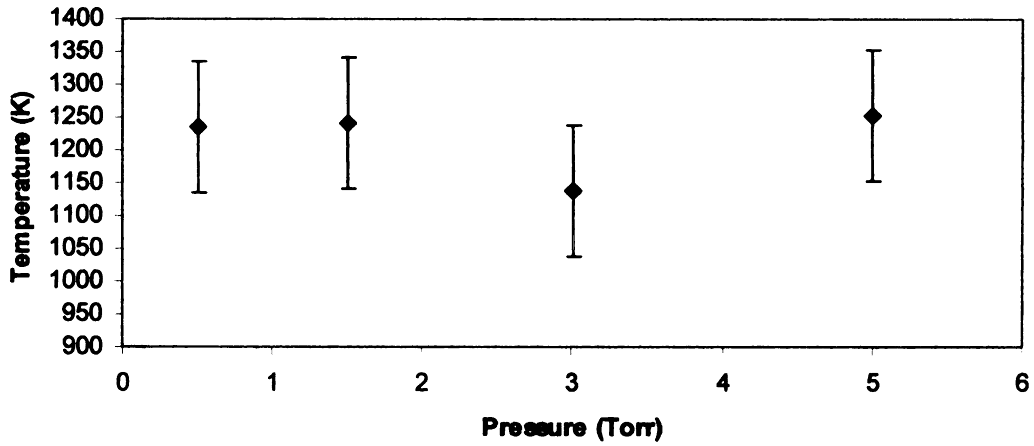

Figure 5.6 Variation of rotational temperature of H_2 with different pressure for H_2 plasma. P_{inc}: 33 W, H_2 flow rate: 2 sccm.

5.2.3 Gas temperature of N_2

5.2.3.1 Experiment procedure

Several OES experiments, using the spectrometer apparatus setup described in chapter 3, were performed to get the rotational temperature of nitrogen discharges. The feed gases used in the experiments were pure N_2 and a mixture of N_2 and Ar. The parameters that were varied include the input power, pressure, and the ratio of the feed gasses flow rates.

The nitrogen discharges created in the microstripline plasma source were assumed to be weakly ionized. Thus, the rotational temperature measurements were performed by analyzing the spectrum of the neutral species. The emission band system for nitrogen commonly known as the Second Positive System (SPS) in nitrogen spectra was used to determine the rotational temperature. The SPS describes the energy level transition from $C^3\Pi_u$ to $B^3\Pi_g$. A wide spectral scan from 3730 Å – 4000 Å as seen in figure 5.3 confirmed that the SPS emission from the nitrogen discharge was detected.

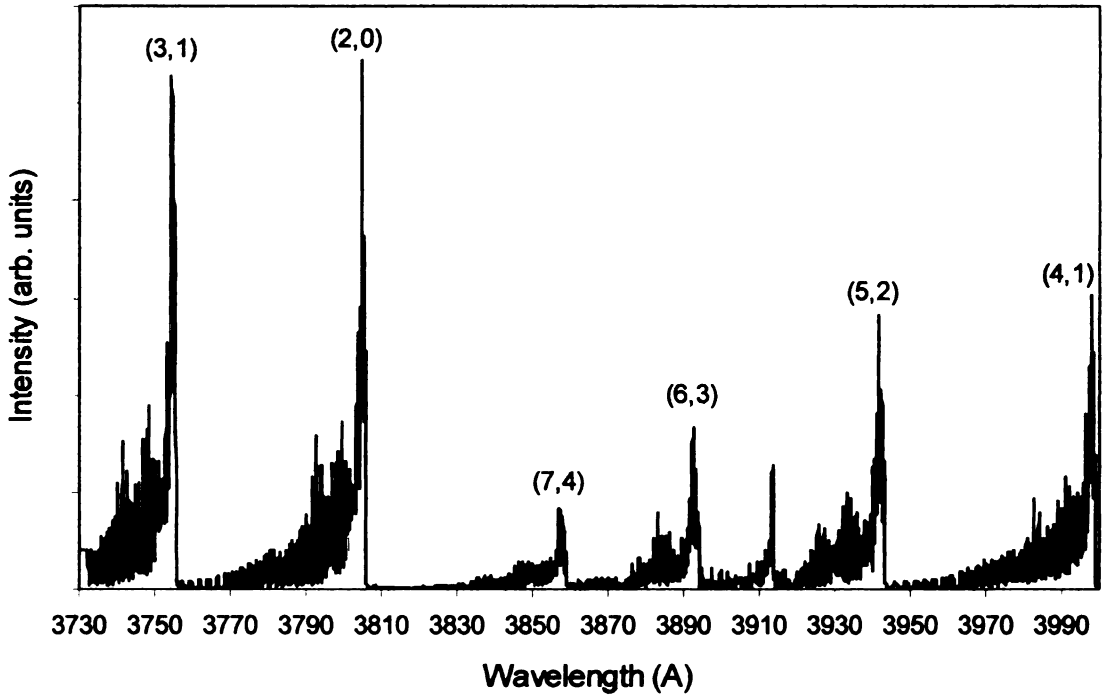

Figure 5.7 Spectrum of nitrogen discharge showing the band heads of the SPS system.

During the wide spectrum scanning experiment, the strongest signal intensity detected by the spectrometer was the (2,0) band-head vibrational transition. Moreover, the fine structures of the rotational lines in that particular band-head were visibly shown. Hence, those rotational lines were used in

determining the gas temperature. Figure 5.4 shows the detail of the R and P branches of the (2, 0) transition in the SPS system. Eleven emission lines (R_{20} – R_{30}) in the spectrum range of 3758 Å – 3783 Å were identified. Conversely, the lower J values of the R branch emissions were not resolved since they coincided with the P branch emissions.

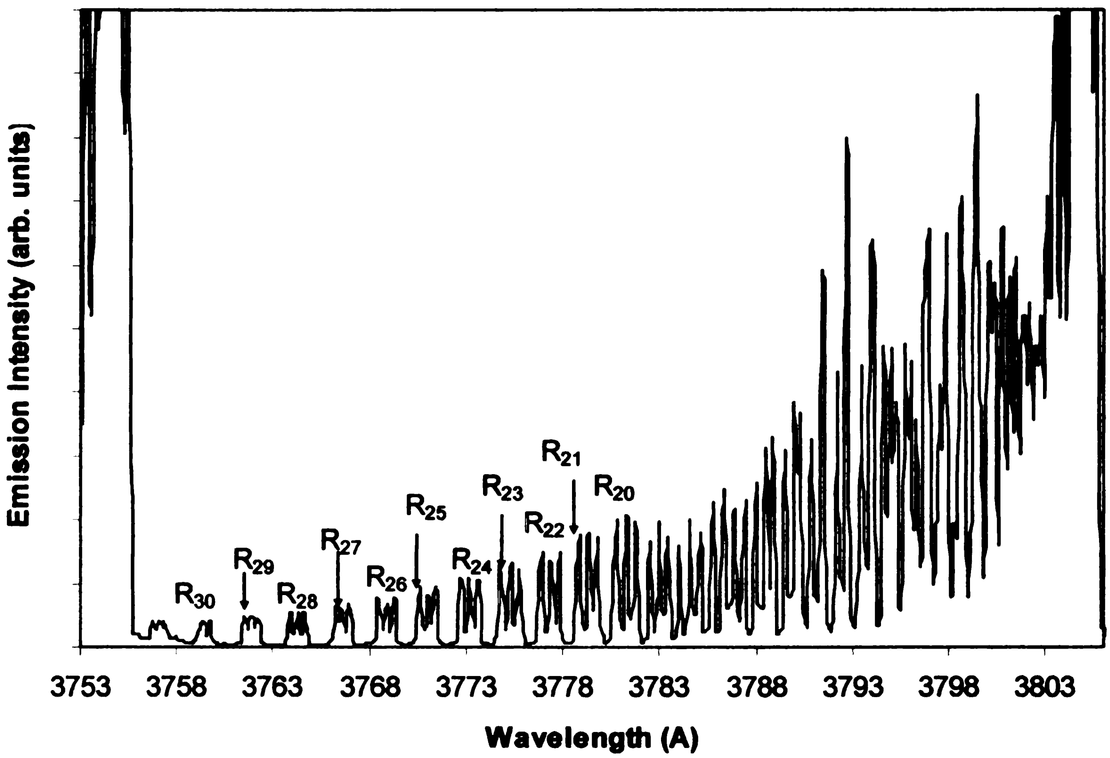

Figure 5.8 Fine structures of the (2,0) SPS system of nitrogen discharge that were used for rotational temperature measurement.

Table 5.3 Energy Level for the R branch of the (2,0) SPS system of nitrogen discharge.

Rotational Line	Wavelength (Å)	Relative upper level energy (cm^{-1})	S
R20	3780.44	837.76	19.8
R21	3778.58	917.42	20.80952
R22	3776.66	1000.67	21.81818
R23	3774.68	1087.51	22.82609
R24	3772.64	1177.95	23.83333
R25	3770.53	1271.97	24.84
R26	3768.37	1369.57	25.84615
R27	3766.14	1470.76	26.85185
R28	3763.86	1575.51	27.85714
R29	3761.51	1683.84	28.86207
R30	3759.11	1795.74	29.86667

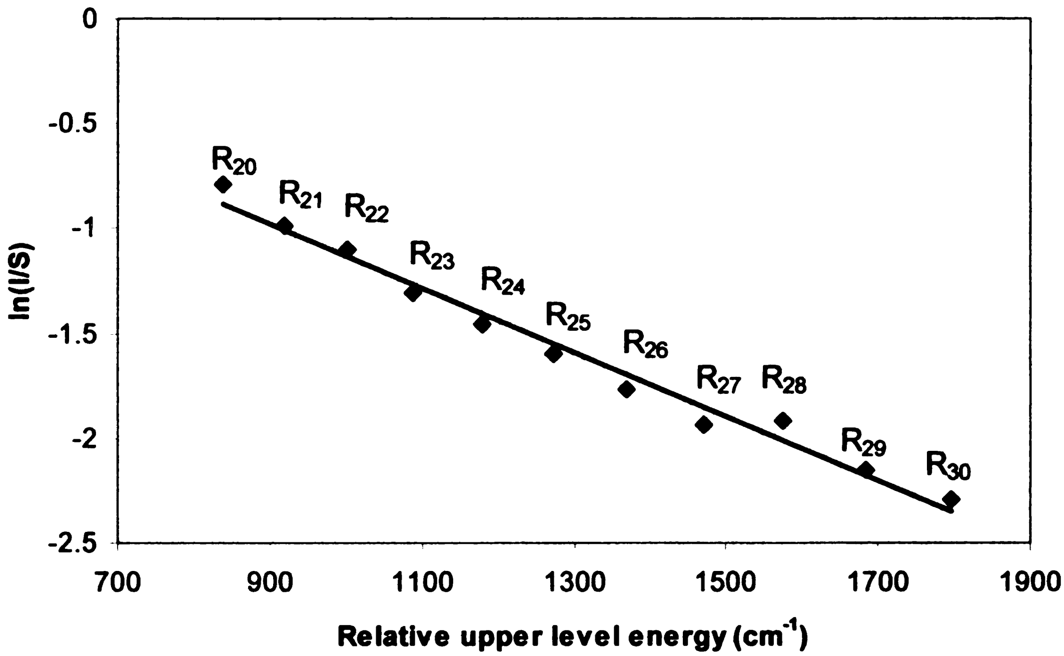

Figure 5.9 Boltzmann plot for the lines $R_{20} - R_{30}$ of N_2 plasma.

The data shown in figure 5.9 was for a mixture of Ar - N_2 plasma operated at 5 Torr pressure, 2 sccm flow rate for both feed gases, and 33 W microwave incident power.

5.2.3.2 Experimental results

The experimental results for the nitrogen rotational temperature are presented below. The accuracy of rotational temperature, determined using this method, is found to be within ± 100 K. This is estimated from the reproducibility of the data obtained.

From figure 5.10, it can be seen that the rotational temperature of Ar - N_2 plasma slightly increases versus pressure from 0.5 – 10 Torr. The temperature ranges from 1025 – 1150 K. From figures 5.11 and 5.12, it can be observed that the rotational temperature of N_2 increases with the increase of Ar flow rate. Thus, the Ar – N_2 mixture has a higher rotational temperature than that of pure N_2 plasma discharges. The rotational temperature of pure N_2 discharges in the pressure ranges from 0.5 – 5 Torr are less than 750 K.

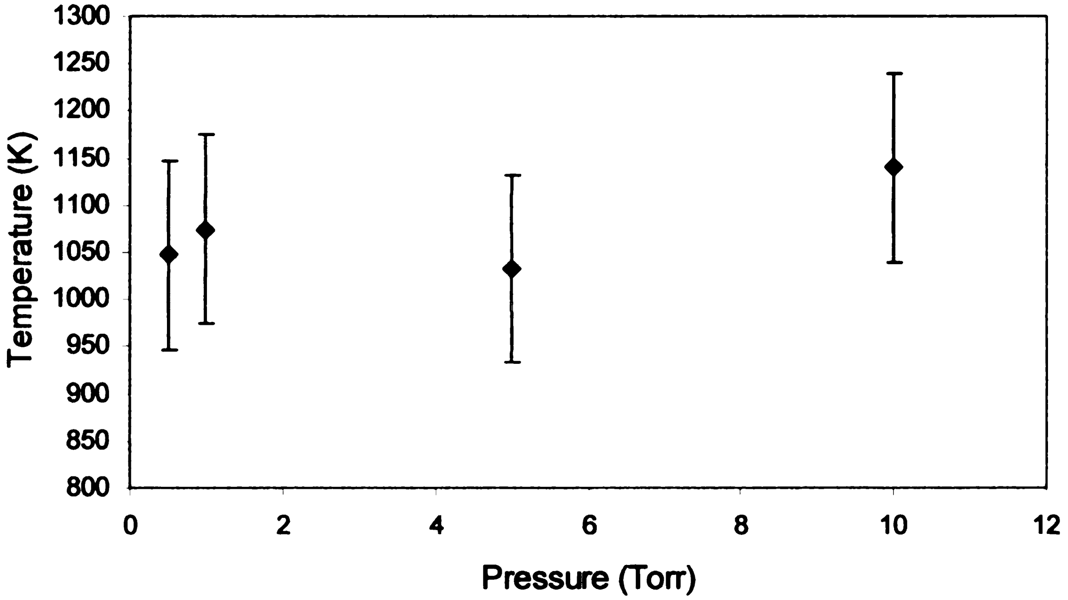

Figure 5.10 Variation of rotational temperature of N_2 with different pressure for N_2 - Ar (10% - 90%) plasma. P_{inc}: 33 W, flow rate: N_2-2 sccm, Ar-18 sccm.

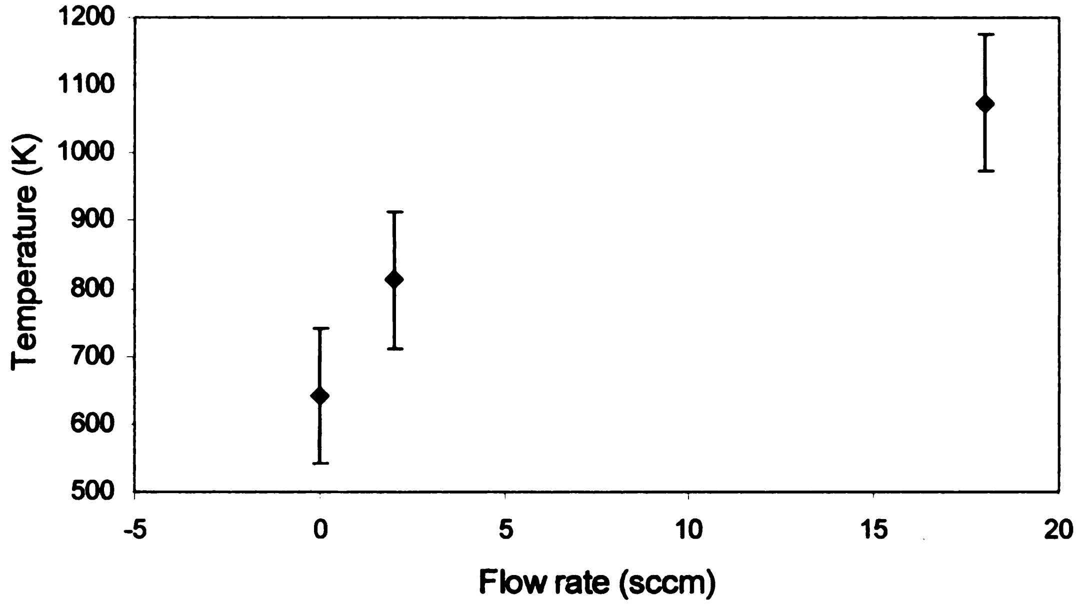

Figure 5.11 Variation of rotational temperature of N_2 with different Ar flow rates in N_2 – Ar plasma. Pressure 0.5 Torr, P_{inc}: 33 W, N_2 flow rate: 2 sccm.

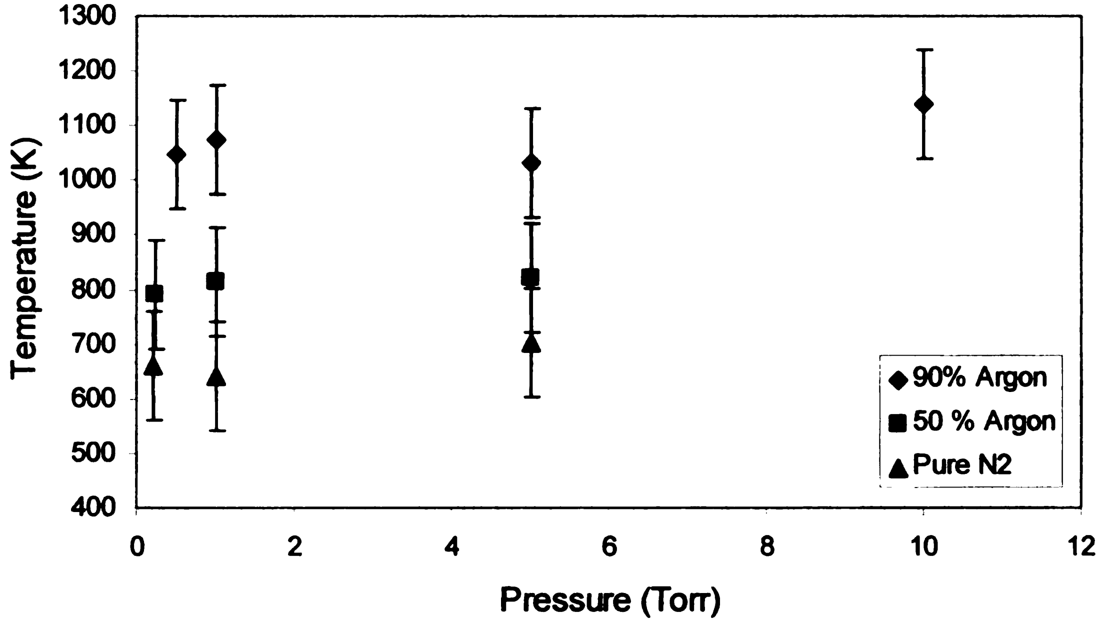

Figure 5.12 Variation of rotational temperature of N_2 with different pressure for pure N_2, and mixtures of Ar – N_2 (50% Ar, and 90% Ar) discharges.

5.3 Stark Broadening

There are many line broadening mechanisms in the optical light emission from a plasma. The two dominant mechanisms are the Doppler broadening and the pressure broadening. Pressure broadening exists in dense plasmas where line shapes are strongly influenced by interactions of the radiating atoms or ions with the surrounding particles. From the physical point of view, pressure broadening can be further subdivided into resonance, Van der Waals, and Stark broadening. In a plasma with ions and electrons present with sufficiently high concentrations ($>10^{13}$ cm^{-3}), the dominant pressure broadening mechanism is the Stark broadening. Stark broadening of spectral lines can be used to determine the electron density of a discharge. This leaves Doppler broadening as the most likely competing mechanism, which must be considered along with the apparatus broadening.

The electron density of the discharge, created using microstripline coupling structure #1, was determined by examining the Stark effect using OES. The emissions of the hydrogen Balmer β and δ transitions (H_β, H_δ) from a mixture of Ar – H_2 plasma were analyzed. Those lines were chosen because they have sufficiently well known Stark profiles and are favorable to measure electron density in the range $10^{13} - 10^{17}$ cm^{-3}.

Purely Stark broadened lines of the hydrogen Balmer series have been computed by Griem [18]. Griem has determined the width of the Stark broadened

Balmer lines as a function of plasma electron density at various electron temperatures. For an electron temperature of 5000 K the plasma density is given by:

$$n = \left[\left(3.99\times10^{8}\right)\left(\Delta\lambda_s/\alpha\right)\right]^{3/2}\ \text{cm}^{-3} \qquad (5.9)$$

where $\Delta\lambda_s$ is the Full Width Half-Maximum (FWHM) of the purely Stark broadened line in Angstroms and α is a coefficient for the various Balmer lines. King [15] summarized the α coefficients along with the useful density range as given in table 5.4.

Table 5.4 Coefficient α for electron density estimates and the fine structure splitting for H_β and H_δ lines of hydrogen Balmer series.

	α	Density	$\Delta\lambda_{fs}$
H_β 486.1 nm	0.0762	~10^{14} cm^{-3}	0.077 Å
H_δ 410.1 nm	0.149	~10^{13} cm^{-3}	0.057 Å

FWHM of the purely Stark broadened line can be deduced from the experimentally observed line by using the following:

$$\Delta\lambda_s = \sqrt{\Delta\lambda_{\exp}^{2} - \Delta\lambda_{fs}^{2} - \Delta\lambda_{inst}^{2}} \qquad (5.10)$$

where $\Delta\lambda_{exp}$ is the FWHM of the observed line, $\Delta\lambda_{fs}$ is the fine structure splitting, and $\Delta\lambda_{inst}$ is the apparatus and Doppler broadening.

Apparatus broadening along with Doppler broadening was estimated by measuring an argon line at 411.9 nm in a low pressure discharge. Since the only significant broadening at this low pressure is expected to be Doppler broadening which is small for Argon. The observed width in the argon emission was assumed to be purely instrumental in origin. $\Delta\lambda_{inst}$ for this experiment has FWHM of 0.3 Å.

The lines presented in figure 5.13 and 5.14 are the H_β and H_δ emission lines from a mixture of Ar - H_2 plasma operated at 1 Torr pressure, 27.5 sccm flow rate for argon gas, 1.5 sccm flow rate for hydrogen gas, and 26.7 W microwave absorbed power.

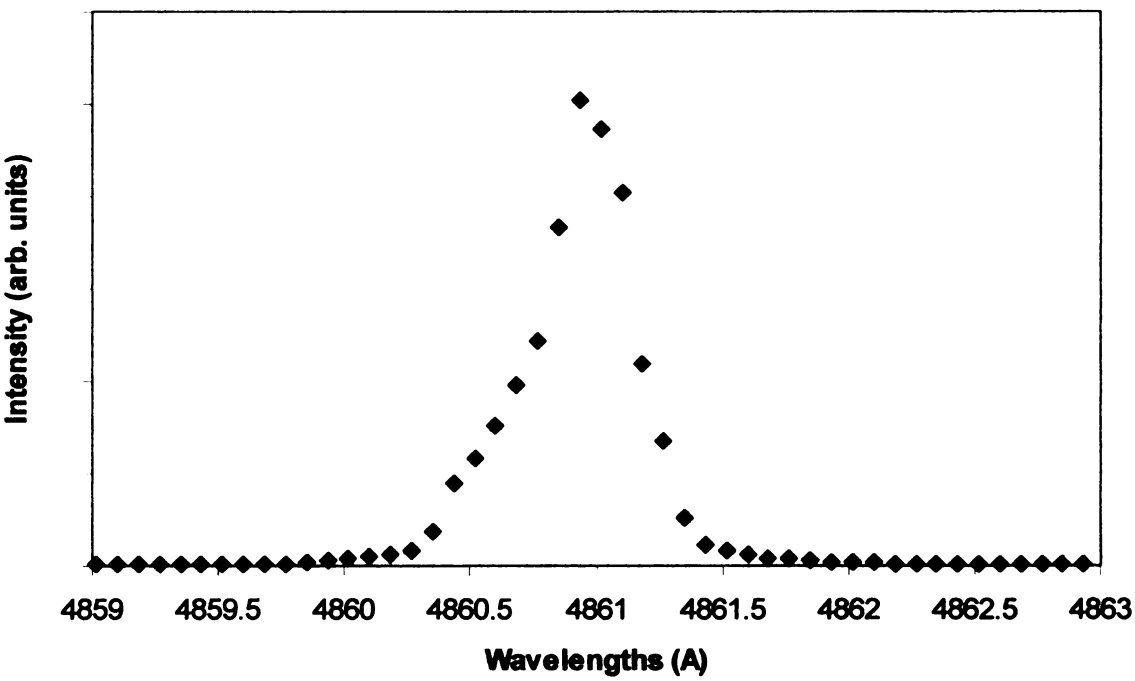

Figure 5.13 The observed broadened H_β hydrogen Balmer line.

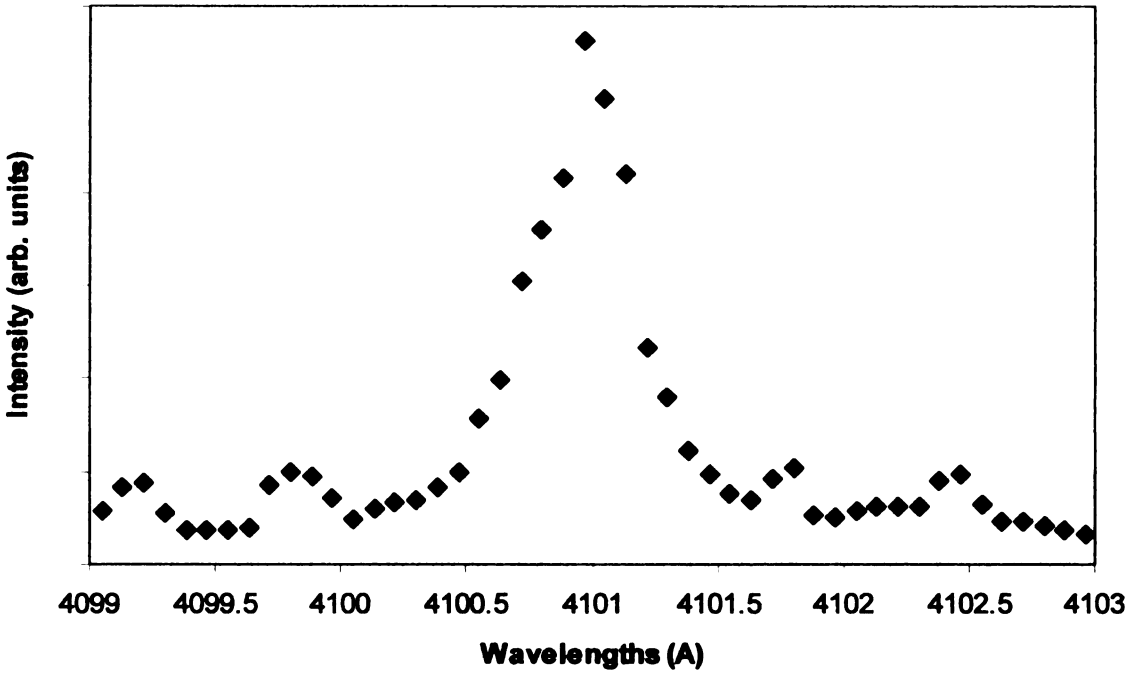

Figure 5.14 The observed broadened H_δ hydrogen Balmer line

The plasma density was determined to be 6.6×10^{13} cm^{-3} and 3.5×10^{13} cm^{-3} from Stark broadened H_β and H_δ measurements respectively. A similar procedure for plasma density measurements was performed on discharge at 100 Torr pressure. The results are listed in table 5.5.

Table 5.5 Measured plasma density from Stark broadened H_β and H_δ lines of hydrogen.

	Pressure (Torr)	Plasma density (cm^{-3})
H_β	1	6.6×10^{13}
H_β	100	1.4×10^{14}
H_δ	1	3.5×10^{13}
H_δ	100	7.1×10^{13}

5.4 Conclusion

The rotational temperature of H_2, Ar – H_2, N_2, and Ar – N_2 microwave plasma discharges were measured. The results showed that increase in pressure slightly increases the temperature. The variation in the gas temperature with argon concentration was of the particular interest, since the global analytical model, discussed in chapter 7, is based on argon discharge. The rotational temperature of Ar – H_2 and Ar – N_2 discharges, with argon as the dominant species, are around 1000 K. This value will be applied in the global analytical model.

The observation of the Stark broadened H_β and H_δ lines of 1 Torr Ar – H_2 discharge shows that the discharge's electron density was on the order of 10^{13} cm^{-3}. This result will be compared to the result from the global model in chapter 7.

Chapter 6

Investigation Using Langmuir Probe

6.1 Introduction and brief review of the Langmuir probe diagnostic

Langmuir Probe diagnostics measures the current – voltage (I-V) characteristics of a discharge. From the I-V characteristics, the electron temperature and the charge density can be determined. In the double Langmuir probes (DLP) diagnostic, two metal probes are inserted into the discharge and a bias voltage is applied across the probes to draw electron and ion current. The bias voltage will draw positive ion current to the negative probe and electron current to the positive probe. As the bias voltage becomes very large, the more negative probe essentially draws the ion saturation current, which is balanced by the net electron current to the other probe. For DLP diagnostics, a Maxwellian electron energy distribution is assumed. Further, the double probe method collects information on the high-energy tail of the electron energy distribution.

In this research, DLP were chosen over single Langmuir probe diagnostic since there was no well-defined ground electrode in the discharge. A typical I-V characteristic obtained from a DLP measurement is shown in figure 6.1. The I-V characteristic is governed by the following equation [16]:

$$\frac{I+I_1}{I_2-I}=\frac{A_1}{A_2}\exp\left(\frac{V}{T_e}\right), \quad V=V_1-V_2 \tag{6.1}$$

where I_1 and I_2 are the ion currents to probe 1 and 2 respectively, A_1 and A_2 are the collection areas, V_1 and V_2 are the probe potentials with respect to the

plasma potential, and T_e is the electron temperature. If $A_1 = A_2$, then $I_1 = I_2 = I_i$, then equation can be simplified to:

$$I = I_i \tanh\left(\frac{V}{2T_e}\right) \tag{6.2}$$

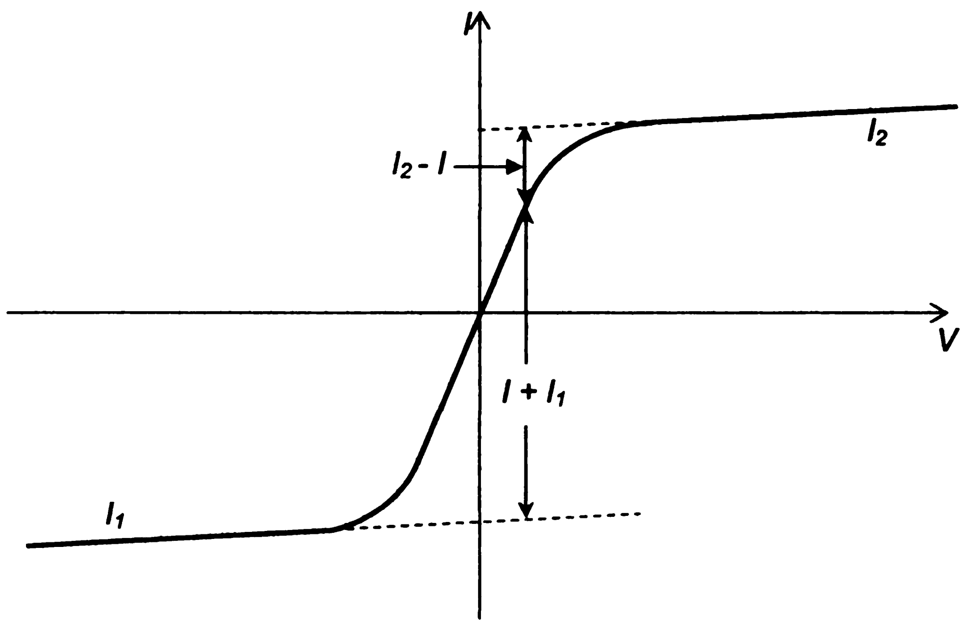

Figure 6.1 Typical current – voltage (I-V) characteristic.

The electron and ion density can be found using [Lieberman]:

$$I_i = e\, n_s\, u_B\, A \tag{6.3}$$

where e is the elementary charge, $n_s \approx 0.61\, n_o$ is the sheath edge density, u_B is the Bohm velocity, and A is the collection area of the probe. The Bohm velocity u_B is given by:

$$u_B = \left(\frac{eT_e}{M}\right)^{1/2} \tag{6.4}$$

where M is the mass of the ion.

The discharge in the DLP diagnostic is assumed to be collisionless. Thus, the simple case of the probe theory, that in which the collisions and magnetic fields are negligible, is used. Collisionless discharge can be achieved when the mean free path of the ion (λ_i) is longer than the discharge sheath thickness (s). The mean free path of ion in argon discharge is defined as [13]:

$$\lambda_i = \frac{1}{330p} \text{ cm} \tag{6.5}$$

where p is the pressure in Torr, and the ion is assumed to have a low-energy (T_i ~ 0.05 eV). The sheath thickness as explained in section 3.5.1 is on the order of a few microns.

When the sheath is thick compared with the probe radius, the current is limited by the orbital motion [19]. Thus, the probe characteristic appears as shown in Figure 6.2 follows for different probe shapes. However, in this experiment, the probe radius is much bigger than the sheath thickness; therefore, the saturation region follows that of the planar probe.

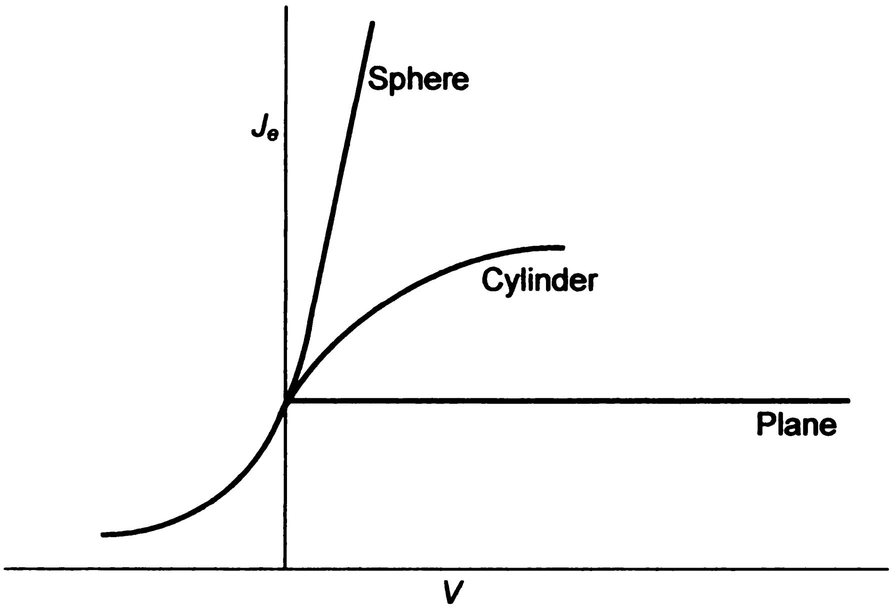

Figure 6.2 Theoretical shape of the saturation current portion of the probe characteristic for various probe shapes when the probe is limited by orbital motions.

6.2 Experimental setup

DLP diagnostics were done for pure argon discharges at pressure ranges from 3 to 10 Torr. The flow rate of the argon feed gas was set to 10 sccm. The microwave power absorbed by the discharges measured was 2 Watts. For the equipment setup detail for this diagnostic, please refer to section 3.5.

The DLP diagnostics at each pressure point were conducted three times in order to check the consistency of the probes performance. As can be seen in figure 6.3, the I-V characteristics have an excellent repeatability, with the exception of a few minor discrepancies in the saturation regions. Also, the average values of the saturation current in the saturation region 1 and in the saturation region 2 were slightly different. This shows that Probe 1 tends to draw a bigger ion current. This may happen due to fact that the collection area of probe 1 was a few tenths of a micron longer than the collection area of probe 2. To verify this, the probes' connections to the multi-meter were switched. The result, as seen in figure 6.3, was that after the probe was switched, the average of the saturation current in region 2 was larger than in region 1. Hence, this proves that the probes used in the diagnostics were not exactly identical.

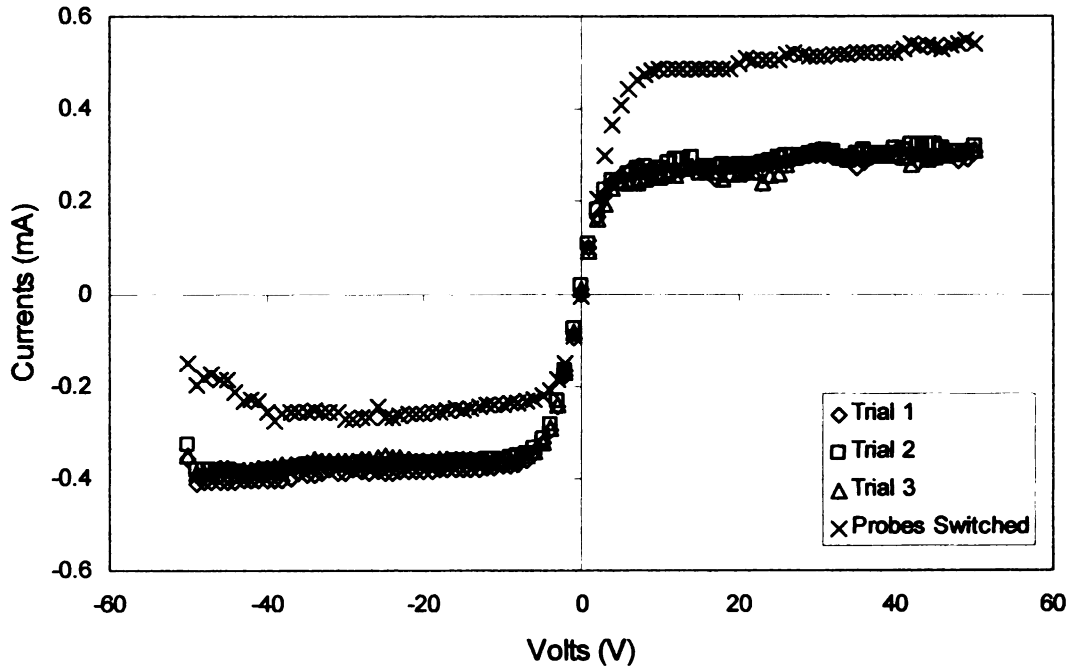

Figure 6.3 I-V curves obtained using DLP diagnostic. Pressure: 10 Torr, P_{abs}: 2.34 Watts, Gas: Argon, flow rate: 10 sccm.

The I-V curves obtained from the DLP measurement have a similar shape to the hyperbolic tangent function described in equation 6.2. Since the saturation ion current was different for each probe, equation 6.1 was used. Re-arranging equation 6.1 into the following form:

$$\ln\left(\frac{I+I_1 / I_2 - I}{A_1 / A_2}\right) = \frac{V}{T_e} \qquad (6.6)$$

the I_1 and I_2 values were obtained by averaging the saturation current for each probe with assumption that the saturation regions were flat line. A_1/A_2 is proportional with the ratio of I_1 and I_2 according to the equation 6.3.

A log plot from equation 6.5 can determine the electron temperature, which is the inverse of the slope. The data points used to generate the log plot were the ones between the two saturation regions.

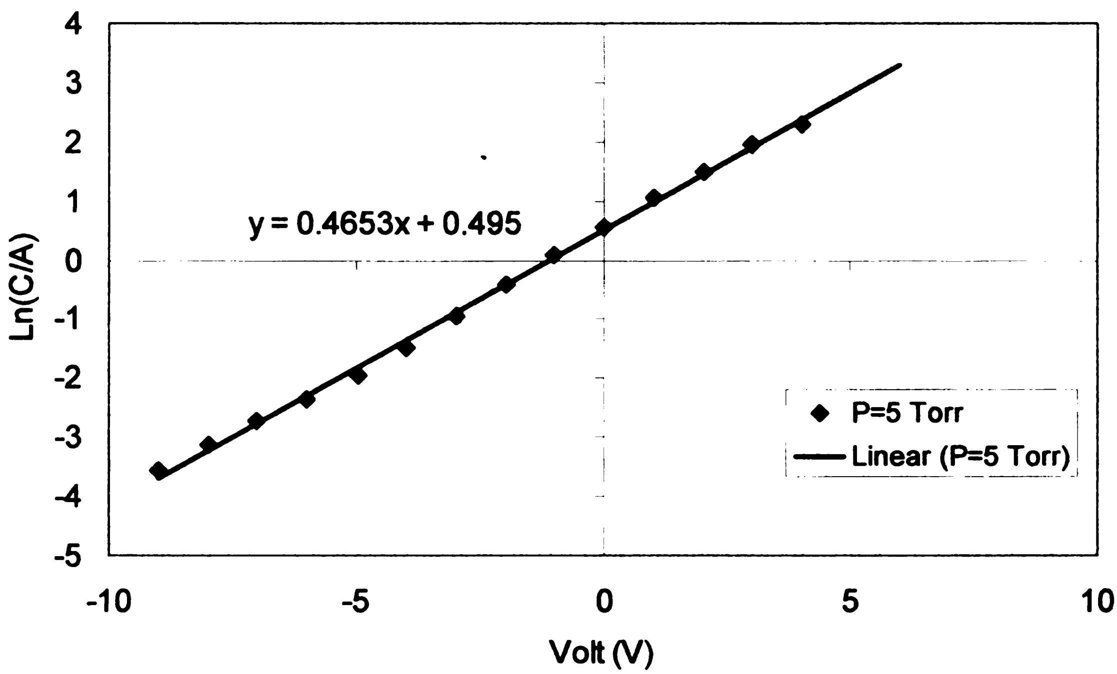

Figure 6.4 Log plot of the I-V characteristic from DLP diagnostic. $C=I+I_1/I_2-I$, $A=A_1/A_2$.

6.3 Results and discussions

The results of DLP diagnostic for argon discharge are presented below. As can be seen in figure 6.5, the electron temperature decreases as the pressure increases. The electron temperature ranges from 2.3 eV – 1.9 eV.

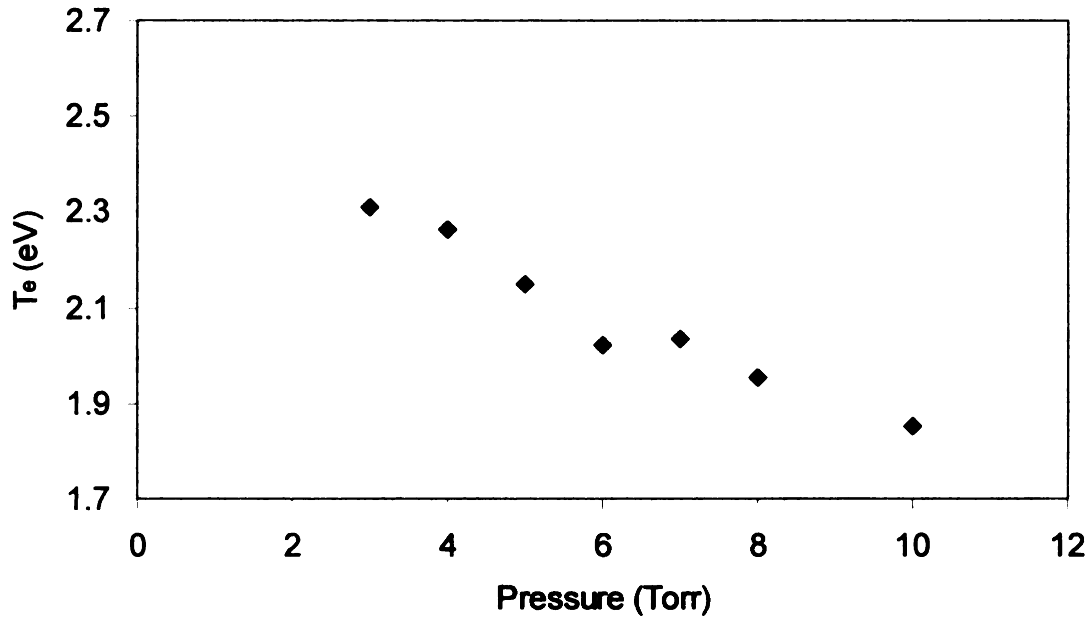

Figure 6.5 Variations of electron temperature for different pressures. Gas: Argon, flow rate: 10 sccm, P_{abs}: 2.34 Watts, Discharge tube size: 2 mm, Microstripline structure #1.

The charge densities of argon discharges as shown in figure 6.6 were measured to be 3 – 6x10^{12} cm^{-3}. As the pressure increases, the charge density increases. The results from electron temperature and charge density measurements confirmed that the assumed sheath thickness, explained in section 3.5, is valid.

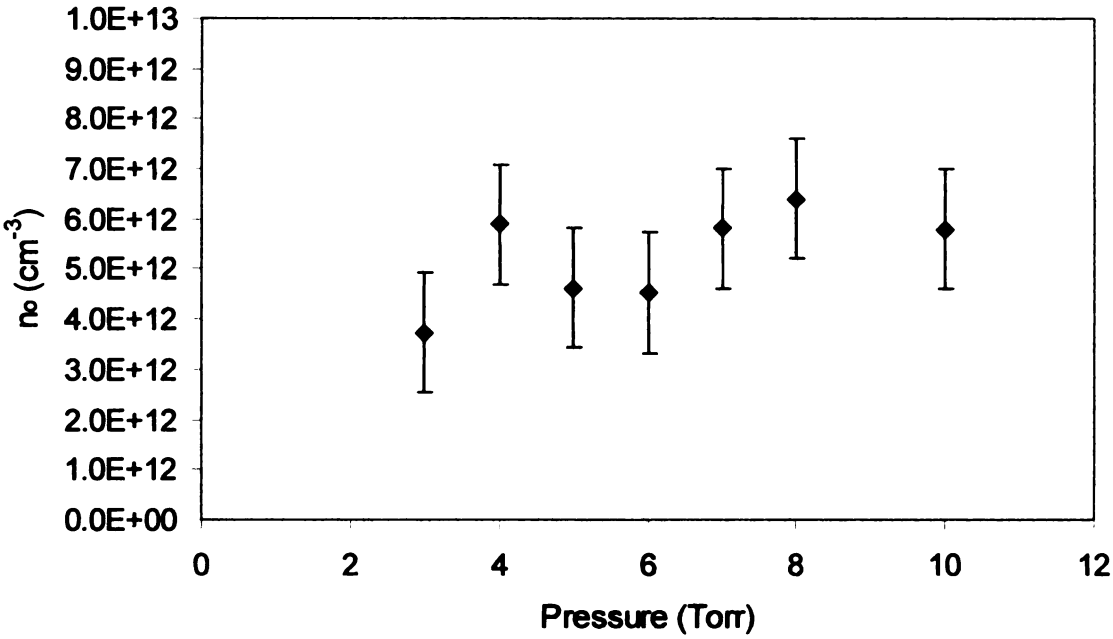

Figure 6.6 Variation of charge density for different pressures. Gas: Argon, flow rate: 10 sccm, P_{abs}: 2.34 Watts, Discharge tube size: 2mm, Microstripline structure #1.

6.4 Conclusion

Experiments to determine the electron temperature and the charge density of argon discharges using DLP diagnostic were done. The I-V characteristics obtained from this DLP measurements shows that the geometry of the probe is large enough compared to the sheath thickness so that the saturation regions is flat. This means that the Debye length of these discharges is very small, thus, the density is high.

The results of the electron temperature and charge density measurements from this DLP diagnostic will be compared to the ones from the global analytical model of argon discharges in chapter 7.

Chapter 7

Global Model Calculations

7.1 Introduction

The electron temperature and charge density in a discharge can be predicted using a Global Model. This chapter describes how the model was built and compares the results with the experimental results from the previous chapters. The global model calculations were done for pure argon discharges, since argon has been use extensively in the experiments.

7.2 Theoretical background

Based on the relation between the pressure and the discharge dimension, the discharge can be categorized into three regimes. They are:

(a) Low pressure: $\lambda_i \geq (R,l)$

(b) Intermediate pressure: $(R,l) \geq \lambda_i \geq \left(T_i / T_e \right)(R,l)$

(c) High pressure: $\lambda_i \leq \left(T_i / T_e \right)(R,l)$

where λ_i is the mean free path of ion-neutral collisions as explained in chapter 6, equation 6.5, R is the radius of the discharge tube, l is the length of the plasma obtained from the discharge volume experiments from chapter 4, T_i is the ion temperature, and T_e is the electron temperature.

In the experiments, the discharge volume was small. However, the mean free path of argon ion never exceeds the discharge dimension because the pressures used were higher than 0.5 Torr. Hence, the discharges fall into the intermediate and high pressure regimes. In addition to that, the discharge has a cylindrical geometry. Thus, all of the calculations presented here are for cylinder geometry.

In the intermediate pressure regime, the electron temperature can be determined from the gas density (n_g) and the effective plasma size (d_{eff}) as can be seen in figure 7.1. Gas density information was obtained from the pressure using the Ideal Gas Law:

$$n_g = \frac{p}{k_B T_g} \tag{7.1}$$

where p is the discharge pressure, k_B is the Boltzmann constant, and T_g is the gas temperature. Gas temperature for argon discharge was found to be around 1000 K from the OES experiments.

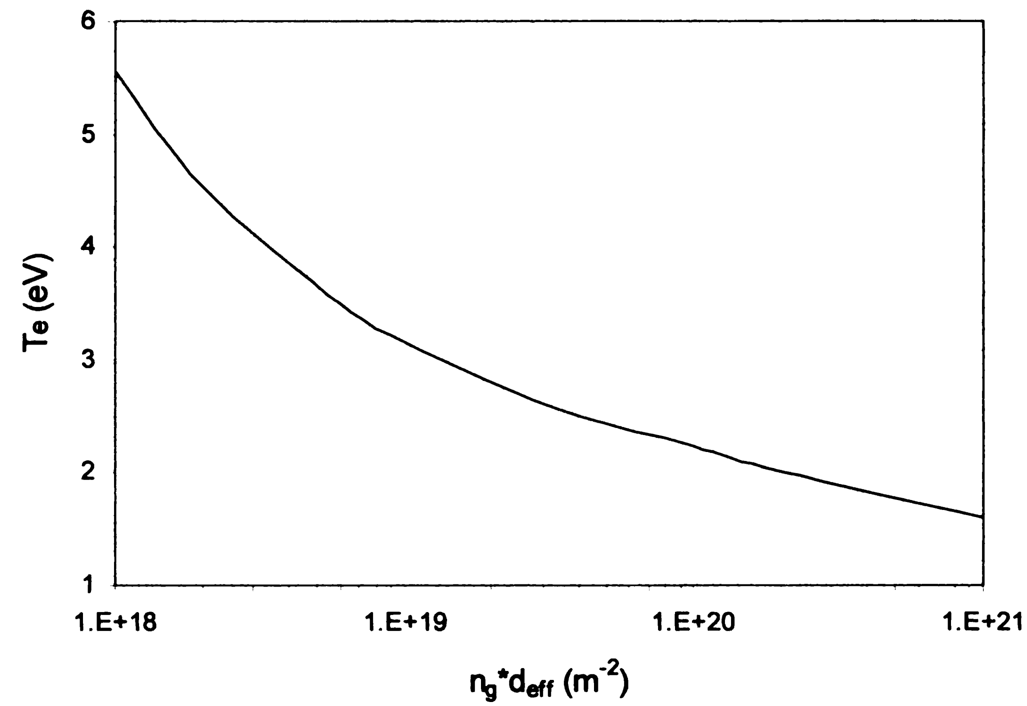

Figure 7.1 T_e versus $n_g \cdot d_{eff}$ for Maxwellian electrons in argon [13].

The effective plasma size as described by Lieberman is

$$d_{eff} = \frac{1}{2}\frac{R\,l}{R\,h_l + l\,h_R} \tag{7.2}$$

where

$$h_l \approx 0.86\left(3 + \frac{l}{2\lambda_i}\right)^{-1/2} \tag{7.3}$$

and

$$h_R \approx 0.80\left(4 + \frac{R}{\lambda_i}\right)^{-1/2} \tag{7.4}$$

h_l and h_R are the density profiles for the axial sheath edge and the radial sheath edge, respectively. They are derived from the diffusion equation.

The estimation of the plasma density (n_o) can be found using

$$n_o = \frac{P_{abs}}{e\,u_B\,A_{eff}\,\varepsilon_T} \tag{7.5}$$

where

$$A_{eff} = 2\pi R(R\,h_l + l\,h_R) \tag{7.6}$$

P_{abs} is the absorbed power obtained from the discharge volume and power density experiments, A_{eff} is the effective area, u_B is the Bohm velocity, and ε_T is the total energy dissipated per ion lost from the system.

The total energy dissipated per ion lost from the system ε_T is the sum of the collisional energy losses ε_c, the mean kinetic energy lost, which for

Maxwellian electrons is equal to *2* T_e, and the mean kinetic energy lost ε_i. For argon discharges $\varepsilon_i \approx 5.2 T_e$.

$$\varepsilon_T = \varepsilon_c + 2T_e + \varepsilon_i \tag{7.7}$$

The value for ε_c is approximated using figure 7.2.

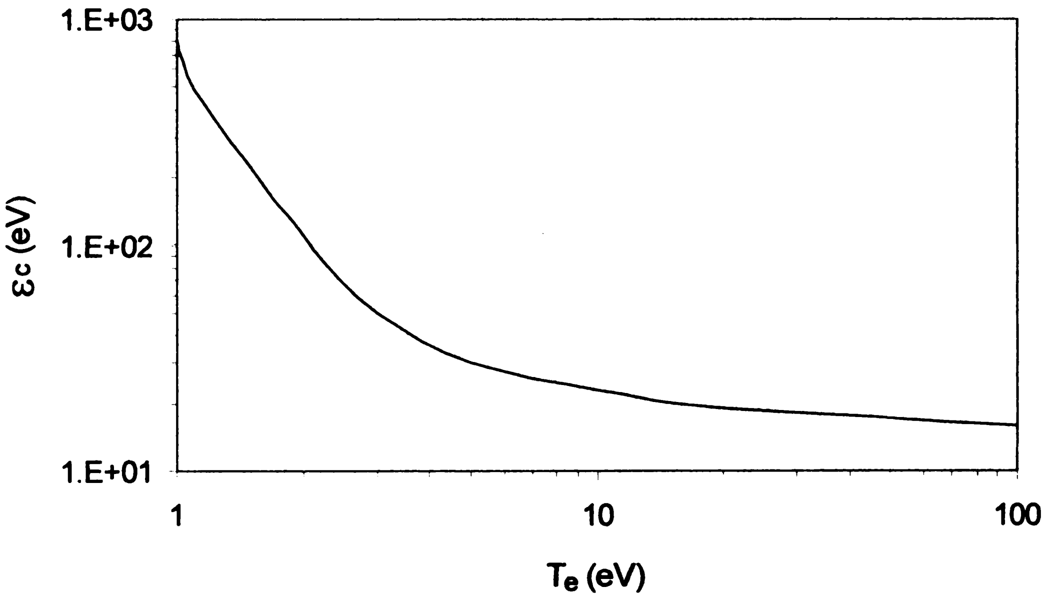

Figure 7.2 Collisional energy loss per electron-ion pair created, ε_c, versus T_e in argon discharge (compiled by Vahedi, 1993) [16].

In the high pressure regime, the discharge density becomes non-uniform. The transport is diffusive and the density profile is well described by a J_o Bessel function variation along the radial axis and a cosine variation along the length of the discharge. In this regime, the electron temperature can be estimated from the gas density (n_g) and the diffusion length (Λ) as can be seen in figure 7.3. Gas density is obtained using equation 7.1.

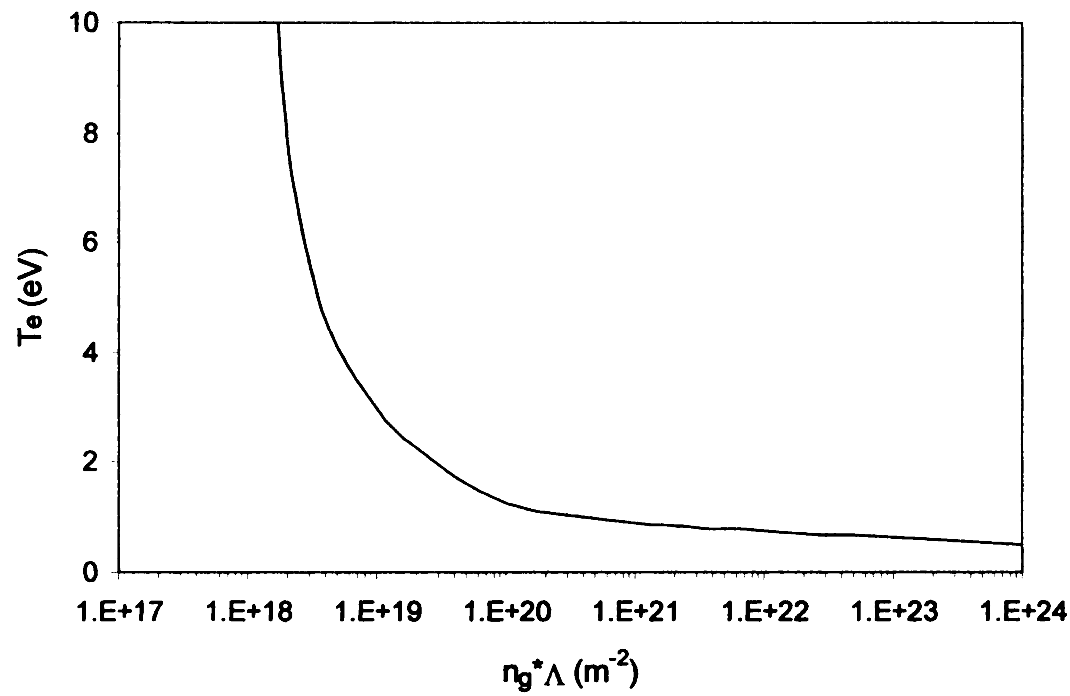

Figure 7.3 T_e versus n_g*Λ for non-uniform argon discharge (compiled by P.Mak, 1994) [ECE989A].

The diffusion length Λ can be derived from the Helmholtz equation for diffusion:

$$\nabla^2 n + \left(\frac{v_{iz}}{D_a}\right) n = 0 \tag{7.8}$$

where v_{iz} is the ionization frequency and D_a is the ambipolar diffusion coefficient. In cylindrical coordinates and assuming that the discharge is ϕ symmetric, equation 7.8 becomes:

$$\frac{\partial^2 n}{\partial r^2} + \frac{1}{r}\frac{\partial n}{\partial r} + \frac{\partial^2 n}{\partial z^2} + \left(\frac{v_{iz}}{D_a}\right) n = 0 \tag{7.9}$$

Using the separation of variables technique $n(r,z) = R(r)Z(z)$ and assuming that the density is zero at the wall and at the ends of the plasma along its length, the solution for the differential equation are:

$$Z(z) = A\cos\left(\frac{\pi}{l}z\right) \tag{7.10}$$

for the axial solution, and

$$R(r) = A\,J_0\left(\frac{\hat{\chi}_{01}}{R}r\right) \tag{7.11}$$

and

$$\frac{1}{\Lambda^2} = \left(\frac{\hat{\chi}_{01}}{R}\right)^2 + \left(\frac{\pi}{l}\right)^2 = \frac{v_{iz}}{D_a} \tag{7.12}$$

for the radial solution, where $\hat{\chi}_{01} = 2.405$ is the first zero of the Bessel function, and $D_a \approx \left(T_e/T_i\right)^{1/2} \lambda_i\, u_B$.

The peak charge density for the high pressure regime can be estimated from the power balance calculation.

$$P_{loss} = e\,\varepsilon_T \oint_A \vec{\Gamma}_A \bullet d\vec{A} = P_{abs} \tag{7.13}$$

The total flux in the axial direction is

$$\int \vec{\Gamma}_{ends} = 2\int_0^{2\pi}\int_0^R \left(\Gamma|_{z=l/2} \bullet \hat{z}\right) r\,dr\,d\theta = 4\pi\, D_a \frac{\pi}{l} n_o \int_0^R J_0\left(\frac{\hat{\chi}_{01}}{R}r\right) r\,dr$$

$$\int \vec{\Gamma}_{ends} = 4\pi\, D_a \frac{\pi}{l} n_o \frac{R^2}{\chi_{01}} J_1(\hat{\chi}_{01}) \tag{7.14}$$

The total flux in the radial direction is

$$\int \vec{\Gamma}_{rad} = \int_{-l/2}^{l/2} \int_{0}^{2\pi} \Gamma \, |_{r=R} \, r \, d\theta \, dz = -2\pi \frac{\hat{\chi}_{01}}{R} D_a \, n_o \, J_1(\hat{\chi}_{01}) \int_{-l/2}^{l/2} \cos\left(\frac{\pi}{l} z\right) dz$$

$$\int \vec{\Gamma}_{rad} = 4\pi \frac{\hat{\chi}_{01}}{R} D_a \, n_o \frac{l}{\pi} J_1(\hat{\chi}_{01}) R \tag{7.15}$$

An equality for P_{abs} and the total flux can be achieved by combining equation 7.14 and equation 7.15 and putting them in the equation 7.13. The peak charge density can be calculated by re-arranging the power balance equation into the following form:

$$n_o = \frac{P_{abs}}{4\pi \, D_a \, J_1(\hat{\chi}_{01}) \left[\frac{R^2 \pi}{\hat{\chi}_{01}} + \frac{l \, \hat{\chi}_{01}}{\pi} \right] e \, \varepsilon_T} \tag{7.16}$$

where $J_1(\hat{\chi}_{01}) \approx 0.519$

7.3 Results and discussions

Using the global model derived above, the electron temperature and electron density of argon discharge were calculated. From chapter 5, the hydrogen and nitrogen rotational temperatures of argon dominated discharges were around 1000K. Thus the gas temperature (T_g) for these calculations was set to 1000 K. However, the rotational temperature slighty increases as the pressure increases. Hence, the error in calculated value may increase as the pressure increases. Global model calculations were performed for pressures lower than 100 Torr.

As shown in figure 7.4, the electron temperature decreases as the pressure increases, and the trends for both microstripline coupling structures are similar. As pressure increases, the number of collisions increases. This makes the electron temperature decrease; because when the electron collides with heavy species, it losses its energy.

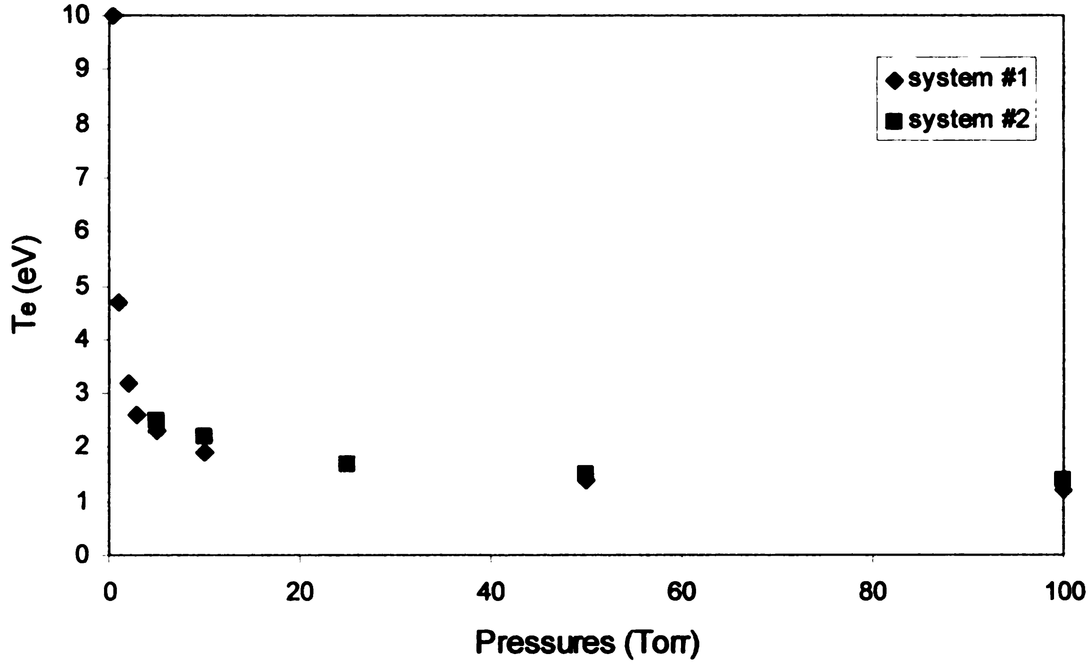

Figure 7.4 Comparison of the global model electron temperatures of argon discharges created in system #1 and system #2.

The measured electron temperatures from DLP diagnostics have slightly lower values as compared to the global model calculations. However, they both shows similar trend as seen in figure 7.5. Aliev [20] remarks for probe diagnostics is that for surface wave (SW) sustained discharges, the perturbation caused by probes inside the plasma and the resultant potential inaccuracies are aggravated by the fact that wave pattern, the basis of plasma maintenance, can be quite noticeably perturbed even outside the plasma, thus enlarging possible deviations of the measured plasma parameters from their unperturbed values.

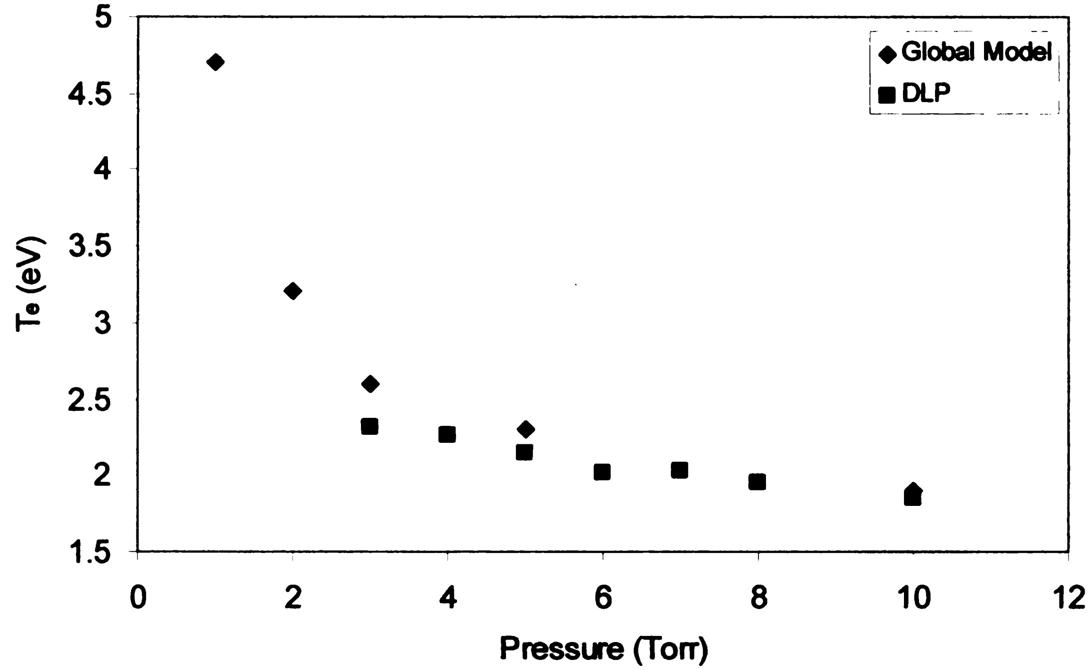

Figure 7.5 Comparison of the electron temperatures between the global model calculations and the results from DLP.

Figures 7.6 – 7.8 show the variation of peak charge densities for different P_{abs}, pressures, discharge tube sizes, and microstripline coupling structures. Overall, the charge density increases as the P_{abs} increases. However, there are cut regions at low P_{abs} where the density abruptly increases. Using the global model, charge density of argon discharges is calculated to be on the order of $10^{12} - 10^{15}$ cm^{-3}.

In terms of discharge tube sizes, higher peak charge density can be obtained using a 1 mm discharge tube rather than a 2 mm one. This follows the first criterion of plasma, discussed in chapter 2, that the smaller the dimension of the system, the higher the density.

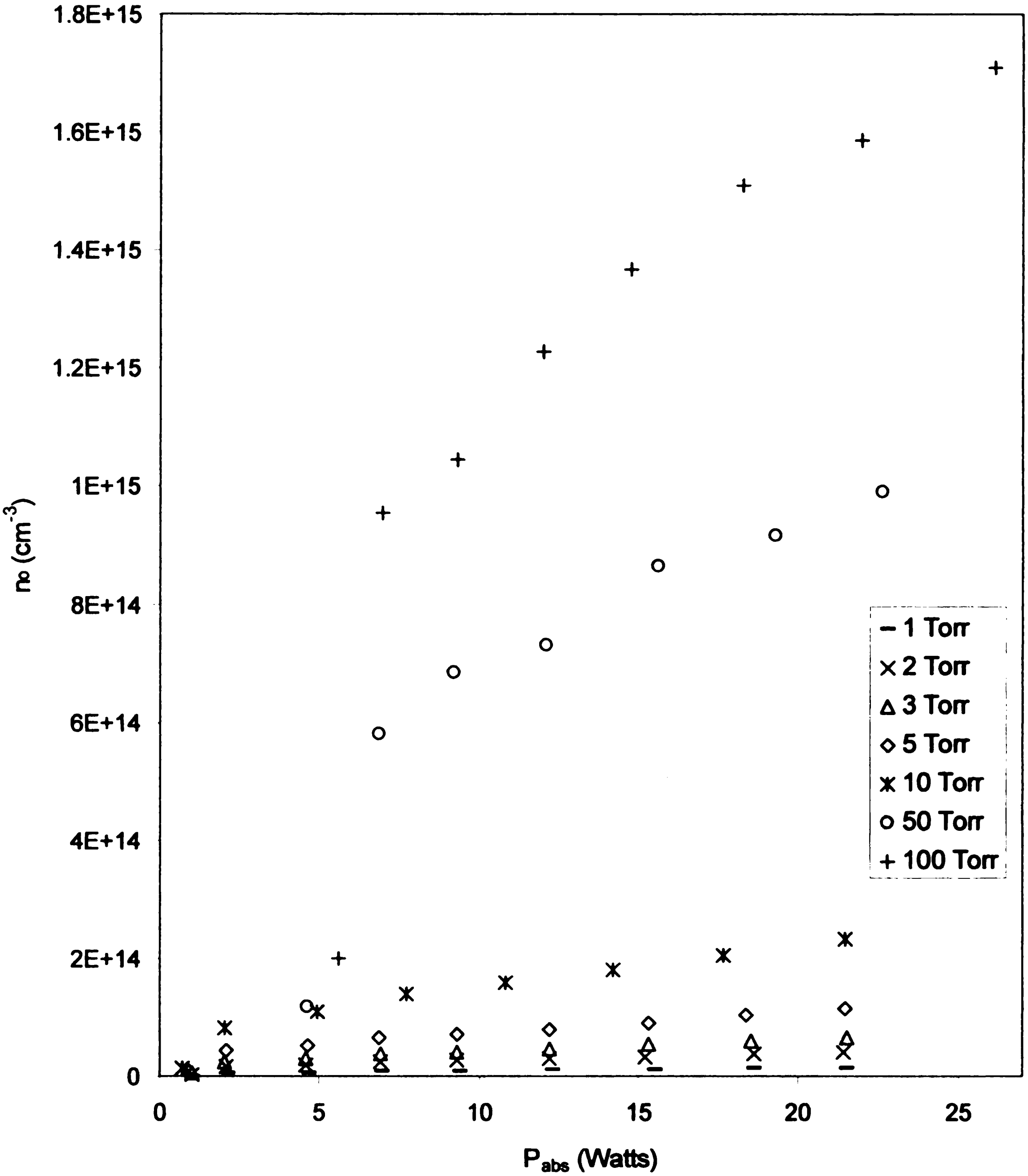

Figure 7.6 Peak charge density of argon discharge created using microstripline structure #1. Discharge tube size: 2 mm i.d.

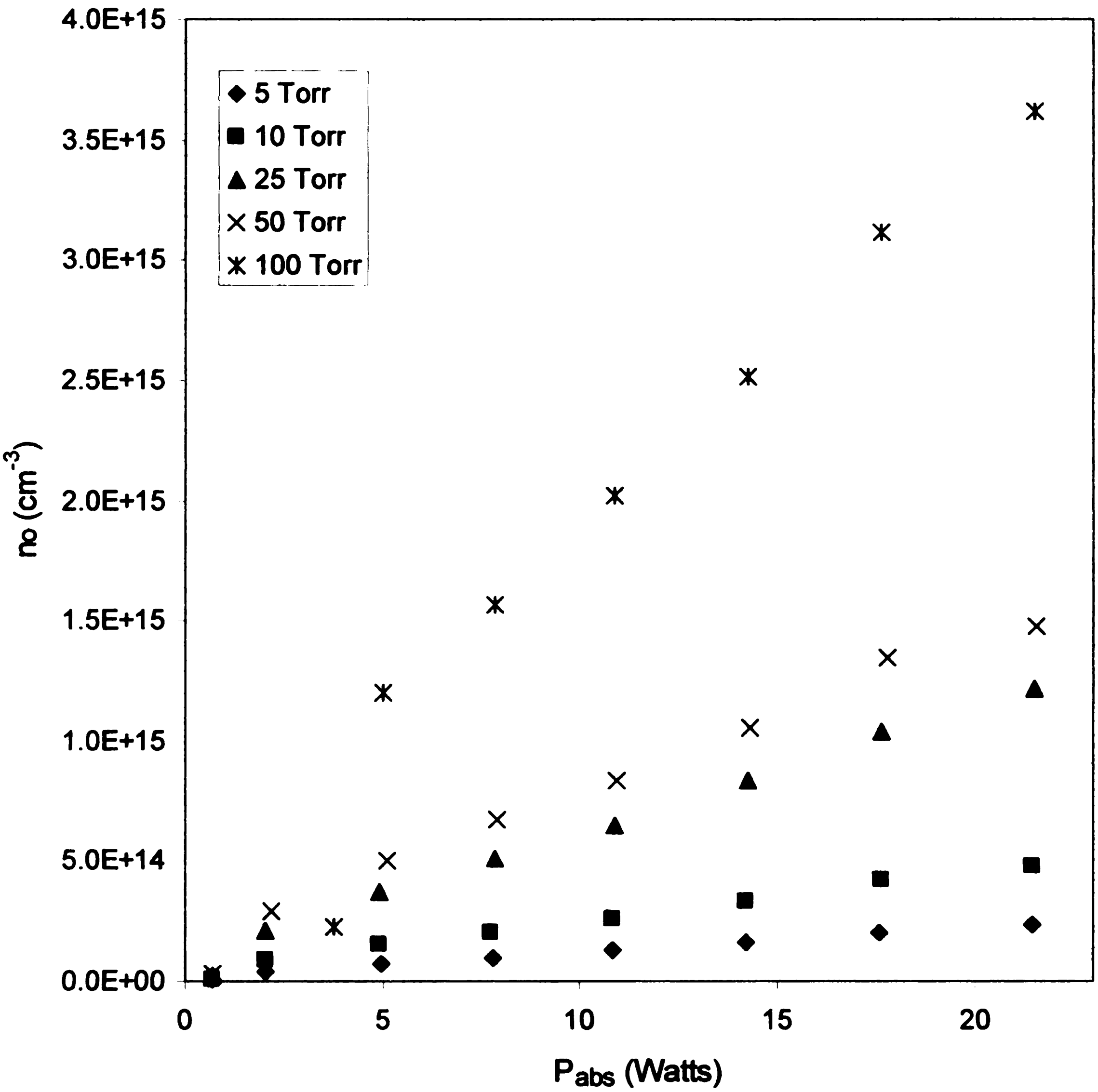

Figure 7.7 Peak charge density of argon discharge created using microstripline structure #1. Discharge tube size: 1 mm i.d.

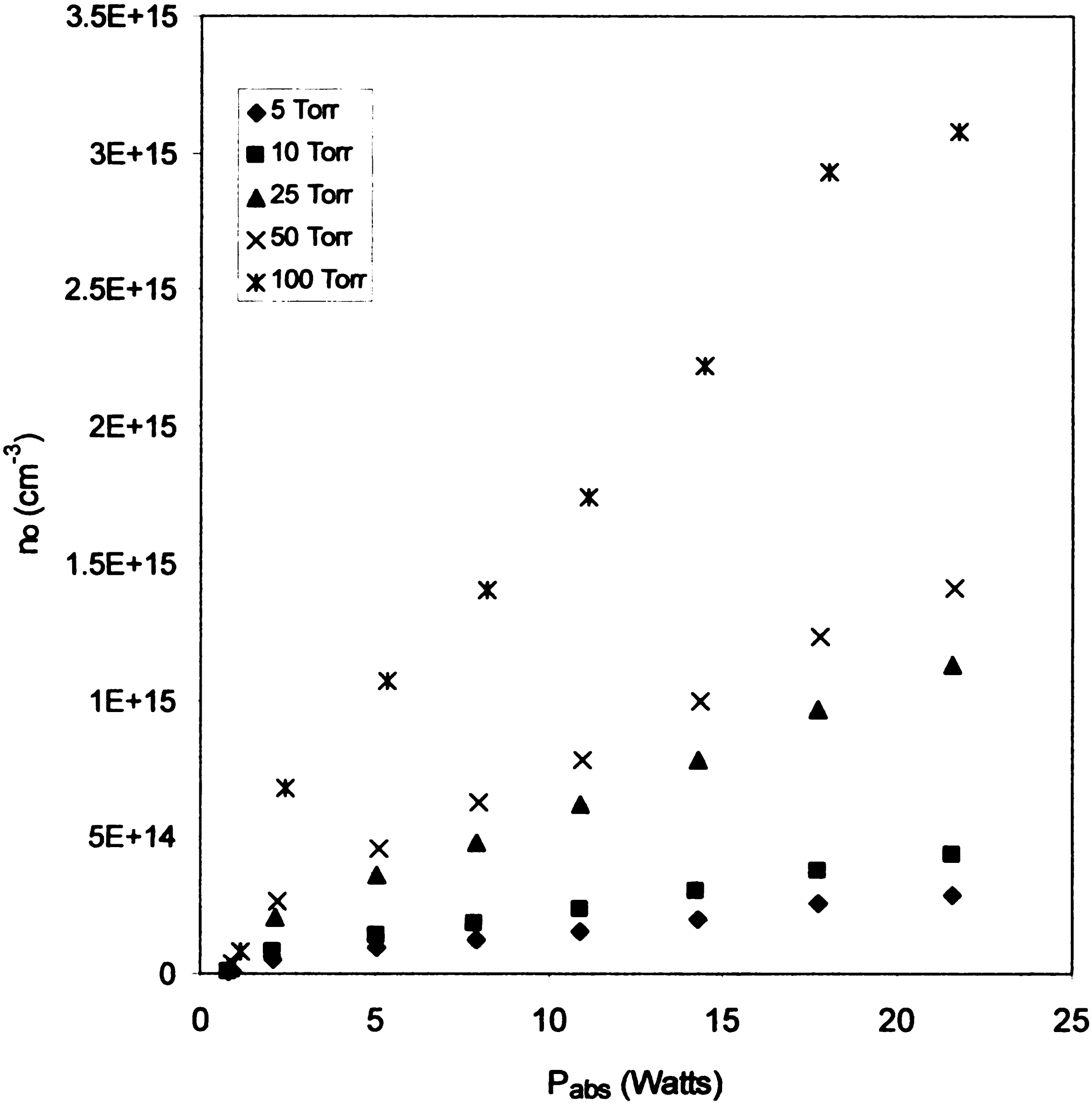

Figure 7.8 Peak charge density of argon discharge created using microstripline structure #2. Discharge tube size: 1 mm i.d.

The performance of both microstripline coupling structures in terms of power density is very similar, as shown in figure 7.7 and 7.8.

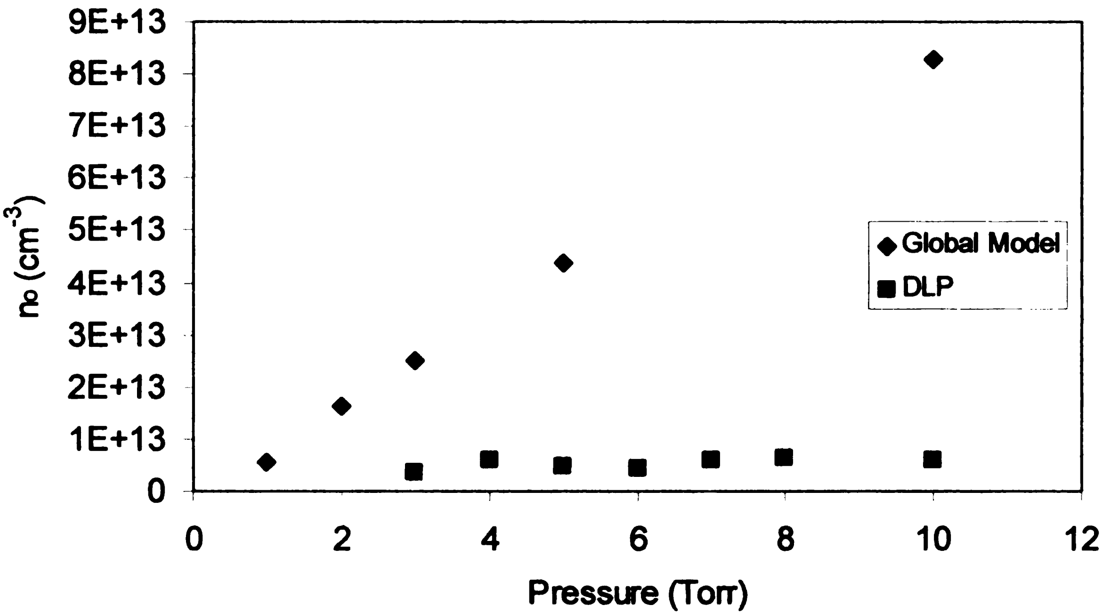

Figure 7.9 Comparison of calculated charge density from global model and measured charge density from DLP diagnostic.

From figure 7.9 it is seen that the measured charge density is lower than the calculated value. DLP diagnostic, discussed in chapter 6, measured the charge density at one end of the discharge. Aliev [20] explains that the axial density profile for surface wave sustained plasmas in cylindrical geometry has a linear function versus the axial coordinate z. The charge density is lower at the extreme z compared to the density near the source. The linear axial decrease of the charge density also depends on frequency, pressure, and discharge radius. The gradient becomes larger as the frequency increases and/or pressure increases and/or discharge radius decreases.

Table 7.1 Comparison of the charge density calculated using global model and measured from the Stark effect

	Global model	H_β	H_δ
Charge density	1.4×10^{13} cm^{-3}	6.6×10^{13} cm^{-3}	3.5×10^{13} cm^{-3}

Table 7.1 shows a comparison between calculated charge density from global model and the measured charge density from the Stark effect using OES. The densities are around 10^{13} cm^{-3}. Minor differences between the calculated and the measured value arise because the charge Stark effect phenomenon was observed from a mixture of Ar – H_2 discharge. Meanwhile, the global model calculations were based on pure argon discharges.

Chapter 8

Summary and Recommendations

8.1 Summary of Results

Two designs of a miniature microwave plasma source using microstripline technology have been developed. The plasma sources were able to create cylindrical discharges inside quartz tubes with 1 – 2 mm radii. The volume of the discharge increases as the power is increased. Discharge absorbed power densities varied from a few 10's W/cm^3 to over 700 W/cm^3 as pressure was increased and discharge tube size was decreased. The plasma sources can create pure argon discharges at atmospheric pressure with as low as 5 W of absorbed power. At atmospheric pressure, filament-like argon discharge can be generated.

At very low power, microstripline applicators generate the discharge in a similar fashion as the parallel plate reactors. However, with increasing power, a plasma surface wave (SW) discharge exists along a tube that extends perpendicular to the stripline. The behaviors of this SW sustained plasma were examined. Discharges can be divided by creating a branched tube.

Characteristics of the discharge were measured using optical emission spectroscopy and the double Langmuir probe. Using OES, the gas temperature of argon discharges was approximated to be around 1000 K for the pressure range from 1 – 10 Torr. As the pressure increased, gas temperature of the discharge slightly increased. The addition of more Ar in a mixture of Ar – H_2

discharge decreased the gas temperature. However, the addition of Ar in a mixture of Ar – N_2 discharge increased the temperature. The charge density was measured by observing the Stark broadened H_α and H_β lines of hydrogen in a mixture of Ar – H_2 discharge at 1 and 100 Torr. The charge density was on the order of 10^{13} cm^{-3} - 10^{14} cm^{-3}.

The charge density was also measured using the DLP diagnostic. The probes were inserted at the end of the discharge. From this measurement, the charge densities of argon plasmas for a pressure range form 3 – 10 Torr were 10^{12} – 10^{13} cm^{-3}. Discrepancies in the charge density measurement using OES and DLP occurred because of the linear decrease of the axial density profile for SW sustained plasmas. Specifically, OES measures the average density and DLP measures the density at the edge of the cylindrical discharge. Using DLP, the electron temperature of a pure argon discharge was observed to decrease as the discharge pressure increased. The electron temperature for argon plasmas in that pressure range were 1.8 – 2.3 eV.

The global analytical model was used to calculate the density and electron temperature for pure argon plasmas, which were created using microstripline coupling structures. The model was calculated based on the measured discharge volume, absorbed power, pressure, and gas temperature. From the global model, the electron temperature and peak charge density of the discharge were obtained. The calculated values of these fundamental plasma parameters roughly matched with the measured values from OES and the DLP diagnostic with only minor differences.

With the knowledge of the fundamental characteristics of the discharge, plasma validity can be checked from the plasma criteria explained in chapter 2. For a pure argon discharge inside a 2 mm tube with 5 Torr pressure, the electron temperature (T_e) is 2.3 eV, gas temperature (T_g) is 1000 K, and electron density (n_e) is $6x10^{13}$ cm^{-3}. Using equation 2.2, the Debye length (λ_d) is found to be $1.45x10^{-4}$ cm. This proves that the discharge fulfills the first criterion of a plasma. Following the finding of λ_d, the second plasma criterion can also be fulfilled. N_d in this case is around 773.

The third criterion deals with the plasma oscillation frequency (ω_{pe}) and mean time between collisions with neutral atom (τ). The approximate formula for plasma oscillation is:

$$\omega_{pe} \approx 2\pi \times 9\sqrt{n_e} \qquad (8.1)$$

and τ is:

$$\tau = \frac{1}{K n_g} \qquad (8.2)$$

where K is the collision rate constant. For argon gas, K is approximately 10^{-13} m^3/s [13], and n_g can be derived using equation 7.1. The calculated value for n_g is $4.83x10^{22}$ m^{-3}. Thus, τ is $2x10^{-10}$ s and ω_{pe} is $4.4x10^{11}$ s^{-1}. This proves that the third plasma criterion also fulfilled.

8.2 Recommendations

This study created a miniature microwave plasma source. Future work on the development of microstripline plasma sources should focus on an improved design to minimize power loss due to radiation leakage or characteristic impedance mismatch. Also, reducing the overall size of the coupling structure is of the interest.

Another study of interest would be using this miniature plasma source design for small scale surface treatments or other applications. The microstripline technology has the potential for being scaled to produce plasmas on a chip.

APPENDICES

Appendix A

Color Pictures of the Miniature Microstripline Plasma Source

Images In this Thesis are presented in color.

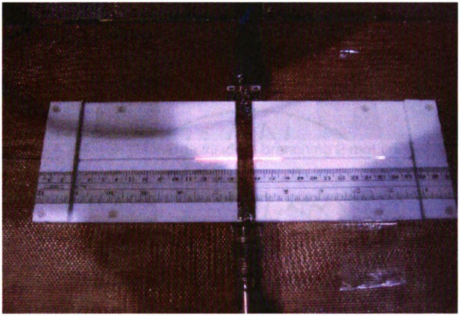

Figure A.1 Argon discharge inside 1 mm i.d. quartz tube generated using microstripline structure #1.

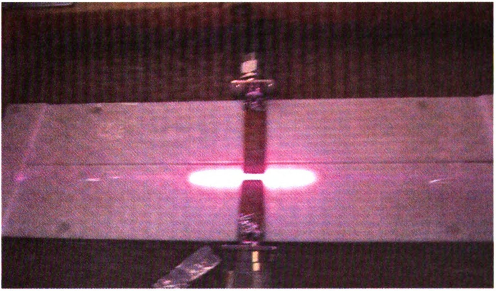

Figure A.2 Argon discharge inside 1 mm i.d. quartz tube generated using microstripline structure #2.

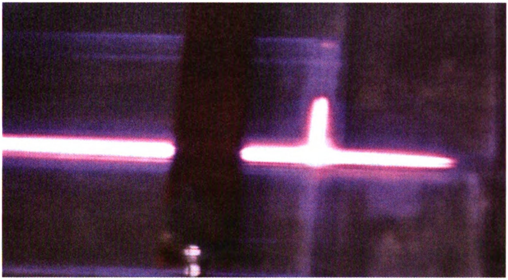

Figure A.3 Argon discharge inside a branching 2 mm i.d. quartz tube.

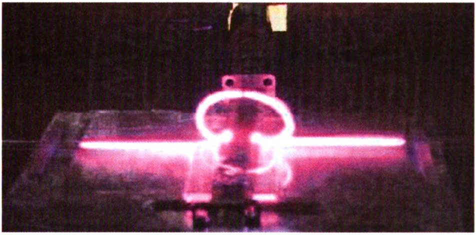

Figure A.4 Argon discharge inside an oval shape 2 mm i.d. quartz tube.

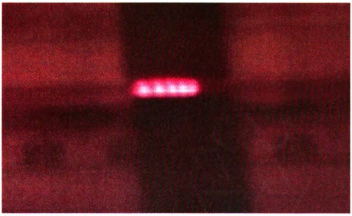

Figure A.5 Atmospheric pressure argon discharge showing five filament-like discharges.

Appendix B

QBasic Program for the Optical Emission Spectroscopy

```
'+-------------------------------------------------------------------------------+
'|Author: Jayakumaran Sivagnaname; Date: July 1998                              |
'|Monochromator Spec: 2400 lines/mm                                             |
'|grating: offset=43x2 Angstrom (updated:08/10/2002)                            |
'|Mcpherson Monochromator must be scanned with increasing wavelength ONLY
'|Re-written by Jefrri Narendra; July 2002                                      |
'|Modified by Stanley Zuo and Kadek Hemawan: August 2002                        |
'+-------------------------------------------------------------------------------+

'$INCLUDE: 'c:\gpib-dos\qbasic\qbdecl.bas'
DECLARE SUB ReportError (fd%, errmsg$)
DECLARE SUB FILEWRT (prev, pico%, cyc%, i%, RSTALN#, resol#, tottim%,
sec%, TEMP$, BUFF$, count%)
DECLARE SUB RESTART ()

CONST black = 0
CONST blue = 1
CONST green = 2
CONST cyan = 3
CONST red = 4
CONST magenta = 5
CONST brown = 6
CONST white = 7
CONST grey = 8
CONST lightblue = 9
CONST lightgreen = 10
CONST lightcyan = 11
CONST lightred = 12
CONST lightmagenta = 13
CONST yellow = 14
CONST brightwhite = 15

COMMON resol#, cyc%, count%, pico%, i%, RSTALN#, ENDLN!, RENDLN!,
speed!, tottim%, sec%, BUFF$, TEMP$, prev

st1$ = "waveln=["
st2$ = "value=["
EN$ = "]"
path$ = "C:\QB45\Data"
```

```
DO WHILE confirm$ <> "y" AND confirm$ <> "Y"
  CLS
  SCREEN 0
  LOCATE 1, 3
  PRINT "Enter a file name [mmddTrialNumber]: ";
  INPUT filenm$
  PRINT "Is the filename correct[y/n]";
  INPUT confirm$
LOOP


'-------- Initialize the device --------
CALL IBDEV(0, 14, 0, T10s, 1, 0, pico%)
IF (pico% < 0) THEN
  CALL ReportError(pico%, "Could not open picoAmpmeter.")
END IF

'---- Clear the picoampmeter and set it to default ----
'CALL IBWRT(pico%, "DCL")
'IF (IBSTA% AND EERR) THEN
  'CALL ReportError(pico%, "Can't clear the picoAmpmeter")
'END IF


CLS    'Clear the screen
OPEN path$ + "\W" + filenm$ + ".m" FOR OUTPUT AS #1'store wavelength
value
PRINT #1, st1$
OPEN path$ + "\D" + filenm$ + ".m" FOR OUTPUT AS #2'store current value
PRINT #2, st2$
LOCATE 2, 3
PRINT "Values of wavelength stored in file "; path$ + "\W" + filenm$ + ".m";
LOCATE 3, 3
PRINT "Values of current stored in file "; path$ + "\D" + filenm$ + ".m";


'-------- Declare temporary variables and constants --------
BUFF$ = SPACE$(20)
TEMP$ = SPACE$(20)
cycle% = 2
count% = 1
prev = 1E-11

'-------- Taking input parameters--------
COLOR green, black
```

```
LOCATE 4, 3
PRINT "Program used for the spectrometer with 2400 lines/mm grating"
COLOR white, black
LOCATE 5, 3
PRINT "Enter the initial scan wavelength [A]";
INPUT STALN!
RSTALN! = 2 * STALN!
RSTALN# = RSTALN!

COLOR yellow, blue
LOCATE 7, 3
PRINT "Set the counter to"; STALN! + (86 / 2)
COLOR white, black
LOCATE 9, 3
PRINT "Enter the final scan wavelength [A]";
INPUT ENDLN!
RENDLN! = 2 * ENDLN!

LOCATE 10, 3
PRINT "End point as observed from the counter [A]"; ENDLN! + (86 / 2);
LOCATE 11, 3
PRINT "Enter the speed scanning drive [A/min]";
INPUT speed!

speed! = speed! * 2     'Scan speed is only half of the reading of at spectro meter

'IF speed! <= 0 THEN
  'speed! = 100
  'LOCATE 11, 3
  'PRINT "Default speed (100) is used. Continue?";
  'INPUT ans$

  'IF ans$ = "Y" THEN
  'END IF
'END IF

LOCATE 13, 3
resol# = speed! / (cycle% * 60)
PRINT "Warning: The minimum number for resolution : "; resol#; " [Angstrom]"
LOCATE 15, 3
PRINT "Enter a resolution multiplication of above (in integer) ";
INPUT multiple!        'The reason of above is to make sure we a precised round
up (see sec%=sec#)
multiple% = multiple!

resol# = resol# * multiple%
```

```
IF resol# = 0 THEN
resol# = speed! / (cycle% * 60)
END IF

COLOR white, red
LOCATE 16, 3
PRINT "Actual resolution you used is: "; resol#; " [Angstrom]"

sec# = resol# * (cycle% * 60) / speed!
sec% = sec#

'--------- Accuracy check of old code, NO need any more --------
'IF (sec% - sec#) > .000001 THEN
  'COLOR white, red
  'LOCATE 16, 3
  'PRINT "Error in calculation is more likely to occur";
'END IF
'-------------------------------------------------------

COLOR white, black
LOCATE 17, 3
PRINT "Data acquisition interval [seconds]"; sec%
TEMP! = ENDLN! - STALN!

IF TEMP! < 0 THEN
  LOCATE 19, 3
  PRINT "Please scan the spectrometer with increasing value of wavelength"
  CALL RESTART
ELSE
  numofsamples# = (RENDLN! - RSTALN!) / resol#
  numofsamples% = numofsamples#
  LOCATE 19, 3
  PRINT "No. of samples will be: "; numofsamples%

  tottim! = numofsamples# / cycle%
  tottim% = tottim!
  LOCATE 20, 3
  PRINT "Total time to be taken [in seconds]: "; tottim%

  endtim# = tottim! / sec#
  endtim% = endtim#

  LOCATE 22, 3
  COLOR white, red
  PRINT "Set Scan drive scanning switch to H";
```

```
LOCATE 23, 3
COLOR white, red
PRINT "Please check the PicoAmpMeter is at RMT mode";

LOCATE 24, 3
PRINT "Start the Program and the Scan drive simultaneously";
COLOR white, black
LOCATE 25, 3
PRINT "Hit any key to start";

'-------- Set GPIB bus on continuous talk --------
CALL IBWRT(pico%, "T0X")

'-------- Set pico% to RMT mode --------
CALL IBWRT(pico%, "REN")
IF (IBSTA% AND EERR) THEN
  CALL ReportError(pico%, "Can't set picoAmpmeter to the remote mode")
END IF

'-------- Set pico$ to AUTO range -------
CALL IBWRT(pico%, "T0X")
CALL IBWRT(pico%, "R0X")
IF (IBSTA% AND EERR) THEN
  CALL ReportError(pico%, "You may have to manually set to AUTO range")
END IF


WHILE INKEY$ = ""
WEND


COLOR green, black
i% = 1

CLS
LOCATE 1, 1
PRINT "Program reads data from picoammeter in "; sec% / cycle%; "- second
interval";

LOCATE 2, 1
PRINT "No. of samples to be taken"; numofsamples%;

LOCATE 3, 1
PRINT "Total time will be: "; tottim%; "seconds";
```

```
  LOCATE 5, 1
  PRINT "Wavelength[A] Current[amps] Sample No. Cycle/Sec. Time
remaining[sec]"

  TIMER ON
    ON TIMER(sec%) GOSUB disp
    start! = TIMER

    DO
    LOOP WHILE (i% - 1) * sec% < tottim%  'keep timer on if remaining time is
greater than 0

    finish! = TIMER
  TIMER OFF

  PRINT " "
  PRINT "Total execution time = "; finish! - start!; "Seconds"
  PRINT #1, EN$
  PRINT #2, EN$

  '------ Store data to files ------
  OPEN path$ + "\X" + filenm$ + ".m" FOR OUTPUT AS #3'store matlab EXE file
    PRINT #3, "clear all;clc"
    PRINT #3, "W" + filenm$
    PRINT #3, "D" + filenm$
    PRINT #3, "plot(waveln,abs(value),'g');pause(3);sm5;xlabel('Wavelength
A');ylabel('Current amps');"
    PRINT #3, "title('Emission Spectrum');grid;"
    PRINT "Execute "; path$ + "\X" + filenm$ + ".m"; " in matlab to view plot"
  CLOSE

  CALL RESTART        'Finish or restart the program

  END

'------ A sub program based on the timer ------
disp:
 FOR cyc% = 1 TO cycle%
 CALL FILEWRT(prev, pico%, cyc%, i%, RSTALN#, resol#, tottim%, sec%,
TEMP$, BUFF$, count%)
 count% = count% + 1
 NEXT cyc%
 i% = i% + 1
RETURN

  END IF     'Following the last else statement
```

```
END          'Whole program ends

SUB FILEWRT (prev, pico%, cyc%, i%, RSTALN#, resol#, tottim%, sec%,
TEMP$, BUFF$, count%)

'--------- Trigger pico% for reading ---------
CALL IBWRT(pico%, "GET")

'--------- Read the picoAmeter ---------
CALL IBRD(pico%, BUFF$)
'IF (IBSTA% AND EERR) THEN
  'CALL ReportError(pico%, "Could not read picoAmpmeter setting.")
'END IF

'To enforce read function, don't use error checking function to
'avoid read failure

'--------- Store the value last read in TEMP ---------
TEMP$ = MID$(BUFF$, 5, 20)
y = VAL(RTRIM$(TEMP$))

IF (y > .00001) THEN
  y = prev
END IF

'--------- Calculate and display parameters onto screen ---------
prev = y
RSTALN# = RSTALN# + resol#
RSTALN! = RSTALN#

WRITE #1, RSTALN!
WRITE #2, -1 * y
LOCATE 7, 1
PRINT RSTALN!, y, count%, cyc%, tottim% - (sec% * i%)

END SUB

SUB ReportError (fd%, errmsg$) STATIC

PRINT "Error =", IBERR%; errmsg$

IF (fd% <> -1) THEN
  PRINT ("Cleanup: taking board off-line")
  CALL IBONL(fd%, 0)
END IF
```

```
STOP   'Abort program

END SUB

SUB RESTART

 '-------- Place the Device Offline --------
 CALL IBONL(pico%, 0)

 '-------- Instruct the User Terminating the Program --------
 PRINT " "
 COLOR white, red
 PRINT "Switch off the Spectrometer drive"
 COLOR white, black
 PRINT "Press any key to restart or end the program";

 WHILE INKEY$ = ""
 HTONE = 2000: LTONE = 550: DELAY = 500
 FOR count = HTONE TO LTONE STEP -10
 SOUND count, DELAY / count
 NEXT count
 HTONE = 780: RANGE = 650
 FOR count = RANGE TO -RANGE STEP -4
 SOUND HTONE - ABS(count), .3
 count = count - 2 / RANGE
 NEXT count
 WEND

END SUB
```

Appendix C

QBasic Program for the Double Langmuir Probe

```
'+----------------------------------------------------------------------------+
'| Double Langmuir Probe I-V curve measurement                                |
'| Programed by Meng-hua Tsai, customized by  Mark  Perrin 9/97               |
'| Modified by Stanley Zuo 02/02                                              |
'+----------------------------------------------------------------------------+

 ' $INCLUDE: 'c:\gpib-dos\qbasic\qbdecl.bas'

  DECLARE SUB ReportError (fd%, errmsg$)  ' Error subroutine

' Bring the Power suppply/ PicoAmp meter on-line

     CALL IBDEV(0, 1, 0, T1s, 1, 0, dm1%)
     IF (dm1% < 0) THEN
         CALL ReportError(dmm%, "Could not open Ampmeter.")
     END IF

     CALL IBDEV(0, 2, 0, T1s, 1, 0, dmm%)
     IF (dmm% < 0) THEN
         CALL ReportError(dmm%, "Could not open Power Supply.")
     END IF

  CLS
  PRINT "           Double Langmuir probe I-V curve Measurement"
  PRINT ""
  INPUT "Input filename for storing data :"; name$
  name$ = "c:\zuo\dlp\" + name$
  PRINT "Data stored in file :"; name$
  OPEN name$ FOR OUTPUT AS #2

  INPUT "Input voltage increment (volt) = "; dv!
  totl% = 100 / dv! + 1
  PRINT #2, totl%
  ini! = 0
  num% = 0

  DO WHILE ini! < 100
    num% = num% + 1
    ini! = (num% - 1) * dv!
```

```
  Vi$ = STR$(ini!)

  LOCATE 8, 1
  PRINT "vi="; Vi$

'Set voltage to volmeter

  devbuf$ = "VSET " + Vi$
  CALL IBWRT(dmm%, devbuf$)
'  CALL IBWRT(dmm%, "VOUT?")

'Request data readings from device

'  LOCATE 20, 1
'  INPUT "Ready to take data (y/n)?", idx$
'  IF idx$ = "n" THEN
'    CALL IBONL(dmm%, 0)
'    CALL IBONL(dm1%, 0)
'    END
'  ELSE

'  ctime$ = TIME$
'  TIME$ = "00:00:00"
'  WHILE TIME$ < "00:00:03"
'    LOCATE 21, 1
'    PRINT TIME$
'  WEND

'Take the average of 20 readings for each vol/cur point
  Vo! = 0
  Io! = 0
  Reading$ = SPACE$(20)

  FOR i% = 1 TO 20

      CALL IBWRT(dmm%, "VOUT?")
     ' IF (IBSTA% AND EERR) THEN
     '     CALL ReportError(dmm%, "Could not trigger multimeter")
     ' END IF

    ' Read data from dmm

      CALL IBRD(dmm%, Reading$)
      IF (IBSTA% AND EERR) THEN
         CALL ReportError(dmm%, "Could not read data from power supply")
      END IF
```

```
     'Remove blank spaces in READING$ and store the result in RD$.

      RD$ = LEFT$(Reading$, IBCNT%)

     'Request current reading from dm1

     'CALL IBWRT(dm1%, "Amp; Auto")
     'IF (IBSTA% AND EERR) THEN
     '   CALL ReportError(dm1%, "Can't  trigger  Ampmeter")
     'END IF

      CALL IBRD(dm1%, Reading$)
      IF (IBSTA% AND EERR) THEN
        CALL ReportError(dm1%, "Can't read data from Amp meter")
      END IF

    ' rd1$ = LEFT$(Reading$, IBCNT%)
      rd1$ = Reading$

    ' LOCATE 9, 1
    ' PRINT LEN(RD$); LEN(rd1$)
    ' PRINT "Voltage/Current read: "; RD$; rd1$

      vol! = VAL(RD$) - 50
      cur! = VAL(rd1$)

      cur! = cur! * 1000
      LOCATE 12, 1
      PRINT "Voltage(V)/current(mA) :                    "
      LOCATE 12, 1
      PRINT "Voltage(V)/current(mA) :"; vol!; cur!

      Io! = Io! + cur!
  NEXT i%
 ' END IF

  Io! = Io! / 20
  PRINT "Average currenr =               "
  LOCATE 13, 1
  PRINT "Average current ="; Io!
  PRINT #2, vol!; Io!
 LOOP


'Take dmm off-line
```

```
  CLOSE #2
  CALL IBONL(dmm%, 0)
  CALL IBONL(dm1%, 0)

  END

SUB ReportError (fd%, errmsg$) STATIC

  PRINT "Error = ", IBERR%; errmsg$

  IF (fd% <> -1) THEN
    PRINT ("Cleanup: taking board off-line")
    CALL IBONL(fd%, 0)
  END IF

  STOP            ' Abort program

END SUB
```

Appendix D

Discharge Volume and Power Density Measurements Results

D.1 Argon Discharges

D.1.1. Microstripline Structure #1

D.1.1.1. 1 mm i.d. discharge tube

D.1.1.1.1. Flow rate: 2 sccm

Pressure: 0.08 Torr					
Absorbed(W)	Left	Right	Length (cm)	Vol(cm^3)	Density(Wcm^{-3})
0.7	6.7	8.1	1.4	1.10E-02	61.8
1.2	6.4	8.1	1.7	1.34E-02	91.8
4.0	5.9	8.9	3.0	2.36E-02	170.9
6.6	5.7	9.0	3.3	2.59E-02	255.6
9.7	5.4	9.2	3.8	2.98E-02	324.6
13.1	5.3	9.3	4.0	3.14E-02	417.4
16.5	5.7	9.0	3.3	2.59E-02	637.8
20.5	4.9	9.6	4.7	3.69E-02	555.7

Pressure: 5.0 Torr					
Absorbed(W)	Left	Right	Length (cm)	Vol(cm^3)	Density(Wcm^{-3})
1.5	6.2	8.5	2.3	1.81E-02	80.3
4.0	5.8	8.9	3.1	2.43E-02	165.4
6.9	5.5	9.1	3.6	2.83E-02	242.3
9.9	5.1	9.5	4.4	3.46E-02	286.9
13.3	5.0	9.6	4.6	3.61E-02	369.2
16.8	5.1	9.4	4.3	3.38E-02	496.1
20.7	4.8	9.8	5.0	3.93E-02	528.1

Pressure: 10 Torr					
Absorbed(W)	Left	Right	Length (cm)	Vol(cm^3)	Density(Wcm^{-3})
1.4	6.2	8.2	2.0	1.57E-02	88.8
4.0	5.8	8.9	3.1	2.43E-02	165.4
7.0	5.3	9.3	4.0	3.14E-02	221.7
10.0	5.0	9.6	4.6	3.61E-02	277.5
13.5	5.0	9.6	4.6	3.61E-02	372.3
16.9	5.0	9.6	4.6	3.61E-02	468.4
20.8	4.8	9.9	5.1	4.01E-02	519.1

Pressure: 25 Torr					
Absorbed(W)	Left	Right	Length (cm)	Vol(cm^3)	Density(Wcm^{-3})
1.5	6.2	8.1	1.9	1.49E-02	97.2
4.2	5.8	8.9	3.1	2.43E-02	172.4
7.1	5.4	9.2	3.8	2.98E-02	237.1
10.1	5.1	9.4	4.3	3.38E-02	300.2
13.6	5.0	9.6	4.6	3.61E-02	375.5
17.0	5.2	9.5	4.3	3.38E-02	502.8
20.9	4.9	9.7	4.8	3.77E-02	554.6

Pressure: 50 Torr					
Absorbed(W)	Left	Right	Length (cm)	Vol(cm^3)	Density(Wcm^{-3})
4.3	5.7	8.1	2.4	1.88E-02	225.6
7.3	5.5	9.1	3.6	2.83E-02	258.2
10.3	5.3	9.3	4.0	3.14E-02	328.1
13.8	5.2	9.4	4.2	3.30E-02	418.0
17.2	5.2	9.4	4.2	3.30E-02	521.6
21.1	5.0	9.7	4.7	3.69E-02	571.0

D.1.1.1.2. Flow rate: 10 sccm

Pressure: 0.08 Torr					
Absorbed(W)	Left	Right	Length (cm)	Vol(cm^3)	Density(Wcm^{-3})
0.6	6.1	8.6	2.5	2.0E-02	29.6
1.9	5.5	9.3	3.8	3.0E-02	63.7
4.8	4.7	10.1	5.4	4.2E-02	113.5
7.6	4.2	10.6	6.4	5.0E-02	152.0
10.6	4.0	10.8	6.8	5.3E-02	199.3
14.1	4.0	10.8	6.8	5.3E-02	263.5
17.5	3.6	11.2	7.6	6.0E-02	293.9
21.4	3.5	11.2	7.7	6.0E-02	353.2

Pressure: 5.0 Torr					
Absorbed(W)	Left	Right	Length (cm)	Vol(cm^3)	Density(Wcm^{-3})
0.7	5.9	8.8	2.9	2.28E-02	30.4
2.0	5.2	9.6	4.4	3.46E-02	58.3
5.0	4.4	10.4	6.0	4.71E-02	105.8
7.8	3.8	10.9	7.1	5.58E-02	140.0
10.8	3.5	11.3	7.8	6.13E-02	176.5
14.2	3.4	11.4	8.0	6.28E-02	225.7
17.6	3.4	11.4	8.0	6.28E-02	280.1
21.5	3.2	11.6	8.4	6.60E-02	325.4

Pressure: 10 Torr					
Absorbed(W)	Left	Right	Length (cm)	Vol(cm^3)	Density(Wcm^{-3})
0.7	5.9	8.8	2.9	2.28E-02	30.4
2.0	5.2	9.6	4.4	3.46E-02	58.3
4.9	4.3	10.4	6.1	4.79E-02	102.9
7.8	3.8	10.9	7.1	5.58E-02	139.0
10.8	3.5	11.3	7.8	6.13E-02	176.5
14.2	3.4	11.4	8.0	6.28E-02	225.7
17.7	3.5	11.3	7.8	6.13E-02	288.2
21.5	3.2	11.6	8.4	6.60E-02	325.4

Pressure: 25 Torr					
Absorbed(W)	Left	Right	Length (cm)	Vol(cm^3)	Density(Wcm^{-3})
0.7	5.9	8.8	2.9	2.28E-02	30.4
2.0	5.1	9.6	4.5	3.53E-02	57.0
4.9	4.3	10.4	6.1	4.79E-02	102.9
7.9	3.8	11.0	7.2	5.65E-02	139.1
10.9	3.5	11.3	7.8	6.13E-02	177.4
14.2	3.4	11.3	7.9	6.20E-02	229.5
17.7	3.4	11.3	7.9	6.20E-02	284.6
21.5	3.3	11.5	8.2	6.44E-02	334.2

Pressure: 50 Torr					
Absorbed(W)	Left	Right	Length (cm)	Vol(cm^3)	Density(Wcm^{-3})
0.7	5.8	8.1	2.3	1.81E-02	38.4
2.2	5.3	9.5	4.2	3.30E-02	66.2
5.1	4.6	10.3	5.7	4.48E-02	113.9
7.9	4.1	10.7	6.6	5.18E-02	152.8
10.9	3.7	11.0	7.3	5.73E-02	190.6
14.3	3.6	11.2	7.6	5.97E-02	239.5
17.8	3.7	11.1	7.4	5.81E-02	305.7
21.6	3.3	11.5	8.2	6.44E-02	335.1

Pressure: 100 Torr					
Absorbed(W)	Left	Right	Length (cm)	Vol(cm^3)	Density(Wcm^{-3})
3.8	5.4	9.3	3.9	3.06E-02	122.9
5.0	5.1	9.6	4.5	3.53E-02	142.6
7.9	4.7	10.1	5.4	4.24E-02	185.4
10.9	4.5	10.3	5.8	4.56E-02	238.6
14.2	4.4	10.5	6.1	4.79E-02	297.2
17.7	4.4	10.5	6.1	4.79E-02	368.5
21.5	4.3	10.7	6.4	5.03E-02	428.3

Pressure: 150 Torr					
Absorbed(W)	Left	Right	Length (cm)	Vol(cm^3)	Density(Wcm^{-3})
3.5	5.6	8.9	3.3	2.59E-02	134.4
4.8	5.4	9.1	3.7	2.91E-02	165.7
7.8	5.0	9.6	4.6	3.61E-02	214.6
10.8	4.8	9.9	5.1	4.01E-02	268.6
14.1	4.7	10.0	5.3	4.16E-02	339.4
17.5	4.8	10.0	5.2	4.08E-02	429.5
21.3	4.5	10.3	5.8	4.56E-02	467.6

Pressure: 200 Torr					
Absorbed(W)	Left	Right	Length (cm)	Vol(cm^3)	Density(Wcm^{-3})
4.5	5.7	8.8	3.1	2.43E-02	183.9
7.5	5.3	9.3	4.0	3.14E-02	239.6
10.6	5.0	9.6	4.6	3.61E-02	294.6
14.0	5.0	9.7	4.7	3.69E-02	379.7
17.4	5.1	9.5	4.4	3.46E-02	504.4
21.2	4.8	9.9	5.1	4.01E-02	530.4

Pressure: 300 Torr					
Absorbed(W)	Left	Right	Length (cm)	Vol(cm^3)	Density(Wcm^{-3})
4.1	5.8	8.6	2.8	2.20E-02	188.3
7.0	5.8	8.8	3.0	2.36E-02	295.5
10.1	5.6	8.9	3.3	2.59E-02	389.0
13.5	5.5	9.0	3.5	2.75E-02	491.4
16.8	5.6	8.8	3.2	2.51E-02	666.6
21.0	5.1	9.9	4.8	3.77E-02	556.1

Pressure: 400 Torr					
Absorbed(W)	Left	Right	Length (cm)	Vol(cm^3)	Density(Wcm^{-3})
9.8	5.5	9.0	3.5	2.75E-02	356.5
13.2	5.4	9.0	3.6	2.83E-02	465.8
16.5	5.5	8.9	3.4	2.67E-02	619.0
20.5	5.4	9.0	3.6	2.83E-02	725.5

Pressure: 500 Torr					
Absorbed(W)	Left	Right	Length (cm)	Vol(cm^3)	Density(Wcm^{-3})
12.7	5.6	8.8	3.2	2.51E-02	503.9

D.1.1.1.3. Flow rate: 20 sccm

Pressure: 0.15 Torr					
Absorbed(W)	Left	Right	Length (cm)	Vol(cm^3)	Density(Wcm^{-3})
0.6	5.9	8.9	3.0	2.36E-02	27.0
2.0	5.2	9.7	4.5	3.53E-02	57.0
4.9	4.4	10.5	6.1	4.79E-02	102.9
7.8	4.0	10.9	6.9	5.42E-02	143.0
10.8	3.7	11.3	7.6	5.97E-02	180.2
14.1	3.6	11.3	7.7	6.05E-02	233.6
17.5	3.3	11.7	8.4	6.60E-02	265.9
21.4	3.2	11.7	8.5	6.68E-02	320.8

Pressure: 5.0 Torr					
Absorbed(W)	Left	Right	Length (cm)	Vol(cm^3)	Density(Wcm^{-3})
0.8	5.6	9.2	3.6	2.83E-02	28.5
2.1	5.0	9.9	4.9	3.85E-02	55.3
5.1	4.2	10.7	6.5	5.11E-02	99.8
7.9	3.7	11.2	7.5	5.89E-02	134.5
10.9	3.4	11.5	8.1	6.36E-02	170.9
14.3	3.2	11.6	8.4	6.60E-02	216.7
17.7	3.4	11.5	8.1	6.36E-02	278.4
21.6	3.0	11.9	8.9	6.99E-02	308.8

Pressure: 10 Torr					
Absorbed(W)	Left	Right	Length (cm)	Vol(cm^3)	Density(Wcm^{-3})
0.8	5.7	9.1	3.4	2.67E-02	30.2
2.1	5.0	9.9	4.9	3.85E-02	55.3
5.0	4.1	10.8	6.7	5.26E-02	95.8
7.9	3.6	11.3	7.7	6.05E-02	130.0
10.9	3.3	11.6	8.3	6.52E-02	166.7
14.2	3.2	11.7	8.5	6.68E-02	213.3
17.7	3.2	11.7	8.5	6.68E-02	265.3
21.6	3.0	12.0	9.0	7.07E-02	305.3

Pressure: 25 Torr					
Absorbed(W)	Left	Right	Length (cm)	Vol(cm^3)	Density(Wcm^{-3})
0.9	5.7	9.2	3.5	2.75E-02	31.4
2.2	5.0	9.9	4.9	3.85E-02	56.7
5.1	4.1	10.7	6.6	5.18E-02	98.3
7.9	3.6	11.3	7.7	6.05E-02	131.0
10.9	3.3	11.5	8.2	6.44E-02	169.7
14.3	3.2	11.7	8.5	6.68E-02	214.1
17.7	3.2	11.7	8.5	6.68E-02	265.3
21.6	3.0	11.9	8.9	6.99E-02	308.8

Pressure: 50 Torr					
Absorbed(W)	Left	Right	Length (cm)	Vol(cm^3)	Density(Wcm^{-3})
0.9	5.8	8.9	3.1	2.43E-02	37.7
2.2	5.1	9.8	4.7	3.69E-02	60.7
5.2	4.3	10.6	6.3	4.95E-02	104.2
8.0	3.9	11.0	7.1	5.58E-02	143.1
11.0	3.5	11.4	7.9	6.20E-02	177.0
14.4	3.4	11.5	8.1	6.36E-02	225.6
17.8	3.4	11.5	8.1	6.36E-02	279.3
21.6	3.2	11.8	8.6	6.75E-02	320.4

Pressure: 100 Torr					
Absorbed(W)	Left	Right	Length (cm)	Vol(cm^3)	Density(Wcm^{-3})
1.1	5.7	9.0	3.3	2.59E-02	44.1
2.5	5.4	9.3	3.9	3.06E-02	80.4
5.4	4.7	10.1	5.4	4.24E-02	126.8
8.2	4.3	10.6	6.3	4.95E-02	165.8
11.2	4.0	10.9	6.9	5.42E-02	205.8
14.5	4.0	11.0	7.0	5.50E-02	263.1
18.0	4.2	10.8	6.6	5.18E-02	347.1
21.8	3.7	11.3	7.6	5.97E-02	364.4

Pressure: 150 Torr					
Absorbed(W)	Left	Right	Length (cm)	Vol(cm^3)	Density(Wcm^{-3})
2.1	5.8	8.8	3.0	2.36E-02	90.2
5.3	5.0	9.7	4.7	3.69E-02	142.7
8.0	4.7	10.1	5.4	4.24E-02	189.4
11.0	4.4	10.4	6.0	4.71E-02	234.3
14.4	4.4	10.5	6.1	4.79E-02	299.6
17.9	4.5	10.4	5.9	4.63E-02	385.9
21.6	4.1	10.8	6.7	5.26E-02	411.2

Pressure: 200 Torr					
Absorbed(W)	Left	Right	Length (cm)	Vol(cm^3)	Density(Wcm^{-3})
3.7	5.7	8.9	3.2	2.51E-02	145.4
5.0	5.4	9.2	3.8	2.98E-02	168.9
8.0	4.9	9.7	4.8	3.77E-02	211.6
11.0	4.7	10.0	5.3	4.16E-02	263.8
14.4	4.6	10.1	5.5	4.32E-02	332.3
17.8	4.7	10.1	5.4	4.24E-02	418.9
21.6	4.4	10.4	6.0	4.71E-02	459.2

Pressure: 300 Torr					
Absorbed(W)	Left	Right	Length (cm)	Vol(cm^3)	Density(Wcm^{-3})
4.4	5.9	8.8	2.9	2.28E-02	191.7
7.5	5.4	9.2	3.8	2.98E-02	250.3
10.6	5.2	9.5	4.3	3.38E-02	313.5
14.0	5.0	9.6	4.6	3.61E-02	387.9
17.4	5.1	9.5	4.4	3.46E-02	504.4
21.3	4.9	9.8	4.9	3.85E-02	553.5

Pressure: 400 Torr					
Absorbed(W)	Left	Right	Length (cm)	Vol(cm^3)	Density(Wcm^{-3})
7.0	5.9	8.9	3.0	2.36E-02	295.5
10.2	5.6	9.1	3.5	2.75E-02	370.9
13.7	5.5	9.2	3.7	2.91E-02	470.7
17.0	5.5	9.1	3.6	2.83E-02	602.5
21.1	5.2	9.4	4.2	3.30E-02	638.9

Pressure: 500 Torr					
Absorbed(W)	Left	Right	Length (cm)	Vol(cm^3)	Density(Wcm^{-3})
9.6	6.0	8.8	2.8	2.20E-02	438.0
13.1	5.9	8.8	2.9	2.28E-02	573.3
16.4	6.0	8.8	2.8	2.20E-02	746.5
20.6	5.6	9.0	3.4	2.67E-02	770.3

Pressure: 600 Torr					
Absorbed(W)	Left	Right	Length (cm)	Vol(cm^3)	Density(Wcm^{-3})
12.7	5.8	8.8	3.0	2.36E-02	539.8

Pressure: 700 Torr					
Absorbed(W)	Left	Right	Length (cm)	Vol(cm^3)	Density(Wcm^{-3})
12.2	6.0	8.7	2.7	2.12E-02	575.9

D.1.1.1.4. Flow rate: 40 sccm

Pressure: .018 Torr					
Absorbed(W)	Left	Right	Length (cm)	Vol(cm^3)	Density(Wcm^{-3})
0.7	5.7	9.2	3.5	2.75E-02	27.3
2.1	5.1	9.9	4.8	3.77E-02	56.4
4.9	4.4	10.7	6.3	4.95E-02	99.6
7.8	4.0	11.3	7.3	5.73E-02	135.2
10.8	3.7	11.4	7.7	6.05E-02	177.9
14.1	3.6	11.6	8.0	6.28E-02	224.8
17.5	3.7	11.5	7.8	6.13E-02	286.4
21.5	3.3	11.8	8.5	6.68E-02	321.6

Pressure: 5.0 Torr					
Absorbed(W)	Left	Right	Length (cm)	Vol(cm^3)	Density(Wcm^{-3})
0.9	5.5	9.9	4.4	3.46E-02	26.6
2.2	5.0	10.0	5.0	3.93E-02	57.0
5.2	4.2	10.9	6.7	5.26E-02	97.9
8.0	3.7	11.9	8.2	6.44E-02	123.9
11.0	3.4	11.7	8.3	6.52E-02	168.5
14.4	3.3	11.8	8.5	6.68E-02	215.0
17.8	3.3	11.8	8.5	6.68E-02	266.2
21.6	3.1	12.0	8.9	6.99E-02	309.6

Pressure: 10 Torr					
Absorbed(W)	Left	Right	Length (cm)	Vol(cm^3)	Density(Wcm^{-3})
0.9	5.4	9.4	4.0	3.14E-02	29.2
2.2	4.9	10.0	5.1	4.01E-02	55.9
5.2	4.1	10.9	6.8	5.34E-02	96.5
8.0	3.7	11.8	8.1	6.36E-02	125.4
11.0	3.4	11.7	8.3	6.52E-02	168.5
14.4	3.2	11.8	8.6	6.75E-02	212.5
17.8	3.3	11.8	8.5	6.68E-02	266.2
21.6	3.1	11.9	8.8	6.91E-02	313.1

Pressure: 25 Torr					
Absorbed(W)	Left	Right	Length (cm)	Vol(cm^3)	Density(Wcm^{-3})
0.9	5.6	9.3	3.7	2.91E-02	31.6
2.2	4.9	10.0	5.1	4.01E-02	55.9
5.2	4.2	10.9	6.7	5.26E-02	97.9
8.0	3.7	11.4	7.7	6.05E-02	131.9
11.0	3.4	11.7	8.3	6.52E-02	168.5
14.4	3.3	11.8	8.5	6.68E-02	215.0
17.8	3.3	11.8	8.5	6.68E-02	266.2
21.6	3.1	11.9	8.8	6.91E-02	313.1

Pressure: 50 Torr					
Absorbed(W)	Left	Right	Length (cm)	Vol(cm^3)	Density(Wcm^{-3})
1.0	5.7	9.2	3.5	2.75E-02	35.5
2.4	5.0	9.9	4.9	3.85E-02	61.1
5.2	4.3	10.7	6.4	5.03E-02	103.6
8.0	3.9	11.1	7.2	5.65E-02	142.1
11.0	3.6	11.5	7.9	6.20E-02	177.9
14.4	3.5	11.6	8.1	6.36E-02	226.5
17.8	3.5	11.6	8.1	6.36E-02	280.2
21.6	3.3	11.7	8.4	6.60E-02	328.0

Pressure: 100 Torr					
Absorbed(W)	Left	Right	Length (cm)	Vol(cm^3)	Density(Wcm^{-3})
2.1	5.6	9.2	3.6	2.83E-02	73.8
2.7	5.3	9.4	4.1	3.22E-02	83.5
5.6	4.6	10.3	5.7	4.48E-02	125.2
8.4	4.2	10.8	6.6	5.18E-02	161.5
11.4	4.0	11.0	7.0	5.50E-02	206.9
14.7	3.9	11.2	7.3	5.73E-02	257.2
18.2	4.0	11.1	7.1	5.58E-02	325.7
22.0	3.7	11.4	7.7	6.05E-02	364.3

Pressure: 150 Torr					
Absorbed(W)	Left	Right	Length (cm)	Vol(cm^3)	Density(Wcm^{-3})
2.5	5.8	9.0	3.2	2.51E-02	98.0
5.5	5.0	9.8	4.8	3.77E-02	145.7
8.3	4.6	10.2	5.6	4.40E-02	189.0
11.3	4.4	10.6	6.2	4.87E-02	231.3
14.7	4.3	10.7	6.4	5.03E-02	292.3
18.1	4.4	10.6	6.2	4.87E-02	371.8
21.9	4.1	11.0	6.9	5.42E-02	403.5

Pressure: 200 Torr					
Absorbed(W)	Left	Right	Length (cm)	Vol(cm^3)	Density(Wcm^{-3})
4.1	5.6	9.2	3.6	2.83E-02	145.1
5.4	5.3	9.5	4.2	3.30E-02	163.1
8.2	4.9	9.9	5.0	3.93E-02	208.9
11.2	4.6	10.2	5.6	4.40E-02	254.8
14.6	4.5	10.3	5.8	4.56E-02	321.3
18.1	4.6	10.3	5.7	4.48E-02	404.4
21.9	4.3	10.5	6.2	4.87E-02	449.0

Pressure: 300 Torr					
Absorbed(W)	Left	Right	Length (cm)	Vol(cm^3)	Density(Wcm^{-3})
4.7	5.9	9.0	3.1	2.43E-02	193.2
7.9	5.5	9.4	3.9	3.06E-02	256.8
11.0	5.1	9.6	4.5	3.53E-02	310.7
14.4	5.0	9.7	4.7	3.69E-02	390.3
17.8	5.1	9.6	4.5	3.53E-02	504.3
21.6	4.8	9.9	5.1	4.01E-02	540.2

Pressure: 400 Torr					
Absorbed(W)	Left	Right	Length (cm)	Vol(cm^3)	Density(Wcm^{-3})
7.2	6.0	9.0	3.0	2.36E-02	307.5
10.5	5.7	9.2	3.5	2.75E-02	383.1
14.0	5.5	9.3	3.8	2.98E-02	469.6
17.4	5.6	9.2	3.6	2.83E-02	616.5
21.4	5.3	9.5	4.2	3.30E-02	649.2

Pressure: 500 Torr					
Absorbed(W)	Left	Right	Length (cm)	Vol(cm^3)	Density(Wcm^{-3})
9.9	6.1	8.8	2.7	2.12E-02	467.5
13.3	6.0	8.9	2.9	2.28E-02	585.7
16.8	6.1	8.8	2.7	2.12E-02	790.1
20.9	5.6	9.2	3.6	2.83E-02	737.4

Pressure: 600 Torr					
Absorbed(W)	Left	Right	Length (cm)	Vol(cm^3)	Density(Wcm^{-3})
13.1	5.9	9.0	3.1	2.43E-02	538.6

Pressure: 700 Torr					
Absorbed(W)	Left	Right	Length (cm)	Vol(cm^3)	Density(Wcm^{-3})
13.1	6.1	8.8	2.7	2.12E-02	618.4

D.1.1.2. 2 mm i.d. discharge tube, flow rate: 20 sccm

Pressure = 0.40 Torr					
Absorbed (W)	**Left (cm)**	**Right(cm)**	**Length (cm)**	**Vol (cm^3)**	**P/Vol(W/cm^3)**
1.0	14.1	16.5	2.4	7.54E-02	13.7
2.2	13.1	17.5	4.4	1.38E-01	16.2
4.8	11.3	19.4	8.1	2.54E-01	18.7
7.0	10.3	20.3	10.0	3.14E-01	22.2
9.4	9.1	21.5	12.4	3.90E-01	24.1
12.5	8.0	22.3	14.3	4.49E-01	27.8
15.6	7.1	22.8	15.7	4.93E-01	31.7
19.0	6.3	22.8	16.5	5.18E-01	36.6
22.1	5.8	23.3	17.5	5.50E-01	40.1

Pressure = 1.0 Torr					
Absorbed (W)	**Left (cm)**	**Right(cm)**	**Length (cm)**	**Vol (cm^3)**	**P/Vol(W/cm^3)**
1.0	14.2	16.4	2.2	6.91E-02	14.9
2.1	13.1	17.5	4.4	1.38E-01	15.4
4.7	11.5	19.4	7.9	2.48E-01	18.9
7.0	10.3	20.3	10.0	3.14E-01	22.2
9.4	9.2	21.3	12.1	3.80E-01	24.7
12.3	8.0	22.3	14.3	4.49E-01	27.4
15.5	7.1	22.7	15.6	4.90E-01	31.7
18.6	6.2	23.1	16.9	5.31E-01	35.0
21.5	5.6	23.3	17.7	5.56E-01	38.7

Pressure = 2.0 Torr					
Absorbed (W)	Left (cm)	Right(cm)	Length (cm)	Vol (cm^3)	P/Vol(W/cm^3)
1.0	14.2	16.4	2.2	6.91E-02	14.9
2.1	13.1	17.5	4.4	1.38E-01	15.0
4.6	11.3	19.5	8.2	2.58E-01	17.8
6.9	10.2	20.3	10.1	3.17E-01	21.8
9.3	9.1	21.5	12.4	3.90E-01	23.9
12.2	7.9	22.3	14.4	4.52E-01	27.0
15.2	7.0	22.9	15.9	5.00E-01	30.4
18.6	6.3	23.1	16.8	5.28E-01	35.2
21.4	5.5	23.3	17.8	5.59E-01	38.2

Pressure = 3.0 Torr					
Absorbed (W)	Left (cm)	Right(cm)	Length (cm)	Vol (cm^3)	P/Vol(W/cm^3)
1.0	14.3	16.1	1.8	5.65E-02	18.2
2.0	13.1	17.5	4.4	1.38E-01	14.6
4.6	11.0	19.5	8.5	2.67E-01	17.2
6.9	10.3	20.3	10.0	3.14E-01	22.0
9.3	9.1	21.5	12.4	3.90E-01	23.9
12.2	8.0	22.3	14.3	4.49E-01	27.2
15.3	7.0	22.9	15.9	5.00E-01	30.6
18.5	6.2	23.1	16.9	5.31E-01	34.8
21.5	5.5	23.4	17.9	5.62E-01	38.2

Pressure = 5.0 Torr					
Absorbed (W)	Left (cm)	Right(cm)	Length (cm)	Vol (cm^3)	P/Vol(W/cm^3)
0.9	14.1	16.5	2.4	7.54E-02	12.2
2.1	13.1	17.5	4.4	1.38E-01	15.0
4.6	11.0	19.4	8.4	2.64E-01	17.6
6.9	10.3	20.3	10.0	3.14E-01	21.8
9.3	9.1	21.5	12.4	3.90E-01	23.9
12.2	7.8	22.5	14.7	4.62E-01	26.4
15.3	7.0	22.9	15.9	5.00E-01	30.6
18.4	6.2	23.1	16.9	5.31E-01	34.6
21.4	5.5	23.3	17.8	5.59E-01	38.3

Pressure = 10.0 Torr					
Absorbed (W)	Left (cm)	Right(cm)	Length (cm)	Vol (cm^3)	P/Vol(W/cm^3)
0.9	14.2	16.3	2.1	6.60E-02	13.9
2.1	13.2	17.5	4.3	1.35E-01	15.7
4.7	11.3	19.3	8.0	2.51E-01	18.7
6.9	10.3	20.2	9.9	3.11E-01	22.0
9.3	9.3	21.5	12.2	3.83E-01	24.2
12.3	8.2	22.3	14.1	4.43E-01	27.8
15.4	7.2	22.6	15.4	4.84E-01	31.8
18.5	6.4	23.0	16.6	5.22E-01	35.4

21.8	5.8	23.2	17.4	5.47E-01	39.8

Pressure = 20.0 Torr					
Absorbed (W)	Left (cm)	Right(cm)	Length (cm)	Vol (cm^3)	P/Vol(W/cm^3)
1.0	14.5	16.1	1.6	5.03E-02	20.5
2.2	13.1	17.3	4.2	1.32E-01	17.0
4.6	11.5	18.7	7.2	2.26E-01	20.3
7.0	10.5	20.0	9.5	2.98E-01	23.3
9.4	9.9	20.5	10.6	3.33E-01	28.2
12.2	8.9	21.5	12.6	3.96E-01	30.9
15.2	8.0	22.3	14.3	4.49E-01	33.8
18.8	7.3	22.5	15.2	4.78E-01	39.3
21.6	6.7	22.9	16.2	5.09E-01	42.5

Pressure = 30.0 Torr					
Absorbed (W)	Left (cm)	Right(cm)	Length (cm)	Vol (cm^3)	P/Vol(W/cm^3)
	-	-	-	-	-
1.5	14.5	16.1	1.6	5.03E-02	28.9
4.3	12.6	17.9	5.3	1.67E-01	25.5
6.6	11.5	18.3	6.8	2.14E-01	31.0
9.4	10.7	20.0	9.3	2.92E-01	32.2
12.4	10.3	20.5	10.2	3.20E-01	38.8
15.4	9.4	21.3	11.9	3.74E-01	41.2
18.9	8.5	21.6	13.1	4.12E-01	46.0
22.3	8.0	22.0	14.0	4.40E-01	50.7

Pressure = 50.0 Torr					
Absorbed (W)	Left (cm)	Right(cm)	Length (cm)	Vol (cm^3)	P/Vol(W/cm^3)
4.6	13.1	17.7	4.6	1.45E-01	32.2
6.9	12.0	18.3	6.3	1.98E-01	34.6
9.2	11.5	18.7	7.2	2.26E-01	40.6
12.1	10.7	19.6	8.9	2.80E-01	43.3
15.6	10.5	20.2	9.7	3.05E-01	51.3
19.3	9.7	21.0	11.3	3.55E-01	54.3
22.6	9.2	21.5	12.3	3.86E-01	58.6

Pressure = 100 Torr					
Absorbed (W)	Left (cm)	Right(cm)	Length (cm)	Vol (cm^3)	P/Vol(W/cm^3)
5.6	13.4	17.5	4.1	1.29E-01	43.3
7.0	13.0	17.9	4.9	1.54E-01	45.2
9.3	12.3	18.3	6.0	1.88E-01	49.3
12.0	12.0	18.6	6.6	2.07E-01	57.8
14.7	11.6	18.9	7.3	2.29E-01	64.2
18.3	11.2	19.4	8.2	2.58E-01	70.9
21.9	10.7	20.1	9.4	2.95E-01	74.3
26.2	10.3	20.7	10.4	3.27E-01	80.1

Pressure = 200 Torr					
Absorbed (W)	Left (cm)	Right(cm)	Length (cm)	Vol (cm^3)	P/Vol(W/cm^3)
9.4	13.2	17.8	4.6	1.45E-01	65.1
12.7	12.7	18.1	5.4	1.70E-01	74.6
15.4	12.4	18.3	5.9	1.85E-01	83.1
18.6	12.0	18.6	6.6	2.07E-01	89.7
21.1	11.8	18.7	6.9	2.17E-01	97.4
24.5	11.3	19.0	7.7	2.42E-01	101.2

Pressure = 300 Torr					
Absorbed (W)	Left (cm)	Right(cm)	Length (cm)	Vol (cm^3)	P/Vol(W/cm^3)
11.3	13.5	17.5	4.0	1.26E-01	90.0
15.4	12.9	17.9	5.0	1.57E-01	98.1
18.9	12.7	18.2	5.5	1.73E-01	109.6
22.3	12.6	18.4	5.8	1.82E-01	122.3
25.1	12.0	18.6	6.6	2.07E-01	121.3

Pressure = 400 Torr					
Absorbed (W)	Left (cm)	Right(cm)	Length (cm)	Vol (cm^3)	P/Vol(W/cm^3)
11.9	13.5	17.2	3.7	1.16E-01	102.0
15.1	13.1	17.8	4.7	1.48E-01	102.0
18.9	12.3	18.0	5.7	1.79E-01	105.7
22.3	12.5	18.2	5.7	1.79E-01	124.5
25.7	12.6	18.4	5.8	1.82E-01	140.8

D.1.2. Microstripline Structure #2, 1 mm i.d. discharge tube, 20 sccm

Pressure: 0.15 Torr					
Absorbed(W)	Left	Right	Length (cm)	Vol(cm^3)	Density(Wcm^{-3})
0.6	5.9	8.9	3.0	2.36E-02	27.0
2.0	5.2	9.7	4.5	3.53E-02	57.0
4.9	4.4	10.5	6.1	4.79E-02	102.9
7.8	4.0	10.9	6.9	5.42E-02	143.0
10.8	3.7	11.3	7.6	5.97E-02	180.2
14.1	3.6	11.3	7.7	6.05E-02	233.6
17.5	3.3	11.7	8.4	6.60E-02	265.9
21.4	3.2	11.7	8.5	6.68E-02	320.8

Pressure: 5.0 Torr					
Absorbed(W)	Left	Right	Length (cm)	Vol(cm^3)	Density(Wcm^{-3})
0.8	5.6	9.2	3.6	2.83E-02	28.5
2.1	5.0	9.9	4.9	3.85E-02	55.3
5.1	4.2	10.7	6.5	5.11E-02	99.8
7.9	3.7	11.2	7.5	5.89E-02	134.5
10.9	3.4	11.5	8.1	6.36E-02	170.9
14.3	3.2	11.6	8.4	6.60E-02	216.7
17.7	3.4	11.5	8.1	6.36E-02	278.4
21.6	3.0	11.9	8.9	6.99E-02	308.8

Pressure: 10 Torr					
Absorbed(W)	Left	Right	Length (cm)	Vol(cm^3)	Density(Wcm^{-3})
0.8	5.7	9.1	3.4	2.67E-02	30.2
2.1	5.0	9.9	4.9	3.85E-02	55.3
5.0	4.1	10.8	6.7	5.26E-02	95.8
7.9	3.6	11.3	7.7	6.05E-02	130.0
10.9	3.3	11.6	8.3	6.52E-02	166.7
14.2	3.2	11.7	8.5	6.68E-02	213.3
17.7	3.2	11.7	8.5	6.68E-02	265.3
21.6	3.0	12.0	9.0	7.07E-02	305.3

Pressure: 25 Torr					
Absorbed(W)	Left	Right	Length (cm)	Vol(cm^3)	Density(Wcm^{-3})
0.9	5.7	9.2	3.5	2.75E-02	31.4
2.2	5.0	9.9	4.9	3.85E-02	56.7
5.1	4.1	10.7	6.6	5.18E-02	98.3
7.9	3.6	11.3	7.7	6.05E-02	131.0
10.9	3.3	11.5	8.2	6.44E-02	169.7
14.3	3.2	11.7	8.5	6.68E-02	214.1
17.7	3.2	11.7	8.5	6.68E-02	265.3
21.6	3.0	11.9	8.9	6.99E-02	308.8

Pressure: 50 Torr					
Absorbed(W)	Left	Right	Length (cm)	Vol(cm^3)	Density(Wcm^{-3})
0.9	5.8	8.9	3.1	2.43E-02	37.7
2.2	5.1	9.8	4.7	3.69E-02	60.7
5.2	4.3	10.6	6.3	4.95E-02	104.2
8.0	3.9	11.0	7.1	5.58E-02	143.1
11.0	3.5	11.4	7.9	6.20E-02	177.0
14.4	3.4	11.5	8.1	6.36E-02	225.6
17.8	3.4	11.5	8.1	6.36E-02	279.3
21.6	3.2	11.8	8.6	6.75E-02	320.4

Pressure: 100 Torr					
Absorbed(W)	Left	Right	Length (cm)	Vol(cm^3)	Density(Wcm^{-3})
1.1	5.7	9.0	3.3	2.59E-02	44.1
2.5	5.4	9.3	3.9	3.06E-02	80.4
5.4	4.7	10.1	5.4	4.24E-02	126.8
8.2	4.3	10.6	6.3	4.95E-02	165.8
11.2	4.0	10.9	6.9	5.42E-02	205.8
14.5	4.0	11.0	7.0	5.50E-02	263.1
18.0	4.2	10.8	6.6	5.18E-02	347.1
21.8	3.7	11.3	7.6	5.97E-02	364.4

Pressure: 150 Torr					
Absorbed(W)	Left	Right	Length (cm)	Vol(cm^3)	Density(Wcm^{-3})
2.1	5.8	8.8	3.0	2.36E-02	90.2
5.3	5.0	9.7	4.7	3.69E-02	142.7
8.0	4.7	10.1	5.4	4.24E-02	189.4
11.0	4.4	10.4	6.0	4.71E-02	234.3
14.4	4.4	10.5	6.1	4.79E-02	299.6
17.9	4.5	10.4	5.9	4.63E-02	385.9
21.6	4.1	10.8	6.7	5.26E-02	411.2

Pressure: 200 Torr					
Absorbed(W)	Left	Right	Length (cm)	Vol(cm^3)	Density(Wcm^{-3})
3.7	5.7	8.9	3.2	2.51E-02	145.4
5.0	5.4	9.2	3.8	2.98E-02	168.9
8.0	4.9	9.7	4.8	3.77E-02	211.6
11.0	4.7	10.0	5.3	4.16E-02	263.8
14.4	4.6	10.1	5.5	4.32E-02	332.3
17.8	4.7	10.1	5.4	4.24E-02	418.9
21.6	4.4	10.4	6.0	4.71E-02	459.2

Pressure: 300 Torr					
Absorbed(W)	Left	Right	Length (cm)	Vol(cm^3)	Density(Wcm^{-3})
4.4	5.9	8.8	2.9	2.28E-02	191.7
7.5	5.4	9.2	3.8	2.98E-02	250.3
10.6	5.2	9.5	4.3	3.38E-02	313.5
14.0	5.0	9.6	4.6	3.61E-02	387.9
17.4	5.1	9.5	4.4	3.46E-02	504.4
21.3	4.9	9.8	4.9	3.85E-02	553.5

Pressure: 400 Torr					
Absorbed(W)	Left	Right	Length (cm)	Vol(cm^3)	Density(Wcm^{-3})
7.0	5.9	8.9	3.0	2.36E-02	295.5
10.2	5.6	9.1	3.5	2.75E-02	370.9
13.7	5.5	9.2	3.7	2.91E-02	470.7
17.0	5.5	9.1	3.6	2.83E-02	602.5
21.1	5.2	9.4	4.2	3.30E-02	638.9

Pressure: 500 Torr					
Absorbed(W)	Left	Right	Length (cm)	Vol(cm^3)	Density(Wcm^{-3})
9.6	6.0	8.8	2.8	2.20E-02	438.0
13.1	5.9	8.8	2.9	2.28E-02	573.3
16.4	6.0	8.8	2.8	2.20E-02	746.5
20.6	5.6	9.0	3.4	2.67E-02	770.3

Pressure: 600 Torr					
Absorbed(W)	Left	Right	Length (cm)	Vol(cm^3)	Density(Wcm^{-3})
12.7	5.8	8.8	3.0	2.36E-02	539.8

Pressure: 700 Torr					
Absorbed(W)	Left	Right	Length (cm)	Vol(cm^3)	Density(Wcm^{-3})
12.2	6.0	8.7	2.7	2.12E-02	575.9

D.2 Argon – Hydrogen Discharges, microstripline structure #1, 2 mm i.d. discharge tube, argon flow rate: 47 sccm, hydrogen flow rate: 3 sccm.

Pressure = 0.35 Torr					
Absorbed (W)	Left (cm)	Right(cm)	Length (cm)	Vol (cm^3)	P/Vol(W/cm^3)
3.5	14.5	16.1	1.6	5.03E-02	68.9
4.9	14.3	16.2	1.9	5.97E-02	82.7
6.9	14.1	16.3	2.2	6.91E-02	100.3
9.3	13.8	16.3	2.5	7.85E-02	118.2
13.4	13.4	17.2	3.8	1.19E-01	112.1
17.1	13.2	17.5	4.3	1.35E-01	126.4
20.1	12.9	17.6	4.7	1.48E-01	136.1

Pressure = 1.0 Torr					
Absorbed (W)	Left (cm)	Right(cm)	Length (cm)	Vol (cm^3)	P/Vol(W/cm^3)
3.5	14.6	16.1	1.5	4.71E-02	73.5
5.1	14.4	16.3	1.9	5.97E-02	85.5
6.9	14.1	16.3	2.2	6.91E-02	100.3
9.3	13.9	16.4	2.5	7.85E-02	118.2
13.2	13.5	17.1	3.6	1.13E-01	116.8
16.6	13.3	17.4	4.1	1.29E-01	128.7
19.9	12.9	17.6	4.7	1.48E-01	134.9

Pressure = 2.0 Torr					
Absorbed (W)	Left (cm)	Right(cm)	Length (cm)	Vol (cm^3)	P/Vol(W/cm^3)
3.6	14.6	16.0	1.4	4.40E-02	82.6
5.3	14.5	16.3	1.8	5.65E-02	93.3
6.9	14.3	16.4	2.1	6.60E-02	105.0
9.5	14.0	16.4	2.4	7.54E-02	125.4
13.4	13.6	17.2	3.6	1.13E-01	118.3
16.6	13.3	17.4	4.1	1.29E-01	128.7
19.9	13.0	17.6	4.6	1.45E-01	137.9

Pressure = 3.0 Torr					
Absorbed (W)	Left (cm)	Right(cm)	Length (cm)	Vol (cm^3)	P/Vol(W/cm^3)
3.5	14.6	16.1	1.5	4.71E-02	73.5
4.9	14.5	16.3	1.8	5.65E-02	87.3
6.9	14.3	16.3	2.0	6.28E-02	110.3
9.3	14.0	16.4	2.4	7.54E-02	123.2
13.0	13.6	17.2	3.6	1.13E-01	115.3
16.6	13.3	17.4	4.1	1.29E-01	128.7
19.9	13.1	17.6	4.5	1.41E-01	140.9

Pressure = 5.0 Torr					
Absorbed (W)	Left (cm)	Right(cm)	Length (cm)	Vol (cm^3)	P/Vol(W/cm^3)
3.5	14.7	16.1	1.4	4.40E-02	78.8
4.9	14.5	16.2	1.7	5.34E-02	92.4
6.9	14.3	16.3	2.0	6.28E-02	110.3
9.3	14.0	16.3	2.3	7.23E-02	128.5
13.0	13.6	17.1	3.5	1.10E-01	118.6
16.6	13.4	17.4	4.0	1.26E-01	131.9
19.9	13.1	17.6	4.5	1.41E-01	140.9

Pressure = 10.0 Torr					
Absorbed (W)	Left (cm)	Right(cm)	Length (cm)	Vol (cm^3)	P/Vol(W/cm^3)
-	-	-	-	-	-
5.1	14.5	16.2	1.7	5.34E-02	95.6
6.9	14.4	16.3	1.9	5.97E-02	116.1
9.3	14.1	16.3	2.2	6.91E-02	134.3
11.7	13.9	16.4	2.5	7.85E-02	148.8
16.6	13.6	17.3	3.7	1.16E-01	142.6
19.8	13.3	17.6	4.3	1.35E-01	146.2

Pressure = 15.0 Torr					
Absorbed (W)	Left (cm)	Right(cm)	Length (cm)	Vol (cm^3)	P/Vol(W/cm^3)
5.3	14.6	16.1	1.5	4.71E-02	111.9
6.9	14.5	16.3	1.8	5.65E-02	122.5
9.3	14.3	16.3	2.0	6.28E-02	147.8
11.7	14.0	16.4	2.4	7.54E-02	155.0
16.6	13.7	17.0	3.3	1.04E-01	159.8
20.3	13.4	17.3	3.9	1.23E-01	165.4
23.1	13.3	17.4	4.1	1.29E-01	179.5

Pressure = 20.0 Torr					
Absorbed (W)	Left (cm)	Right(cm)	Length (cm)	Vol (cm^3)	P/Vol(W/cm^3)
5.2	14.4	16.0	1.6	5.03E-02	104.2
7.3	14.3	16.1	1.8	5.65E-02	128.4
9.7	14.0	16.2	2.2	6.91E-02	139.8
12.5	13.8	16.3	2.5	7.85E-02	159.4
17.6	13.4	16.9	3.5	1.10E-01	159.7
21.4	13.1	17.3	4.2	1.32E-01	162.4

Pressure = 25.0 Torr					
Absorbed (W)	Left (cm)	Right(cm)	Length (cm)	Vol (cm^3)	P/Vol(W/cm^3)
3.8	14.5	16.0	1.5	4.71E-02	80.1
6.0	14.4	16.0	1.6	5.03E-02	119.8
8.3	14.2	16.1	1.9	5.97E-02	139.2
11.1	14.0	16.2	2.2	6.91E-02	159.9
13.6	13.7	16.3	2.6	8.17E-02	166.7
19.2	13.2	17.2	4.0	1.26E-01	152.6

D.3 Pure Hydrogen Discharges, microstripline structure #1, 2 mm i.d. discharge tube, 5 sccm.

Pressure = 0.34 Torr					
Absorbed (W)	Left (cm)	Right(cm)	Length (cm)	Vol (cm^3)	P/Vol(W/cm^3)
3.6	14.9	16.0	1.1	3.46E-02	105.1
5.3	14.9	16.1	1.2	3.77E-02	139.9
7.1	14.8	16.2	1.4	4.40E-02	161.4
9.1	14.7	16.2	1.5	4.71E-02	193.5
11.3	14.7	16.3	1.6	5.03E-02	225.8
14.2	14.6	16.3	1.7	5.34E-02	266.0
16.2	14.5	16.4	1.9	5.97E-02	271.5

Pressure = 1.0 Torr					
Absorbed (W)	Left (cm)	Right(cm)	Length (cm)	Vol (cm^3)	P/Vol(W/cm^3)
5.3	14.8	16.2	1.4	4.40E-02	119.9
6.9	14.7	16.2	1.5	4.71E-02	147.0
8.9	14.7	16.3	1.6	5.03E-02	178.0
11.0	14.6	16.2	1.6	5.03E-02	219.1
13.7	14.6	16.3	1.7	5.34E-02	256.5
15.9	14.5	16.3	1.8	5.65E-02	280.6

Pressure = 2.0 Torr					
Absorbed (W)	Left (cm)	Right(cm)	Length (cm)	Vol (cm^3)	P/Vol(W/cm^3)
5.3	14.8	16.1	1.3	4.08E-02	129.2
6.8	14.7	16.2	1.5	4.71E-02	143.5
8.6	14.7	16.3	1.6	5.03E-02	171.3
10.8	14.7	16.3	1.6	5.03E-02	215.7
13.5	14.6	16.3	1.7	5.34E-02	253.4
15.9	14.6	16.3	1.7	5.34E-02	297.1

Pressure = 5.0 Torr					
Absorbed (W)	Left (cm)	Right(cm)	Length (cm)	Vol (cm^3)	P/Vol(W/cm^3)
-	-	-	-	-	-
6.6	14.9	16.1	1.2	3.77E-02	174.8
8.6	14.8	16.2	1.4	4.40E-02	195.8
11.0	14.7	16.2	1.5	4.71E-02	233.7
13.5	14.7	16.3	1.6	5.03E-02	269.2
15.9	14.7	16.3	1.6	5.03E-02	315.7

Pressure = 10.0 Torr					
Absorbed (W)	Left (cm)	Right(cm)	Length (cm)	Vol (cm^3)	P/Vol(W/cm^3)
8.6	14.8	16.0	1.2	3.77E-02	229.4
11.3	14.7	16.0	1.3	4.08E-02	277.6
13.8	14.7	16.1	1.4	4.40E-02	314.7
16.4	14.6	16.1	1.5	4.71E-02	347.2

D.4 Pure Nitrogen Discharges, microstripline structure #1, 2 mm i.d. discharge tube, 5 sccm.

Pressure = 0.0 Torr					
Absorbed (W)	Left (cm)	Right(cm)	Length (cm)	Vol (cm^3)	P/Vol(W/cm^3)
3.9	5.9	7.2	1.3	4.08E-02	96.1
5.6	5.9	7.2	1.3	4.08E-02	136.6
7.6	5.8	7.2	1.4	4.40E-02	172.7
9.7	5.8	7.3	1.5	4.71E-02	205.0
12.2	5.8	7.3	1.5	4.71E-02	258.5
15.0	5.7	7.3	1.6	5.03E-02	298.9
17.7	5.7	7.3	1.6	5.03E-02	352.4

Pressure = 0.50 Torr					
Absorbed (W)	Left (cm)	Right(cm)	Length (cm)	Vol (cm^3)	P/Vol(W/cm^3)
3.6	6.0	7.2	1.2	3.77E-02	95.1
5.4	5.9	7.2	1.3	4.08E-02	132.4
7.6	5.8	7.3	1.5	4.71E-02	161.2
9.7	5.8	7.3	1.5	4.71E-02	205.0
12.2	5.8	7.4	1.6	5.03E-02	242.3
15.0	5.7	7.4	1.7	5.34E-02	281.3
18.1	5.7	7.4	1.7	5.34E-02	338.0

Pressure = 1.0 Torr					
Absorbed (W)	Left (cm)	Right(cm)	Length (cm)	Vol (cm^3)	P/Vol(W/cm^3)
3.6	5.9	7.2	1.3	4.08E-02	87.8
5.2	5.9	7.3	1.4	4.40E-02	119.1
7.3	5.8	7.3	1.5	4.71E-02	154.0
9.5	5.8	7.3	1.5	4.71E-02	201.4
12.2	5.8	7.4	1.6	5.03E-02	242.3
15.5	5.7	7.4	1.7	5.34E-02	290.8
18.4	5.7	7.4	1.7	5.34E-02	344.3

Pressure = 2.0 Torr					
Absorbed (W)	Left (cm)	Right(cm)	Length (cm)	Vol (cm^3)	P/Vol(W/cm^3)
3.6	5.9	7.2	1.3	4.08E-02	87.8
5.1	5.9	7.3	1.4	4.40E-02	115.3
7.4	5.8	7.3	1.5	4.71E-02	157.6
9.5	5.8	7.4	1.6	5.03E-02	188.8
12.5	5.7	7.4	1.7	5.34E-02	234.4
15.9	5.7	7.4	1.7	5.34E-02	297.1
18.9	5.7	7.4	1.7	5.34E-02	353.8

Pressure = 3.0 Torr					
Absorbed (W)	Left (cm)	Right(cm)	Length (cm)	Vol (cm^3)	P/Vol(W/cm^3)
2.9	6.0	7.2	1.2	3.77E-02	77.2
4.9	5.9	7.2	1.3	4.08E-02	120.0
7.1	5.9	7.3	1.4	4.40E-02	161.2
9.2	5.8	7.3	1.5	4.71E-02	194.3
11.8	5.8	7.4	1.6	5.03E-02	235.6
15.2	5.7	7.4	1.7	5.34E-02	284.5
18.1	5.7	7.5	1.8	5.65E-02	319.2

Pressure = 5.0 Torr					
Absorbed (W)	Left (cm)	Right(cm)	Length (cm)	Vol (cm^3)	P/Vol(W/cm^3)
4.9	5.9	7.2	1.3	4.08E-02	120.0
7.1	5.9	7.3	1.4	4.40E-02	162.5
9.4	5.8	7.3	1.5	4.71E-02	200.2
11.6	5.8	7.3	1.5	4.71E-02	246.5
14.2	5.8	7.4	1.6	5.03E-02	282.1
15.8	5.8	7.4	1.6	5.03E-02	314.3

Pressure = 10.0 Torr					
Absorbed (W)	Left (cm)	Right(cm)	Length (cm)	Vol (cm^3)	P/Vol(W/cm^3)
7.7	5.9	7.2	1.3	4.08E-02	188.0
9.1	5.9	7.3	1.4	4.40E-02	207.2
11.9	5.8	7.3	1.5	4.71E-02	251.6

REFERENCES

[1] F. F. Chen, Introduction to Plasma Physics and Controlled Fusion Vol1: Plasma Physics, Plenum Press, New York, 1984.

[2] Y. Yin, J. Messier, and J. A. Hopwood, "Miniaturization of Inductively Coupled Plasma Sources", *IEEE Trans. on Plasma Science*, 27, 1516-1524, 1999.

[3] D. J. D. Hartog, D. J. Craig, G. Fiksel, and J. S. Sarff, "Impurities, temperature and density in a miniature electrostatic plasma and current source", *Plasma Sources Sci. Technol.*, 6, 492-498, 1997.

[4] E. Stoffels, A. J. Flikweert, W. W. Stoffels, and G. M. W. Kroesen, "Plasma needle: a non-destructive atmospheric plasma source for fine surface treatment of (bio) materials", *Plasma Sources Sci. Technol.*, 11, 383-388, 2002.

[5] J. R. Rogers, Properties of Steady – State, High Pressure, Argon Microwave Discharges, Ph.D. Dissertation, Michigan State University, 1982.

[6] M. L. Brake, A Theoretical And Experimental Investigation of The Chemical Kinetics of An Oxygen Microwave Discharge, Ph.D. Dissertation, Michigan State University, 1983.

[7] M. Brake, J. Rogers, M. Peters, J. Assmusen, and R. Kerber, "Electron Density Measurements of Argon Surface-Wave Discharges", *Plas. Chem. and Plas. Processing*, 5, 255-261, 1985.

[8] B. C. Wadell, Transmission Line Design Handbook, Artech House, Inc., Norwood, 1991.

[9] A. M. Bilgic, U. Engel, E. Voges, M. Kuchkelheim, and J. A. C. Broekaert, "A new low-power microwave plasma source using microstrip technology for atomic emission spectroscopy", *Plasma Source Sci. Technol.*, 9, 1-4, 2000.

[10] U. Engel, A. M. Bilgic, O. Hasse, E. Voges, and J. A. C. Broekaert, "A Microwave-Induced Plasma Based on Microstrip Technology and Its Use for the Atomic Emission Spectrometric Determination of Mercury with the Aid of the Cold-Vapor Technique", *Anal. Chem.*, 72, 193-197, 2000.

[11] H. N. Chu, E. A. D. Hartog, A. R. Lefkow, J. Jacobs, L. W. Anderson, M. G. Lagally, and J. E. Lawler, "Measurement of the gas kinetic temperature in a CH_4-H_2 discharge during the growth of diamond", *Phys. Rev. A*, 44, 6, 1991.

[12] J. Sivagnaname, Optical Emission Spectroscopy Investigation of Microwave Plasmas, M.S. Thesis, Michigan State University, 1998.

[13] J. Zhang, L. Liu, T. Ma, and X. Deng, "Rotational temperature of nitrogen glow discharge obtained by optical emission spectroscopy", *Spectrochim. Acta A*, 58, 1915-1922, 2002.

[14] A. N. Goyette, J. R. Peck, Y. Matsuda, L. W. Anderson, and J. E. Lawler, "Experimental comparison of rotational and gas kinetic temperatures in N_2 and He-N_2 discharges", *J. Phys. D: Appl. Phys.*, 31, 1556, 1998.

[15] G. L. King, Temperature and Concentration of Ionic and Neutral Species in Resonant Microwave Cavity Plasma Discharges, Ph.D. Dissertation, Michigan State University, 1994.

[16] M. A. Lieberman and A. J. Lichtenberg, Principles of Plasma Discharges and Materials Processing, John Wiley & Sons, Inc., New York, 1994.

[17] G. Herzberg, Molecular Spectra and Molecular Structure: I. Spectra of Diatomic Molecules, Van Nostrand, New York, 1950.

[18] H. R. Griem, Spectral Line Broadening by Plasmas, Academic Press, New York, 1974.

[19] R. H. Huddlestone and S. L. Leonard, Plasma Diagnostic Techniques, Academic Press, New York, 1965.

[20] Y. M. Aliev, H. Schulter, and A. Shivarova, Guided-Wave-Produced Plasmas, Springer, Berlin, 2000.